Continuous Measurements for Detection of Cavitation Caused by Transients in Hydropower Plants and Fluid Transport Systems

Kjetil Guddal Ruud

NTNU

Norges teknisk-
naturvitenskapelige universitet

Institutt for energi- og prosessteknikk

MASTEROPPGAVE

for

Student Kjetil Guddal Ruud

Våren 2014

Kontinuerlig måling for deteksjon av kavitasjon forårsaket av transienter i vannkraftverk og væsketransportsystemer

Contious measurements for detection of cavitation caused by transients in hydropower plants and fluid transport systems

Bakgrunn og målsetting

Fenomener som skjer ved store lastendringer er av stor interesse for vannkraftbransjen. I tillegg til den transiente moment/kraftoverføringen kan også kavitasjon som oppstår gjennom transienten være uheldig. Kavitasjon vil nødvendigvis ikke skje for alle lastendringer, og vil derfor være avhengig av start- og stoppnivå på transienten.

Kandidaten har i sin prosjektoppgave evaluert vandring av vannturbin i ytelsesdiagrammet og potensiell påvirkning på kavitasjonsforhold ved lastendringer. Denne tilnærmingen har benyttet ideelle analytisk tilnærminger, og det er naturlig å prøve å finne om effekten er tilstede i et virkelig kraftverk.

Flow Design Bureau AS (FDB) gjennomfører våren 2014 to omfattende kontinuerlige målinger, inklusive sanntidsanalyse på sensordata, på vannkraftverk i midt-Norge. Et av disse vannkraftverkene har påvist kavitasjon og en deteksjon og evaluering av transienter kan gjennomføres på denne.

Kandidaten gjennomfører en oppgave der hensikten er å etablere en kontinuerlig måling. Da oppfølging av kontinuerlig måling blir vanskelig blir oppgaven todelt: 1) I samarbeid med veileder på NTNU velges et system på laboratoriet som skal kontinuerlig måles og analyseres. 2) I samarbeid med FDB skrives en algoritme som implementeres i FDBs analyseprogram.

Oppgaven bearbeides ut fra følgende punkter

1. LabView programmeringsmetoder skal forklares med et spesielt fokus på sanntidsprogrammering.
2. En algoritme skal dokumenteres og programmeres og presenteres for FDB. Det kan tas utgangspunkt i prosjektoppgave av Sigrid Skodje høsten 2012.
3. Det skal utvikles et selvstendig program som skal kjøres på NI RT plattform. Hardware ved NTNU benyttes.

4. I tilfelle FDB gjennomfører en kalibreringsrunde av sensorer på kraftverk vil kandidaten inviteres inn med sine instrumenter. Det lages en selvstendig analyse på disse data.
5. Data kandidaten får basert på sin egen algoritme og tall/analyser fra FDBs kontinuerlige målinger behandles selvstendig av kandidaten

" - "

Senest 14 dager etter utlevering av oppgaven skal kandidaten levere/sende instituttet en detaljert fremdrift- og eventuelt forsøksplan for oppgaven til evaluering og eventuelt diskusjon med faglig ansvarlig/veiledere. Detaljer ved eventuell utførelse av dataprogrammer skal avtales nærmere i samråd med faglig ansvarlig.

Besvarelsen redigeres mest mulig som en forskningsrapport med et sammendrag både på norsk og engelsk, konklusjon, litteraturliste, innholdsfortegnelse etc. Ved utarbeidelsen av teksten skal kandidaten legge vekt på å gjøre teksten oversiktlig og velskrevet. Med henblikk på lesning av besvarelsen er det viktig at de nødvendige henvisninger for korresponderende steder i tekst, tabeller og figurer anføres på begge steder. Ved bedømmelsen legges det stor vekt på at resultatene er grundig bearbeidet, at de oppstilles tabellarisk og/eller grafisk på en oversiktlig måte, og at de er diskutert utførlig.

Alle benyttede kilder, også muntlige opplysninger, skal oppgis på fullstendig måte. For tidsskrifter og bøker oppgis forfatter, tittel, årgang, sidetall og eventuelt figurnummer.

Det forutsettes at kandidaten tar initiativ til og holder nødvendig kontakt med faglærer og veileder(e). Kandidaten skal rette seg etter de reglementer og retningslinjer som gjelder ved alle (andre) fagmiljøer som kandidaten har kontakt med gjennom sin utførelse av oppgaven, samt etter eventuelle pålegg fra Institutt for energi- og prosessteknikk.
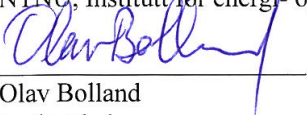
Risikovurdering av kandidatens arbeid skal gjennomføres i henhold til instituttets prosedyrer. Risikovurderingen skal dokumenteres og inngå som del av besvarelsen. Hendelser relatert til kandidatens arbeid med uheldig innvirkning på helse, miljø eller sikkerhet, skal dokumenteres og inngå som en del av besvarelsen. Hvis dokumentasjonen på risikovurderingen utgjør veldig mange sider, leveres den fulle versjonen elektronisk til veileder og et utdrag inkluderes i besvarelsen.

I henhold til "Utfyllende regler til studieforskriften for teknologistudiet/sivilingeniørstudiet" ved NTNU § 20, forbeholder instituttet seg retten til å benytte alle resultater og data til undervisnings- og forskningsformål, samt til fremtidige publikasjoner.

Besvarelsen leveres digitalt i DAIM. Et faglig sammendrag med oppgavens tittel, kandidatens navn, veileders navn, årstall, instituttnavn, og NTNUs logo og navn, leveres til instituttet som en separat pdf-fil. Etter avtale leveres besvarelse og evt. annet materiale til veileder i digitalt format.

☒ Arbeid i laboratorium (vannkraftlaboratoriet, strømningsteknisk, varmeteknisk)
☒ Feltarbeid

NTNU, Institutt for energi- og prosessteknikk, 14. januar 2014

Olav Bolland
Instituttleder

Torbjørn K. Nielsen
Faglig ansvarlig/veileder

Medveileder(e): Morten Kjeldsen, FDB

Preface

This master thesis was written at the Waterpower Laboratory at the Norwegian University of Science and Technology during the spring semester 2014. The work includes an experimental investigation of hydraulic transients and cavitation as well as development of stand-alone surveillance software in LabVIEW. The assignment was truly widespread and covered many subjects. This made it challenging to achieve very specific results.

I want to thank my supervisor professor Torbjørn Kristian Nielsen for his invaluable knowledge of dynamics in the hydropower system, and his peculiar way of asking the right questions to push me in the right direction. PhD.-Students Bjørn Winther Solemslie and Peter Joachim Gogstad have been teachers, discussion partners, motivators and friends during a long year at the laboratory. They are great resources for the master students and examples to follow with regard to their contribution. I also want to thank the guys at FDB AS for sharing their competence and experience in LabVIEW programming and for being patient with my many questions.

Finally, my fellow students have created a great environment for achieving the goals of my own and for making the path there cheerful.

Trondheim June 10 2014

Kjetil Guddal Ruud

Abstract

Surveillance of operating power plants is a progressing science in the hydropower sector. The efficiency improvements are closing in on the limits and reducing the costs by improvement of turbine life time seems to be a profitable approach. Continuously updated knowledge of the state of the mechanical parts of the turbine, will improve the ability to plan and execute maintenance work in a more efficient manner and in more suitable periods. It is therefore an important task to address the challenges connected to determination and quantification of relevant parameters, as well as development of reliable and applicable surveillance systems.

This study does an experimental investigation of the coherence between hydraulic transients induced by governing and the relevant parameters used to describe the tendency of cavitation in Francis turbines. Theory relevant to these subjects is inquired to describe the problem sufficiently. An embedded application is built in LabVIEW to acquire and process data during experiments. The application is constructed using the Real-Time module of LabVIEW to investigate how this type of acquisition and data processing can be done in stand-alone surveillance systems. Sub-VIs for Real-Time analysis of acquired data are implemented and tested. Amongst other, a modified Gibsons Pressure-Time method is implemented to do transient flow rate measurements in Real-Time. The ability of the system to control external systems is proved by controlling the speed of an electric motor upon user interaction.

The experiment results confirm that hydraulic transient from governing in turbines influence the parameters that describe the conditions for inception of cavitation. Real-Time data acquisition and processing prove its applicability to surveillance of these phenomena in operating turbines. No deduction can be made with regard to detection of cavitation with this experimental set up. The experimental set up may further be used to investigate the frequency response of governing in model turbines. The application built in this study may be developed further and more Real-Time processing methods may be implemented to yield more advanced surveillance systems.

Sammendrag

Overvåkning av kraftverk i drift er en vitenskap i utvikling i dagens vannkraftbransje. Forbedringer i virkningsgrad er inkrementelle og kostnadsreduksjoner ved økt turbin-levetid virker å være en annen økonomisk gunstig tilnærming. Kontinuerlig oppdatert informasjon om tilstanden til de mekaniske deler av turbinen vil forbedre mulighetene til å planlegge og gjennomføre vedlikeholdsarbeid på en mer effektiv måte og i mer gunstige tidsperioder. Det er derfor en viktig oppgave å undersøke utfordringene ved å bestemme og tallfeste de relevante parameterne, samt å utvikle pålitelige og anvendbare overvåkningssystemer.

Den gjennomførte studien er en eksperimentell undersøkelse av sammenhengen mellom hydrauliske transienter med opphav i regulering, og de parametere som er beskrivende for kavitasjon i francisturbiner. Relevant teori for dette er inkludert for å belyse problemet. En innebygget applikasjon er bygget i LabVIEW for å samle inn og prosessere data under forsøk. Applikasjonen er bygget med sanntidsmodulen (Real-Time) i LabVIEW for å undersøke hvordan denne type innsamling og prosessering kan utføres i frittstående overvåkningssystemer. Under-VIer for sanntids behandling av innsamlet data er implementert og testet. Blant annet er en modifisert Gibsons Trykk-Tid metode implementert for å måle volumstrøm i transiente forløp i sanntid. Systemets evne til å kontrollere annet utstyr er vist ved å kontrollere rotasjonshastigheten til en elektrisk motor ved brukerinteraksjon.

Resultater fra eksperimentene bekrefter at reguleringsinduserte hydrauliske transienter påvirker parameterne som beskriver betingelsene for at kavitasjon skal inntreffe. Sanntids datainnsamling og prosessering er vist å være anvendbart i overvåkningsøyemed av disse fenomenene i turbiner i drift. Det kan ikke gjøres noen deduksjon vedrørende kavitasjonsdeteksjon med oppsettet av dette eksperimentet. Metodikken med periodisk variasjon av ledeskovlsvinkel kan videre benyttes i forsøk der frekvensresponsen fra regulering i modellturbiner undersøkes. Sanntidsapplikasjonen kan videreutvikles og flere sanntids prosesseringsmetoder kan implementeres for å skape et mer avansert overvåkningssystem.

Scope

In this study, an initial investigation of real time monitoring of hydraulic transients in hydropower plants has been performed. The main objective is to investigate implications from the transients to cavitation parameters for Francis turbines in an embedded LabVIEW Real-Time application. The LabVIEW Real-Time package contains great opportunities for data acquisition, control and processing from a wide range of sensors and measurement devices. The francis turbine rig in the waterpower laboratory at NTNU were chosen to test the surveillance program in coherence with hydraulic transients and cavitation. The phenomenon was investigated in a numerical simulation study in a project thesis last fall. The results of that thesis are of such kind that it is desirable to do an experimental investigation of the same subject. In the work on the subject, equal weight are put onto experiments and the application development.

Great effort was put into the development of a stable and reliable surveillance program with sufficient data acquisition rates, fast and seamless data processing and proper error handling. Debugging and tuning of the program functionality were prioritized over building a host computer user interface. The development process were time consuming, but invaluable insight in the programming structure of LabVIEW Real-Time applications was achieved. As an inexperienced LabVIEW programmer the entry level to Real-Time application building was high, but achievable. A singleboardRIO was used for some initial tutorials. For the development process and the experiments, a compactRIO available at the Waterpower laboratory was used. A frequency analysis program made in LabVIEW by Sigrid M. Skodje (2012) was modified to yield the required output and used along with self-developed programs to analyze the acquired data. Comprehensive documentation of the LabVIEW environment, libraries and functionality is available online [12].

The experiments were conducted in May, 2014. The Francis rig was modified by installation of an electric motor with a gearbox to operate the guide vanes in a rigid periodic manner. Initially, an open loop configuration of the Francis test rig were attempted to obtain a free surface and reservoir simulation. In this configuration, the draft tube tank pressure could not be lowered and the influence of insufficient submergence could not be investigated. Therefore all experiments were conducted in the closed loop configuration.

Calibrated sensors and measurement devices for pressure, flow rate and guide vane angle were installed along with accelerometers for vibration measurements. The pressure sensors were installed to investigate the hydraulic transients and the influence of the periodic guide vane to the pressure and flow conditions. The installed flowmeter were not expected to react fast enough to detect the hydraulic transients such that the idea of a Real-Time Gibson method flow rate determination was introduced. The methodology was derived and an implementation of this was conducted such that pressure data from two upstream cross sections are processed to yield an estimated flow rate. Accelerometer data from the guide vane arm and the friction torque bearing were collected to investigate if structural vibrations originating from cavitation could be detected in these locations. The compactRIO and the cModules were installed and proper cabling were laid. The compactRIO was connected to the network at all times to allow supervision and user interaction with output controls. A network-setup procedure was developed and is attached in the appendix of this thesis.

At first, field experiments were planned, and an initial survey were conducted at Svorka power plant. At this power plant a simple algorithm was planned to be installed along with hardware and an embedded application of a PhD-student at the laboratory. The time-horizon of his project were changed, and the measurements were delayed such that no data are collected from field experiments. The calibrations of instruments for these experiments are therefore not conducted. The laboratory is under a tight schedule and the different projects are of very different set ups. This lead to a late semester experiment conduction for this study, as the field experiments were expected to be the main objective and the semester was planned accordingly. A survey of the risks of doing experimental work in the field or in the laboratory is included in the appendix.

Contents

List of Figures

List of Tables

Nomenclature

A	Area	m^2
a	Sound wave propagation speed	$m\ s^{-1}$
b	Height at runner inlet	m
C	Coefficient	$-$
c	Absolute velocity vector	$m\ s^{-1}$
D	Diameter	m
E	Energy	$J\ kg^{-1}$
F	Force	N
f	Friction factor	$m^{5/9}\ s^{-2}$
g	Acceleration of mass due to gravity	$m\ s^{-2}$
H	Global head	m
h	Local head	m
k	Constant in friction furmulas	$s^2\ m^{-5}$
L	Length	m
m	Mass	kg
p	Pressure	Pa
Q	Flow rate	$m^3\ s^{-1}$
r	Local runner radius	m
T	Period time	s
t	Time	s
u	Peripheral velocity vector	$m\ s^{-1}$

Greek letters

α	Angle of the absolute velocity vector to the peripheral velocity vector	$^{\circ}$
Δ	Increment/difference	
ω	Angular frequency	$rad\ s^{-1}$
ω	Frequency Hz	s^{-1}
ρ	Density	$kg\ m^{-3}$
σ	Cavitation coefficient	$-$
ξ	Loss coefficient	$-$

Sub- and superscripts

*	Best point of operation
^{n}	Timestep n of numeric variables
$_0$	Initial value
$_1$	Runner inlet or reservoir inlet
$_2$	Runner outlet or surge shaft position
$_3$	Runner outlet
$_4$	Draft tube outlet
$_A$	Available
$_b$	Barometric
$_e$	Effective
$_f$	Friction
$_h$	Hydraulic
$_R$	Reflection, Required
$_S$	Submergence
$_s$	Surge
$_u$	Peripheral velocity component
$_w$	Water
$_\infty$	Reference point
$_{dto}$	Draft tube outlet

$_{ref}$ Reference

$_{tw}$ Tailwater

Abbreviations

AI   Analog Input

ALU   Arithmetic/Logic Unit

AO   Analog Output

BEP   Best Efficiency Point

CLB   Configurable Logic Blocks

CPU   Central Processing Unit

DFT   Discrete Fourier Transform

DMA   Direct Memory Access

FFT   Fast Fourier Transform

FIFO   First In First Out

FPGA   Field Programmable Gate Array

GUI   Graphical User Interface

GV   Guide Vane

IEPE   Integrated Electronic Piezoelectric (signal conditioning)

mlc   Meters of liquid column

NI   National Instruments

NPSH   Net positive suction head

NTNU   Norwegian University of Science and Technology

ODE   Ordinary differential equation

OS   Operative System

PDE   Partial differential equation

RAM   Random Access Memory

RTOS   Real Time Operative System

VI   Virtual Instrument

Chapter 1

Introduction

The current trend in hydropower is increased speed numbers for similar runners, and thereby greater dimensions and larger velocities in the runner. This reduces the hydrostatic pressure and requires greater submergence of the runners. If the runner is not sufficiently submerged, problems with regard to cavitation will occur. In high head power plants, surge arrangements are introduced into the conduit system to prevent the water hammer pressure rise to exceed the safety limits of the mechanical installations in the turbine. These surge arrangements introduce slow periodic hydraulic transients to the system upon governing. The closure or opening of governed turbines will induce these transients due to the inertia of water in the conduits. Different types of surge arrangements exist, and the behavior of the transients depends upon the particular design of the arrangement. In the project thesis by Ruud (fall, 2013), this phenomenon where investigated using numerical and analytical methods. The increasing number of load change cycles performed in hydropower plants do also increase the occurrence of these slow hydraulic pressure transients. If the conditions for cavitation are severely affected by these transients and the operational point of the turbine is one where cavitation normally don't occur, the pressure transient may introduce hill diagram wandering into operational points where cavitation do occur.

Several companies, such as Flow Design Bureau AS in Norway, specialize in surveillance and flow control in hydropower plants. The concept of surveillance in power plants is to increase the knowledge of the state of the installations. Cavitation result in erosion of the material surfaces the cavities collapse upon. This degrades the installations life time, and leads to increased cost of maintenance and an increase of time that the power plant is inoperable. Knowledge of the condition of the installation is therefore important, such that maintenance planning and progression can be performed in an efficient manner. The appearance of cavitation is not visually detectable in operating prototype power plants. Therefore, the common procedure is to stop the generation and disassemble the turbine to do a visual inspection. To increase the interval between these inspections, it is desirable to develop embedded

stand-alone software and hardware that are designed to detect and approximate cavitation, its intensity and erosion rate. As part of the work to achieve this, the phenomenon must be adequately described and understood.

Several investigations of cavitation in hydraulic turbines are performed. Common for most of them is that they investigate either the erosion, the detection of cavitation or the implications to the efficiency in known operational points where cavitation occurs. Escarles et al. (2006) perform a cavitation detection study in different turbines with proven cavitation using frequency analysis, while Sun et al. (2004) establishes an experimental study of erosion by cavitation induced water jets. Kumar and Saini (2009) summarize previous research of cavitation in hydraulic turbines. Jarle V. Ekanger, Phd.-student at NTNU is currently performing an investigation of post processing of vibrational data and storage of relevant describing parameters from the analysis. No previous work known to the author investigate the influence from slow pressure transients to the inception of cavitation in hydraulic turbines. Therefore, this thesis will describe an experimental investigation of this phenomenon carried out in a Francis test turbine at the waterpower laboratory at NTNU in Trondheim. LabVIEW soft- and hardware will be used to highlight the possibilities of implementation of real time data analysis and surveillance tasks. This kind of application is not ”Off the shelf”, so it must be designed and implemented for the use in mind.

Chapter 2

Theoretical background

2.1 Hydraulic transients

Hydraulic transients in hydropower plants are usually a result of dynamic operation of the mechanical components in the system. Normally, closing or opening flow controlling equipment introduces these transients. An increase or a reduction in bulk velocity of an incompressible liquid, changes the pressure in the flow according to the equations of momentum and continuity [28]. As a consequence, the level of any free surfaces in the system changes accordingly. The full set of equations are available in the project thesis by Ruud (2013) [22]. Important in the context of this study, is the frequency of the u-tube oscillations. The phenomenon is of periodic nature and will change the pressure in a cyclic manner until it is dampened out by friction losses and elastic effects in the water.

In order to maintain stability and to limit the amplitude of the pressure changes related to closing or opening equipment, surge arrangements are introduced to the conduit system. A blasted shaft with a free surface to atmosphere at the hydraulic grade line at that current point is the most common arrangement. Air cushion chambers are the alternative, and they are introduced where it is technical or economically beneficial or where the topology don't allow a vertical shaft to ambient pressure. The main difference between the two arrangements is the pressure of the air above the free surface. The air cushion chamber utilize the compressibility of air to dampen the surges and has the benefit of ability to be located closer to the controlled turbine to reduce the reflection time of propagating pressure pulses [18].

The variation in level of the free surface in the surge shaft or the pressure of the air cushion in the surge chamber is deterministic for the effective head in the turbine. An increase in level/pressure will increase the head and a reduction will decrease it as long as the surface of the discharge reservoir is at a constant level. With inclusion of a downstream surge arrangement, the transient behavior is more

3

complex and the effect is more difficult to describe. Ruud (2013) simulated the effect of such an arrangement and found that the downstream surge frequency affected the effective head as well as the flow, although at less amplitudes than upstream [22]. The result of a periodic surface level is that the effective head varies in a similar manner. The characteristics of the turbine is determining for the flow conditions at the instantaneous pressure conditions.

The theoretical period of surges between the surge arrangement and other free surfaces in the system is given by the following equation [18]

$$\omega_s = \sqrt{\frac{g}{A_s \frac{L}{A_t}}}, \qquad \text{and then} \qquad T_s = \frac{2\pi}{\omega_s}. \tag{2.1}$$

For a surge shaft, the shaft area is given by A_s and is defined as the area of the free surface of water. For an air cushion chamber, the area is given by another relation including the polytropic exponent, the initial pressure head in the chamber, h_0, and the gas volume [18]:

$$A_s = \frac{1}{\frac{1}{A_{Chamber}} + \frac{nh_0}{V_{air,0}}}. \tag{2.2}$$

2.1.1 Turbine Characteristics

The turbine characteristics describe the relationship between the determining parameters of the turbine. These parameters are the guide vane opening degree, the flow, the effective head, the power and the efficiency. An analytical expression for this relationship is not achievable, such that the turbine characteristics are usually a data set where measured data from a wide range of operational points are collected in laboratory or field tests. The data set is often presented graphically in a hill diagram, which is a two dimensional plot of the data with iso-curves drawn in the plot to visualize and represent the multi-dimensional nature of the data set. In the hill diagram, the abscissa represent the speed factor n_{ED} and the ordinate represent the flow factor Q_{ED}. These factors is defined by the IEC [11] and is constant for geometrically equal runners.

$$Q_{ED} = \frac{Q}{D^2\sqrt{gH}} \qquad n_{ED} = \frac{nD}{\sqrt{gH}} \tag{2.3}$$

The influence from hydraulic transients is not the same for all operational points. The effects may vary depending on the initial point of operation. Hydraulic transients may be traced in the hill diagram when the factors for speed and flow are known. This is interesting because the occurrence of cavitation often is connected to specific operational points which may be identified in the hill diagram. A numeric investigation of such events were carried out in the project thesis by Ruud (2013) and is found in reference [22].

Another aspect is that the machine will operate at a constant speed of rotation when it is connected to the grid. The phenomena studied in this thesis, implies that the runner will operate connected to the grid, and the grid frequency is determining the speed of rotation. The variation in speed of rotation is then only influenced by the variation in grid frequency, which in Norway is limited to ± 0.1 Hz and is therefore assumed constant in the following. The assumption of constant speed of rotation has some further implications to the variation of n_{ED}, which will be constant under constant pressure conditions and the effective head will be the only variable in the speed factor.

2.2 Outlet pressure conditions

At the runner outlet, high fluid velocity implies a low static pressure according to the principles of Bernoulli's equation [28]. The low static pressure may be reduced below the vapor pressure of water and sustain a low pressure for sufficient time for cavitation to occur. The pressure conditions at the outlet of the runner also affect the pressure upstream the runner as the reference pressure changes [17]. This means that inlet cavitation may be induced by a reduced pressure at the outlet. In order to describe the pressure conditions at the runner outlet, some parameters must be defined. Derivations of these quantities are given in the thesis by Ruud (2013) [22].

2.2.1 NPSH - Net Pressure Suction Head

The net positive suction head describes the instantaneous pressure head at the runner outlet. The NPSH depends on the runner submergence below the tailwater level. Under variable downstream surface level, the available suction head changes correspondingly. The flow rate at the outlet does also affect the available head by change in pressure upon change in velocity. The derivation of this is based on the Bernoulli equation for irrotational flow with losses [28] [2].

$$h_3 = h_4 + h_b + z_4 - \frac{c_3^2}{2g}(1 - \xi) + \frac{c_4^2}{2g} - z_3 [22].$$
(2.4)

After rearrangement, the available net positive suction head is given by

$$NPSH_A = h_b + (-H_s) - h_{va}.$$
(2.5)

The submergence of the runner is given by the total energy at the draft tube outlet subtracted for the runners geodetic height.

$$-H_s = \left(\frac{c^2}{2g} + h + z \right)_4 - z_3$$
(2.6)

$$NPSH_R = a\frac{c_{m2}^2}{2g} + b\frac{u_2^2}{2g}. \qquad (2.7)$$

	Turbines
a	1.05 < a < 1.15
b	0.05 < b < 0.15

Table 2.1: *Semi-empirical range of values used to determine $NPSH_R$ in Equation 2.7*

Determination of the available head can be done by measurements and may be acquired with fair accuracy. The determination of what head is required under any point of operation to avoid cavitation occurrence is a more challenging task. The required head depends upon the runner design and the point of operation, due to large changes in outlet velocities [5]. The required suction head may be represented by the loss term in Equation 2.4. This term is difficult to determine with accuracy due to the chaotic flow patterns in the draft tube, and thereby transient friction. Approximating formulas is developed, and according to Brekke (2001), an old Kværner formula is much used in Norway [2] [4].

In Equation 2.7, the subscript 2 refers to the outlet of the runner. This is according to conventional use of notation in runners and deviates from subscripts used for the total conduit system. The constants a and b are empirical and is chosen based on runner geometry and in some cases model tests [5]. The constant are chosen in the interval shown in Table 2.1

2.3 Cavitation

Cavitation is a phenomenon occurring in liquids. Cavitation may be defined as "The breakdown of a liquid medium under very low pressures" [8]. "Weak spots" in the liquid is not able to withstand pressures below the vapor pressure of the liquid and liquid evaporates into the cavity that forms from the "weak spot". For the duration of the low pressure the cavity, or bubble, will continue to grow until the external pressure rises above the vapor pressure or the critical size of the bubble is reached [8]. In liquid flow, a pressure rise will retard and reverse the increasing bubble diameter and force the bubble to implode and condense vapor back to liquid [7]. The "weak spots" of a liquid may be air trapped in the flow, air trapped in imperfections in the material surfaces surrounding the flow or particles carried along with the flow. All of them are points where a vapor bubble may form and grow under sufficiently low pressure. Bubbles collapsing close to a material surface may under certain circumstances erode the surface. The collapsing bubble form a jet pulse of liquid water, which may hit the surface. If the force from the pressure pulse is larger than the strength of the material, the jet will create a pit in the material surface [7]. Upon longer periods of cavitating flow, these pits may grow and form larger indents in the material surface and disturb the flow in the channel

additionally [6]. Escaler et al. (2006) [7], divides cavitation into three different forms; Traveling bubbles, attached cavities and cavitating vortexes. All of these may be present in hydraulic turbines, even at the same time. A full theoretical description of cavitation can be found in the book Fundamentals of Cavitation by Franc, J.P. and Michel, J.M. (2011) and a short description of the relevant equations can be found in the project thesis by Ruud (2013) [22]. The relevant chapter in the latter project thesis is included in its whole in appendix B for further reading.

2.3.1 Thoma cavitation number

The Thoma cavitation number describes the margin between the external pressure and the vapor pressure. It may be expressed by the relations below and is also described in Appendix B

$$\sigma_v = \frac{p_\infty - p_v(T)}{\Delta p} \qquad [8].$$ (2.8)

In Equation 2.8, p_∞ represent the external static reference pressure in the flow and $p_v(T)$ represent the vapor pressure of water at the the current temperature. This value is tabulated in water property tables, e.g. in [15]. If the reference pressure is lowered, or the pressure difference is increased, the Thoma cavitation number is decreased [22]. The Thoma number at cavitational inception is termed σ_{vi} [8].

A more applicable relation for the Thoma number in hydro power applications is Equation 2.9 (from Equation B.2)

$$\sigma_{pl} = \frac{NPSH}{H_e}.$$ (2.9)

Then, as stated by Ruud (2013) [22], when the effective head is influenced by pressure transients at the runner inlet or outlet, the cavitation number is influenced directly.

2.3.2 Detection of cavitation

Detection of cavitation by measurements in an operating power plant is proven to be a difficult task, as the phenomenon occurs in a random manner. It is a challenge that the location of cavitation inception affect the measurements and ability to detect the occurrence. The different turbine designs also influence how the vibrations are carried from the source of the vibrations to the sensor [7]. In francis turbines, leading edge cavitation is considered to be most damaging, as bubbles originating from the leading edge often collapses in the runner channels where it damages the runner material surfaces [7]. Cavitation in the flow at the outlet affects the efficiency according to the sigma drop curve and the draft tube

swirl influence the operation stability. [7]. Excaler et al. (2006) [7], presents methodology to detect cavitation in hydro turbines. They consider a few key points for detection by vibrations:

- Adequate sensors should be applied to reduce noise from other hydrodynamic or mechanical phenomena.

- Commom locations of the sensors are the turbine guide bearing pedestal, the guide vane arm (top cover) and the draft tube wall.

- Measurements should be made at a range of of different operating conditions to monitor the complete operating range.

- The measured signal must be sampled at sufficiently high frequency to avoid aliasing.

According to Escaler et al. (2006) [7], the dynamic behavior of cavitation on a 2D hydrofoil is following a Strouhal law. However, they are not able to recognize this relation in hydraulic prototype runners. They state that other frequencies, such that the blade passing frequency and the guide vane passing frequency induce the shedding of erosive cavities. These driving mechanisms indicate that a pressure change, or pulse of short duration, will influence the prerequisite for cavitation inception. If phenomena of such short duration is inducing cavitation at certain points of operation, longer period and medium amplitude phenomena such as surge chamber transients may be assumed to exert the same influence to the flow conditions. Cavitation is assumed to incept according to a certain time constant from cavitation free flow to a cavitating flow [17]. It is expected that slow phenomena such as surge chamber transients might be of sufficient duration to trigger cavitation.

It is difficult to predict at which frequencies cavitation may be detected, especially in model turbines. Escaler et al. [7] have done proto type experiments and the results indicate that a significant increase in amplitudes and auto power spectrum in the range of 5-25 kHz should be observed. Mørch and Anderson (2012) [1], investigate the tensile strength of water exposed to pressure pulses of short duration and states that pressurized water will increase its tensile strength. This means that the pressurized water at the inlet of the turbine has an increased tensile strength and the flow are actually less likely to cavitate. This is reduced over time and the pressure are reduced through the turbine. Mørch also states that cavitation bubble can incept, grow to critical radius and collapse within 40 microseconds [16]. This indicates that slow transients in the range of 250-1000 milliseconds will be sufficient to incept cavitation if the operational point is close to the limit where bubbles occur.

2.4 The Gibson method

The pressure-time method, better known as the Gibson method, is a method to determine the flow rate in a conduit with governed equipment installed. Normally, the initial flow rate is determined based on the pressure difference between two cross sections upstream closing equipment, in this case a governed turbine. The concept is that when the flow is retarded, a pressure-rise is induced in front of the closing turbine. Newtons 2nd law is applied to a fluid control volume where forces acting on the control volume are considered. The derivation of the method is given in Appendix A. Equation 2.10 is the final result of the derivation.

$$\Delta Q = Q - Q_0 = \frac{gA}{L} \int_{t_0}^{t} (\Delta h - \Delta h_f) dt. \tag{2.10}$$

The common procedure using the Gibson method is to operate the turbine at a constant operational point before the guide vanes are closed completely in a short period of time. The pressure difference is recorded for the full closing time. Both the pressure and the head loss is a function of time, but the head loss is more difficult to measure and must therefore be approximated. The initial head loss at the initial flow rate may be determined by considering the equilibrium level of the pressure before and after the closure. The head loss is then approximated by an iteration process for all t by an approximated formula using the flowrate in the previous time step [9]. The equilibrium level is used together with the measured differential pressure data to do the integration in Equation 2.10. In the conventional method, the time it takes to close the guide vanes are considered to be the limits in time, i.e. the initiation of the closure happens at t_0 and the finalization happens at $t = t_{closed}$. Then the equation may be rearranged and solved for Q_0. Any leakage flow must be accounted for [9]. A complete procedure for computation of the initial flow is given in the thesis by stud. techn. H. Francke (2006) [9].

2.4.1 Modified Gibsons method

The purpose of this modification to Gibsons method is to be able to measure the flow rate in a turbine that is exposed to transient hydraulic conditions. Such conditions may be governed guide vanes, slow pressure transients or faster changing flow patterns. The idea of this modification and application, was introduced during discussions with prof. Torbjørn K. Nielsen regarding the flowmeter. Under influence of quickly changing flow rates, the resolution of current flowmeters may be too poor to measure the flow rate at a desired level of accuracy. Another method is therefore desirable. The difference in this kind of application is that the method is used to determine the flow rate without a complete closure of the guide vanes. This requires some considerations regarding the time interval of the integration in Equation 2.10. The head loss must be determined to achieve the required accuracy.

The head loss at a certain known steady flow rate may be determined by the use of the differential pressure. Then there is no acceleration or retardation of the flow and the only source of a pressure difference is the head loss. The friction head loss in a steady flow are approximated using Equation 2.11.

$$\Delta h_f = kQ^2 \tag{2.11}$$

In the laboratory, flowmeters are available, such that the flow rate under steady conditions may be determined. In an operating power plant, established turbine characteristics and the opening ratio may be used do approximate the flow rate. Using the characteristics to determine the flow rate requires knowledge of the effective head and the opening ratio and may not be very accurate. Using the measured or approximated flow rate, the friction constant in Equation 2.11 may be determined. By rearranging the equation, one gets:

$$k_{init} = \frac{\Delta h_f}{Q^2_{init}}. \tag{2.12}$$

The constant k in Equation 2.12 is assumed to be constant at flow rates in the near proximity of the steady flowrate. Due to the implicit nature of Equation 2.10 an iteration process must be performed to obtain the change of flowrate with greater accuracy. For any steady flowrate, this change in flowrate should be zero according to the fact that the pressure difference between the two measurement section is equal to the head loss with the consequence of the integrand in Equation 2.10 being zero. This is considered to be the initialization process of the methodology. Then, Equation 2.10 is applied to find the flowrate in the next time step. $(t = t_0 + \Delta t)$

- perform the iteration process to improve accuracy of the flow rate. The initial guess of the new flowrate in the iteration process is the flowrate in the previous time step $(t = t_0)$

- Add ΔQ calculated by Equation 2.10 to the flow rate in the previous time step, Q_0.

This procedure is implemented in the surveillance program that is developed for use in this master thesis and is more thoroughly described in Chapter 5.

2.5   Uncertainty

The international electrotechnical commission defines error as *the difference between the measured and the true value* [11]. The uncertainty of a measureand may be defined as how likely it is that a measured sample is part of a certain range of values. A 95 % confidence interval is normally the requirement. Solemslie (2010) [21] list three types of errors.

- Spurious errors

- Systematic errors

- Random errors

The spurious error is considered to origin from human error or instrument dysfunction [21]. These errors are normally discarded from the measurements if their value lies more than two standard deviations away from the other data. The systematic errors are errors originating from faulty calibrations, hysteresis or unknown coherence between the output signal and the measured quantity. The measurements may be influenced by random errors which are errors that yield different measurements even when measuring the same physical quantity. [21]. The random errors are assumed to behave according to a normal distribution lying around the mean value when the number of measurement points exceed about 30 samples, according to the central limit theorem [26]. For fewer points, the student t-distribution is applied [21].

In typical experiments, the quantity may be measured or sampled several times to reduce the uncertainty of the measurements. In dynamic processes, this may be hard to achieve such that only single samples may be acquired. This give the uncertainty of a single measurement and not the uncertainty mean value of a set of test samples. [27]. There will not be performed an uncertainty analysis in this thesis. A preliminary investigation were made to investigate the possibility to include uncertainty calculation into the surveillance system implemented in LabVIEW, but this was discarded due to the limited RAM resources of the compactRIO. The methodology for these kind of uncertainty analysis may be found in the book Introduction to Engineering experimentation by Wheeler and Ganji (p. 199 2nd ed. 2004) [27].

2.6 Post-processing tools

2.6.1 The fourier transform

The Fourier transform is a complex integral transformation. A time dependent signal can be transformed into a composition of sinusoidal elements. The transform yields what is known as a spectral representation of the signal [14]. If the time signal is a continuous function, the complex Fourier transform is given by:

$$\hat{f}(\omega) = \frac{1}{\sqrt{2\pi}} \int_{-\infty}^{\infty} f(t)e^{-i\omega t}dt. \tag{2.13}$$

Using the Euler identity

$$e^{\pm i\omega t} = \cos\omega t \pm i\sin\omega t$$

it is evident from Equation 2.13 that the Fourier transform may be utilized to describe the frequencies in the signal and the amplitude and phase shift of the sinusoids in the original signal.

Fast Fourier Transform

In empirical methods where analog data is sampled with finite time steps, another method is required. The resulting discrete data set may be handled by interchanging the integral by a finite sum over the elements. To obtain a transform, a complex trigonometric polynomial may be determined. This polynomial must interpolate the discrete points of the data set. The resulting transform, called the Discrete Fourier Transform (DFT) can be expressed by vector components [14]

$$\hat{f}_n = \sum_{k=0}^{N-1} f(t_k) e^{-it_k n},$$
(2.14)

where f_n is the nth component of the vector composing the Fourier transformed signal. N is the total number of discrete points. In order to avoid aliasing, the number of vector components should be less than half the number of the sampled points. Aliasing means that there is more than one polynomial that interpolates the discrete points. Such a faulty polynomial will not be descriptive for the physical system investigated. Travis and Kring (2006) [25] proposes that Nyquist's Theorem can be stated as following: *To avoid aliasing, the sampling rate must be greater than twice the maximum frequency component in the signal to be acquired.*

Sampling at a high frequency yields a vast number of points even at short logging periods. According to Kreyszig (2006), the DFT requires a number of calculations of order $O(N^2)$. e.g., a logging time of 1 second at 100 Hz requires $100^2 = 1000$ calculations. Therefore, the Fast Fourier Transform (FFT) is developed. The FFT reduces the task into several smaller odd and even tasks of size N=2 to reduce the number of calculations. Complete development of this theory and methods can be found in several books on the subject, like Kreyszig (2006) [14], Pickering (1986)[19] and many more. National Instruments also provides the relevant theory to correctly implement the built in signal processing functionality of their software LabVIEW. This information is published in public accessible NI white-papers available online at www.ni.com. A critique of these white-papers using the sources previously mentioned proves their accuracy and reliability with regard to these tools in their software.

The number of points or frequency lines in the spectrum is determined by the number of sampled point in the discrete time data set.

$$N_f = \frac{N_t}{2}$$
(2.15)

The width of the spectrum is determined by the sampling rate and the number of sampled points. The spectrum starts with the DC-component of the signal and ends at the frequency given by

$$f_{end} = \frac{F_s}{2} - \frac{F_s}{N}.$$
(2.16)

The resolution of the spectrum may be determined using the sampling rate of the discrete time signal and the number of acquired points or using the number of points and the time increment between successive points.

$$\Delta f = \frac{F_s}{N} \qquad (2.17)$$

It is important to note that frequencies deviating from multiples of Δf is included in frequency "bins" centered at such multiples of Δf, which means that the resolution is not infinite. In this study, built in functionality in LabVIEW and DIAdem will be utilized.

2.6.2 Savitsky-Golay Filtering

In order to reduce the ratio between the random noise of the measurements and the measured signal, a filter may be applied to the data series. As the sampling rate often is far greater than the frequency of the phenomena under investigation, the filtering is assumed to remove no vital information from the data sets. If phenomena such as the water hammer effect were to be investigated, such filtering should be carefully considered. The requirements that applies to use this type of methods are that the data is uniformly distributed along one of the axes, normally the time axis, and that the points must be fairly continuously distributed when plotted [23].

There are several ways to filter a time-domain signal. Most common might be the running mean method, where a value at a distinct value of t are averaged using the neighboring values [23]. Mathematically this may be described as

$$\bar{Y}_j = \frac{\sum\limits_{i=-m}^{m} C_i Y_{j+1}}{N} \qquad [23]. \qquad (2.18)$$

In Equation 2.18, N=2m+1 and m is the width of the averaging bin. The constant C is, for the running mean case equal to one, but may be tuned to weight the running average by weighted convolution. However, this kind of averaging is not conserving the information of sharp peaks in the data set. Therefore, another method using the method of least squares are applied. Then, polynomials are fitted to a set of data points of size N, and the value of the polynomial are compared to the measured value for the same time t_j. The difference is minimized for all values in the data subset using the method of least squares to obtain the best fitted polynomial. The size of the data subset and the degree of the polynomial determines the final result of the filtering. An increased number of points in the data set will filter out more information and an increased polynomial degree will maintain larger deviations. This method is somewhat more tedious mathematically and the derivation is given

in the article by Savitzky and Golay (1964) [23]. The final equation for the method is

$$\sum_{k=-m}^{m} b_{nk} \sum_{i=-m}^{m} i^{k+r} = \sum_{i=-m}^{m} y_i i^r \qquad (2.19)$$

In Equation 2.19, i is running from $-m$ to m, n is the number of points, k is the order of the terms in the polynomial, r is the number of equations running from 0 to n. y_i is the value of the data set in the i'th point [23]. The method is implemented into the standard library of LabVIEW and is easily implemented by applying a data set, specifying the width of half the data sub set and the degree of the polynomials. However, great care must be taken when specifying these parameters with regard to the area of application and loss of significant information.

2.6.3 Non-parametrical splines

Non-parametrical splines is a method of piecewise polynomial interpolation. The basic concept of spline interpolation is to create a piecewise function that interpolates points of a sub data set. This avoids the problems known as Runge phenomenon when using one single polynomial to fit all points. Runges phenomenon may be explained by the infinite limit of the interpolation error as the number of sample points approaches infinity [14]. This is important to avoid, especially when handling large data sets of thousands of distinct points.

The splines are determined by solving a linear system to obtain a set of functions which together creates a continuous function that interpolate the data set [14].

$$F_s = \begin{cases} q_0\,(t) = a_{00} + a_{01}\,(t - t_0) + a_{02}(t - t_0)^2 + a_{03}(t - t_0)^3 \\ q_1\,(t) = a_{10} + a_{11}\,(t - t_1) + a_{12}(t - t_1)^2 + a_{13}(t - t_1)^3 \\ \vdots \\ q_i\,(t) = a_{i0} + a_{i1}\,(t - t_i) + a_{i2}(t - t_i)^2 + a_{i3}(t - t_i)^3 \end{cases} \qquad (2.20)$$

The coefficients in the functions are determined using Taylor formula and a set of boundary conditions. Proof and derivation of this method is found in the book in advanced engineering mathematics by Kreyszig (2006). In DIAdem, this method is implemented and it requires that the t-values are *"strictly monotonic"*, which means that the increment between all values of t should be equidistant. The method applied in this thesis is one called approximating splines. These splines do not pass through all points, but use the least square error method to minimize the distance to the points of the data set. The approximating splines use a weighing factor which may be manipulated to achieve the desired degree of fit. High weighing factors will approach the natural splines which are interpolating and passing through all points. The purpose of introduction of this method is to obtain curves which are easier to

investigate visually for first order periodic behavior such as the guide vane angle in periodic movement. The approximating splines reduces the noise of the signal, and dampens the amplitudes but maintain the periodicity.

Chapter 3

LabVIEW

In this chapter, a description of the graphical programming language labVIEW is presented along with some of the key concepts in this software. LabVIEW is an abbreviation for Laboratory Virtual Instrument Engineering Workbench. In LabVIEW the user constructs a custom virtual instrument program (VI), built up by a front panel and a block diagram. In the block diagram, functional blocks connected by data-flow wires determines the functionality of the program. The user may control the program through the front panel containing elements which controls, represent or display the functional blocks of the block diagram. The LabVIEW Real-Time module allows the user to construct data acquisition and post processing tasks in the graphical user interface before it is compiled and transferred to stand-alone hardware units. An example of such stand alone hardware is the RIO products from National Instruments. The reliability of the process is increased by running directly on the hardware instead of in an operative system or in an OS based application. [10] This is considered to be highly advantageous, as monitoring systems require high up-time reliability [12].

3.1   RIO - Reconfigurable I/O

A reconfigurable in/out unit is a hardware unit built up by a real time processor, a field programmable gate array and a modular in/out unit. The microprocessor is using a real time operative system (RTOS) and a graphic user interface. There is several different RIO's in the commercial market. Different type of chassis with a wide range of specifications is available. The most important specifications to this thesis were the internal memory, data transferability and the number of slots for cModules. A NI cRIO-9074, available at the waterpower laboratory was found suitable for the application in mind. A cModule is an unit constructed to widen the application of the cRIO chassis. A wide range of cModules is available for most application in data acquisition and output for control. All modules fits in slots in

Table 3.1: *cRIO-9074 specifications as given by National Instruments [12]*

Embedded system specifications	
Chassis	NI cRIO-9074
Operating system	Real-Time OS
FPGA chip	Spartan-3
FPGA # of gates	2.000.000
Chassis # of slots	8
Input voltage range	19-30 V

Table 3.2: *cModule specifications as given by National Instruments [12]*

NI cModules	I/O channels	Signal/max sampling rate
NI-9203	8 + COM	4-20 mA AI 200 kS/s
NI-9233	4	$\pm$ 10 V IEPE AI 50 kS/s
NI-9263	8 + COM	0-10 V AO 100 kS/s
NI-9239	4 isolated channels	$\pm$ 10 V AI 50 kS/s

the chassis and the required modules is chosen to acquire or deliver the required signal input or output from a variety of channels [12]. The specifications of the compactRIO and the cModules are presented in Tables 3.1 and 3.2.

All cables for sensors and controllable equipment is connected to the compact RIO via the cModules. The type of connection varies depending on the type of cable used. In these experiments, common $\pm$ wires with isolation and coaxial cables were used as well as special cables for the accelerometers. For the accelerometers, BNC connectors were used as the cModule is equipped with these. On the contrary, the coaxial cable had BNC connector, while the module did not. A solution was found, where a BNC plug were connected to the module by wires and then connected to the coaxial cable.

3.1.1 Processor

The functions of a central processing unit (CPU) are carried out by the microprocessor. The microprocessor receives and send instructions from other units in the device such as RAM, ROM and other hardware. The microprocessor is made up by only one single integrated circuit. The microprocessor perform three fundamental operations; using the Arithmetic/Logic Unit (ALU), move data between locations and make decisions and switch to another set of instructions based on previous decisions. The CPU loads the RTOS to the local Random access memory (RAM) and executes all commands that is given to the OS either from the user or from other applications in the device. This unit does most of the data handling and all the processing of the data set. In a fully embedded system, this unit will also send processed data to a host-VI running on the computer CPU to handle user input,

graphical display of data and data storage tasks. The specific task of the cRIO CPU in this thesis will be described later in Chapter 4.

3.1.2 FPGA

The field programmable gate array is a silicon chip or parts of a chip. In LabVIEW applications, the FPGA is used in combination with a microprocessor. In difference to the microprocessor, the FPGAs have true parallel functionality such that simultaneous tasks and operations do not require the same resources. Each part of the compiled FPGA-embedded code is assigned to a specific selection of the chip through internal rewiring of the internal blocks. The functionality of one path on the chip is independent from operations in other paths on the chip. That implies that the addition of more calculations or operations do not influence the performance of previous implemented operations. The array consists of a finite number of predefined resources called configurable logic blocks (CLB). The CLBs is connected by programmable interconnections and also to the I/O ports of the chip. The FPGA is missing the opportunity to communicate with an OS or a hard drive and is therefore, as in this case, often constructed together with a microprocessor in a hybrid architecture. The FPGA functionality is configured using LabVIEW to define the tasks. The program is then compiled and uploaded to the hardware RIO. Early hardware description languages are complex and difficult to program without comprehensive knowledge in the hardware functionality due to the parallel behavior and structure of the FPGA. This is made achievable with the LabVIEW FPGA compilation tools.

3.1.3 FIFO - First In First Out

The data transfer to and from the FPGA is handled using direct memory access to utilize the memory blocks of the CPU device. Data is transferred using the first in, first out (FIFO) concept such that the first values to be written to the data stream are the first to be read. The FIFO-buffer has to be set up such that the direction of the data flow is determined beforehand and proper data type is selected according to the input/output channels. The cModules are usually configured with a default data type. Conversion of the default data type to another data type should be done with care to avoid losing significant data in the conversion.

The FIFOs must be configured with a preset buffer size. A buffer is a dedicated memory which is available to the FIFO to temporarily store data while other data is read in the RT-target. The buffer size should be set with great care as the resources are limited. However, the buffer must be of sufficient size such that no data is lost due to a filled buffer.

3.1.4 Programming structure

In embedded RIO systems, the programming is different from traditional LabVIEW programming to utilize the specific advantages of the different hardware units. Therefore, three different levels of programming is established.

First, the FPGA is programmed to do the data acquisition and simple operations such as creating a table of channel data, writing to the FIFO and send and receive status messages. The FPGA can also do several simple operations and these operations are useful when they should be executed for every single data points. The resources of the FPGA are as indicated in Section 3.1.2 limited and the compilation process is extended in time when the number of operations is increased.

Second, The Real-Time target is programmed. The RT-target read data from the FIFO, distribute data to its desired location, processing and handling of data and writing data to a storage location. The RT-target also handles the running/operation of the FPGA target and most FPGA program properties can be accessed from the RT program. Data, either raw, or processed may be sent from this level to the HOST level. Processing in Real-Time is advantageous with regards to limiting the amount of stored data, but may introduce some issues with loss of information when the raw data is used to establish derived units. Raw data may be necessary to store where specific applications requires the data in a specific form.

Last, the computer CPU runs a VI that reads data sent from the RTOS/CPU and sends user input back to the RT-target. The host computer usually handles graphical display better due to its superior hardware. Additional processing may also be made on this level where the available resources on the real time target are exceeded. The transfer of data from the embedded target to the host computer require the use of event handled network queues to keep the embedded target to run independent of the running of the host-VI.

3.2 DIAdem

DIAdem is a graphical user interface data processing software tool delivered by National Instruments. The software include many tools for post processing, presenting and viewing acquired data. DIAdem fully utilize the .tdms file format of LabVIEW and the data is well structured in groups and channels for better overview and to collect data series that are related. The functionality of the post processing tools are the same as functionality available in the LabVIEW libraries. However, the GUI is easier to handle, when the objective is not known, due to its flexibility and versatility. Therefore, DIAdem has been used introductorily to handle the acquired data sets. This gives a quick and complete overview of the findings in the data material. The report generation of DIAdem has some short-comings, such that data has been exported to Matlab to create the figures of this report.

Chapter 4

Method

4.1 The laboratory francis test rig

The hydropower laboratory at NTNU is equipped with a flexible francis test rig. It is flexible in terms of opportunities with regard to operation range and configuration. The rig may be operated with pressures up to 4 bar ($\approx$ 40 mlc.) inlet pressure in a closed loop configuration and with 12 mlc head in an open loop free surface reservoir configuration. In both configurations, centrifugal pumps deliver the available head. The open loop carries the advantage of keeping a fairly constant head, introduce an u-tube between the pressure tank and a constant discharge water level in the pressure tank. The closed loop adds flexibility to operation range with greater head and flexible control of the head and the suction pressure in the draft tube by reduction of the pressure in the draft tube tank.

4.1.1 The francis turbine

The francis runner currently installed in the laboratory is a model runner designed by Ole Gunnar Dahlhaug to the specifications of Tokke power plant in Norway [5]. The specifications of the model is given in Table 4.1 along with some of the main specifications of the prototype runner.

The closed loop of the laboratory is illustrated in Figure 4.1. The rig consist of several main parts described in the following

- Pumps: The pumps is located in the basement below the surface of the lower reservoir of the laboratory to achieve sufficient submergence. The pumps may be operated in four different settings. Each pump may be operated separately, the pumps may be operated in parallel or in series depending on the requirement in head and flow. The pumps are initially used to fill the

Table 4.1: *Specifications of model runner in francis test rig.*

	Model
Rated head [mlc]	30
Rated flow m^3/s	0,33
Rated speed [RPM]	540
Number of full runner vanes	15
Number of splitter blades	15
Total number of blades	15
number of guidevanes	28
b_1 [m]	0,0596
D_1 [m]	0,6305
D_2 [m]	0,3491

components of the closed loop, and later to deliver the required pressure in the loop.

- Pressure tank: The pressure tank is a closed chamber with an air relief valve. Upon filling of the loop, the relief valve is open until the desired water level, and thereby the air volume, is reached and then the valve is closed. The water level must be chosen sufficiently high such that no air is drawn into the pipes running to the turbine, but that is usually not a problem. The pressure tank is basically an air cushion chamber both in closed loop and open loop configuration.

- Gibson measurement pipe stretch: The rig is recently modified to include a straight pipe before the spiral casing inlet to do a differential pressure measurement to calculate the volumetric flow rate according to the Gibson method described in Chapter 2.4.

- Turbine: The turbine is a Francis turbine with spiral casing, stay vanes, guide vanes, runner and a draft tube. The guide vanes is also modified lately to be controlled cyclic by an electric motor, and this will be explained later in Section 4.2. The draft tube is equipped with a transparent draft tube cone to let the operator observe the flow at the runner outlet. This also exposes the lower parts of the blades.

- Draft tube tank: The draft tube tank main task is to be the lower reservoir for the discharge water from the turbine. The tank contains a water free domain which may be utilized to control the pressure level in the draft tube, and thereby the pressure at the runner outlet. A vacuum pump controls the reference pressure at the free surface in the tank and then also the effective submergence of the turbine center.
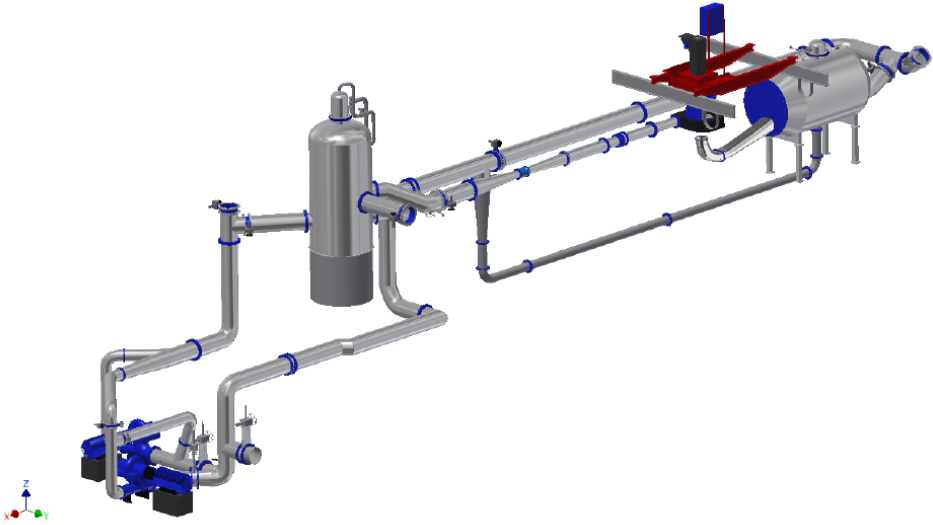
Figure 4.1: Model of the closed loop configuration in the laboratory.

4.2 Guidevane operation

In order to induce the desired hydraulic transients, several different methods were considered. The physical phenomena of a sudden load change by a single stroke by the governor cylinders and the following up and down surges in the surge arrangement described in Section 2.1 is not achievable in the Francis test rig. The air cushion chamber i.e. the pressure tank will not allow the amplitudes and period times a large hydropower plant experiences. Therefore, the possibility of running the test rig in an open loop with free surface reservoir and introduction of a change in guide vane angle were not appropriate. This solution would also not allow the pressure in the draft tube tank to be varied as the open loop discharges water to the sump reservoir. The vacuum pump controlling the reference pressure level in the draft tube tank would then only lift the surface level in the tank and not lowering the pressure with the consequence that the submergence is increased instead of reduced. A solution where transient cyclic movement impressed to the guide vanes was chosen due to the flexibility of submergence. The cyclic movement will affect the flow and head according the turbine characteristics described in Section 2.1.1.The main difference from the physical phenomenon studied is that the guide vane angle is not kept at a constant setting. Therefore, the speed and flow factor will vary slightly different in the experiment than a prototype runner exposed to surge shaft transients would do. The external influence to the turbine is impressed to the guide vanes by a electric frequency controlled motor instead of by the surge shaft transients. The continuous change of flow rate will influence the level in the

23

Table 4.2: *Guide vane motor specifications given by the producer (VEM/Bonfiglioli).*

VEM three phase asynchronous motor and Bonfiglioli gear	Spec.
Power [W]	370
Nom. speed [RPM]	1370
Nom. Voltage [V]	230
Nom. current [A]	1,84
Efficiency [-]	0,678
Weight [kg]	7,8
Gear ratio [-]	1:28

pressure tank, i.e. the air cushion chamber and the draft tube tank and therefore result in surge shaft transient in addition to the guide vane movement. This is a source of conceptual error in the experiment, but will clearly introduce pressure transients in the runner, and is therefore found adequate for the scope of the thesis.

The guide vanes of the Francis rig is normally operated by an electric step motor. This motor is adequate for a single change in opening angle in one direction, but for a periodic change, another solution was sought. To achieve the desired guide vane movement, a motor and a gearbox were installed next to the guide vane adjustment arm. A crank arm was connected between the motor and the guide vane adjustment arm. The shaft of the motor was modified to exert a excentric movement to the crank arm at the motor end which in turn moves the guide vane adjustment arm. This concept was designed in cooperation with Joar Grilstad, divisional engineer, and professor Torbjørn K. Nielsen. The excenter was made to obtain a ±5% change in guide vane angle and the movement arm was stiffened such that the flex should be minimal. A slight deviation from perfect sinusoidal movement is expected due to flex, backplay in connections and the opening torque of the guide vanes at the specific guide vane angle. This deviation is not considered to be of particular influence to the phenomenon in mind as the movement still is periodic.

The setup of the motor with its gearbox and its excentric shaft is shown in Figure 4.2. The motor and the gear box is found online at grabcad.com [29]. The excentric shaft, the crank arm and bearing is drawn by the author. The shaft with excentric top and bearing is illustrated in Figure 4.3.
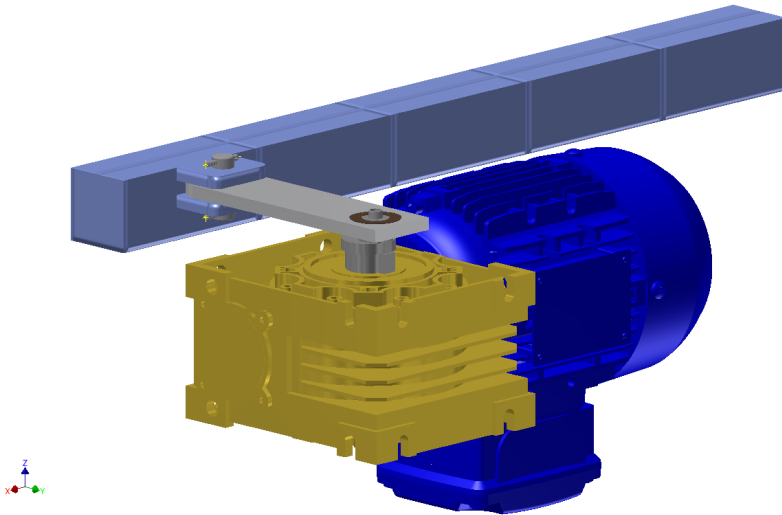
Figure 4.2: 3D sketch of guide vane motor with gear box, excentric shaft, crank arm and parts of the guide vane adjustment arm. (Motor modified from doxsyde at grabcad.com [29]).
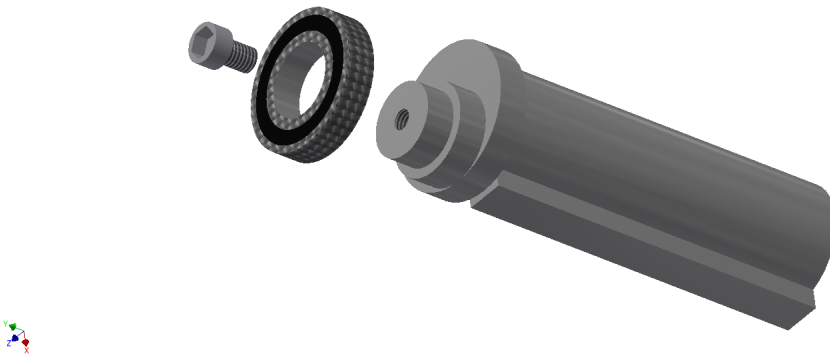
Figure 4.3: Illustration of shaft with bearing and fastening bolt.

4.3   Measurements

To conduct measurements, several sensors and devices are installed to the laboratory test rig. A description of application and positioning are given in the sections below. All measurements are made using the compactRIO and the corresponding cModules. The different data acquisition rates are displayed in Table 4.3

4.3.1   Vibration measurements

The vibration measurements are carried out with two accelerometers from Brüel og Kjær with a frequency range from 1 Hz -25 kHz. The placement of the sensors are according to Escaler et als. [7] recommendation at the guide vane arm and the friction torque bearing side wall. The accelerometers are unidirectional and have a low transverse sensitivity (1,4% of main axis sensitivity). The accelerometers are screwed onto studs that are glued onto the metal surface where the sensor is to be placed. Special shielded cables to connect the accelerometer to the cModules on the cRIO chassis are used.

4.3.2   Flow measurements

Measurements of the flowrate is carried out to compare the calculated flowrate using the method of Gibson in Section 2.4. The measurements are made using an electromagnetic flowmeter. Using the relations of Faradays law, a voltage signal is induced when water flows through an electromagnetic field. The magnetic field is induced by the flowmeter device. The voltage is proportional to the magnetic flux and the diameter of the pipe constraining the water. Assuming an uniform magnet field and that the pipe itself is nonconductive, the flowrate may be expressed as

$$Q = Ac_{avg}B \qquad [3].\qquad\qquad (4.1)$$

Table 4.3: *Sample rate of measured quantities and abbreviation for sensors.*

Location	Abbreviation	Sample rate
Pressure tank air cushion	p_0	1000 Hz
Gibson pressure	p_1	1000 Hz
Turbine inlet pressure	p_2	1000 Hz
Draft tube outlet pressure	p_3	1000 Hz
Guide vane arm	V_{GV}	50 kS/s
Friction torque bearing	V_{FTB}	50 kS/s
Flowmeter	Q_{init}	1000 hz
Guide vane angle	α_{GV}	1000 hz
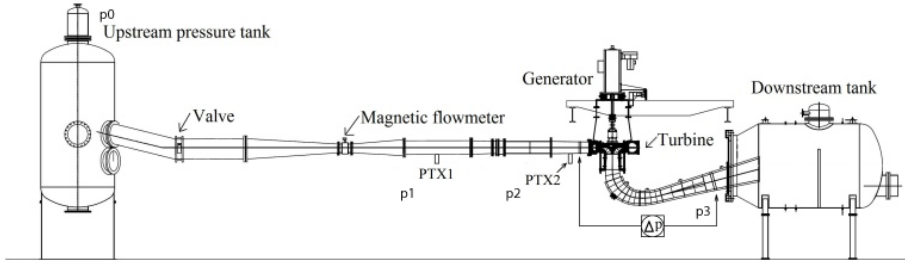
Figure 4.4: Figure showing the location of the different sensors used for measurements of pressure and flow in the Francis rig. The flowmeter is moved slightly left since the figure were made. Figure from the Francis 99 project [20]. Figure is modified with sensor names

In Equation 4.1, A is a calibration constant, c_{avg} is the average fluid velocity in the pipe and B is the magnetic flux of the device. Even though this is a simple formula, the velocity field is rarely symmetric and the magnetic field may vary across the pipe diameter such that the flowmeter should be calibrated to achieve adequate accuracy [3].

4.3.3 Pressure measurements

Pressure measurements are made using four different sensors placed in four different locations on the rig. The pressure measured at the pressure tank is the air pressure of the air cushion above the liquid surface in the tank. This pressure is important to measure as the transient pressure and behavior of the slow periodic transients are well detected in this location. The Gibson pressure sensor is located a few meters upstream of the turbine inlet. Four different pressure taps are located equally spaced around the circumference of the pressure pipe as recommended by Kjølle (2003) [3]. A minimum of four pressure taps are required and they should be placed such that no sensor is placed at the highest or lowest point of the pipe circumference [3]. Placement of the pressure taps at such locations may result in air being trapped or debree being collected. The reference line for the pressure measurement is then identical to the center-line of the pipe cross section [3]. The laboratory personnel has been responsible for the design of the pressure taps, and it is assumed that IEC 60193 standard [11] for model tests are fulfilled. The same configuration is applied for the pressure at the turbine inlet. The differential pressure between these two measurement cross sections make up the basis for the Gibson flow rate method. Normally, a differential pressure sensor would have been used, but due to the embedded system, pressure sensors at the inlet and the outlet of the turbine were necessary to obtain the effective head over the turbine. The outlet pressure is measured at a cross section near the outlet of the draft tube. The draft tube is not circular, but the principles are the same. The angles between the pressure taps
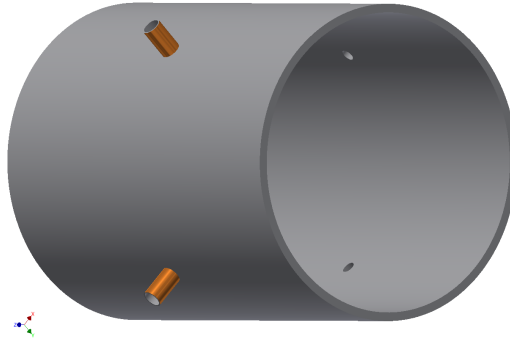
Figure 4.5: Distribution of pressure taps on a pipe segment to obtain average hydrostatic pressure.

Table 4.4: *Range and specification of pressure senors.*

Position	Sensor	Serial number	Range
Pressure tank	Druck PTX 1400	Z00227/07	0-4 bar gage
Gibson crossection	Druck PTX 1400	Z00580/02	0-2,5 bar gage
Turbine inlet	Druck PTX 1400	Y21674/07	0-10 bar gage
Turbine outlet	Druck PTX 1400	D20661/04/2011	0-10 bar gage

are changed to obtain a reference line coincidental with the center line of the draft tube cross section.

4.3.4   Guide vane angle measurements

As the guide vanes are moving continuously during the experiments, an analog measurement device was necessary. A 4-20 mA analog output measuring transducer for angle of rotation is applied. The sensor was calibrated using a rotary encoder already installed in the laboratory. This method of calibration may lead to large uncertainties, but is considered adequate. The rotary encoder has a poor resolution due to its 8 bit grey code output. This resolution is improved by the use of the 4-20 mA analogue input. The accuracy could have been increased if the runner had been disassembled from the turbine, to get an absolute reference for calibration. This was found unviable in the time horizon of the schedule of laboratory experiments. The guide vane angle were pre-set using the rotary encoder and the regular guide vane position electric motor. This angle is the stationary guide vane angle that is the starting point of the periodic movement of the guide vanes. Therefor, if the AI is offset due to calibration with encoder, the relative change is measured with only the uncertainty of the analogue device.

4.3.5 Guide Vane motor control

The guide vanes are operated using a frequency controlled electric motor. A frequency converter alters the 50 Hz grid frequency to the required frequency. The required frequency is set using a 0-10 V signal delivered by the NI-9263 Analogue output cModule (see Table 3.2). The motor is geared, such that the rotational speed output is dependent on the gear ratio and frequency of the input signal. There is a deviation from linearity in the frequency converters output from a certain input from the cModule. A simple calibration is made to obtain the correct output rotational speed from the input signal. The gear ratio is 1:28 such that 1 RPM output corresponds to 28 RMP in the motor, see Table 4.2. The frequency range of the frequency converter is selected based on the desired output. The output of 15-60 RPM yields an interval of 428-1680 RPM in the motor. The motor operates at 1370 RPM at 50 Hz input. The frequency input for any motor output speed may be found by Equation 4.2.

$$f_{motor} = \frac{50 n_{motor} R_{gear}}{1370} \tag{4.2}$$

This result in a frequency range from the converter of $15, 62 - 61, 31$ for operation between $15 - 60$ RPM output from the geared guide vane motor. When the guide vane angle rate of change is addressed, both the speed of the guide vane motor in RPM and the frequency in Hz of the guide vane cyclic movement are used to describe the magnitude of the speed.

4.4 Experiment execution

All measurements are performed the same day in the closed loop set up of the francis rig at the waterpower laboratory. The experiment methodology was checked and the test-rig were inspected the day in advance to verify the operativeness. A systematic approach, where the draft tube tank was set to a constant suction pressure and measurements were taken at different rotational speeds of the guide vane motor. Then the suction pressure were changed, and measurements for the same rotational speeds were made for a range of different suction pressures (see Table 4.6). The alteration of the draft tube tank effectively changes the turbine setting level, and thereby changes the submergence of the runner $(-H_S)$. The experiment program was created using previous visual cavitation detection tests performed under the model tests of the runner at the waterpower laboratory in 2007. Then cavitation was detected on all blades under operation at a certain point that were attempted reconstructed for these tests (see Table 4.5).

Table 4.5: *Operational point for laboratory tests.*

Operational point	Value
Head [mlc]	26,8
Flow [m^3/s]	0,33
n_{gen} [RPM]	540
n_{pump} [RPM]	740-770
n_{ED} [-]	0,19
Q_{ED} [-]	0,165

Table 4.6: *Program for measurements.*

$H_{suction}$	GV motor rotational speed				
-6,0	0	15	30	45	60
-6,5	0	15	30	45	60
-7,0	0	15	30	45	60
-7,5	0	15	30	45	60
-8,0	0	15	30	45	60
-8,5	0	15	30	45	60
-9,0	0	15	30	45	60

Chapter 5

Surveillance program

According to the information given in Chapter 3, the surveillance programs implemented in LabVIEW are usually programmed in three levels. In this thesis however, several issues with data transfer from the cRIO to the HOST computer made it unachievable to make the Host-VI to run reliably. The cRIO did manage to run the tasks of displaying some data and receiving commands from the Real-time VI and this was found to work as a temporary solution.

5.1 Project hierarchy

All elements built for the different applications are collected in LabVIEW projects. A project holds all different VIs, targets, variables, library dependencies of the project, and the specifications of the build for compiled projects. In the case of RT programming, the three different programmatic levels are contained within the project. The VIs related to a specific target at which it runs, are placed at this location in the project window. Depending on what target the VI runs on, the functionality of the VI changes. A VI designed to run at FPGA level do only allow use of FPGA approved functionality. Similarly, VIs created to run in RT targets contains more functionality designed to run at CPU based targets. The project file contains all information needed to build and execute the final application. In order to deploy and compile the VIs to a remote target, the target must be connected to the project. This is done using the NI-MAX software and an explanation to the network set up is given in Appendix D.

5.2   FPGA VI

The FPGA Main VI is the program that does the data acquisition in the desired manner. As described in section 3.1.2, the FPGA is physically reprogrammable to meet the needs of the programmer. In this thesis, four different modules are used to acquire data from different sensors. The FPGA chip must then be programmed to handle the functionality of all four modules. The number of slots in the cRIO is eight and the number of channels available (see Table 3.1) on the FPGA chip far exceeds the required number used in this project. The FPGA program is compiled into a bit-file when the desired functionality is implemented in the VI. This file is uploaded to the chip in the compilation process and cannot be done without being connected to the FPGA target.

The FPGA program is called from the RT-main VI and the properties of controls in the FPGA VI are accessible from the RT VI. Therefore, the configuration of FPGA functionality is usually left to the RT VI. This is done to make sure that the user has full control of the FPGA functionality from a CPU based target and to reduce the possibility of faulty configured tasks. The FPGA in this project is set up with a flat sequence structure to force execution in a desired manner. A Interrupt Request call is made in the first frame of the Flat sequence to hold execution of the program until the real time target VI is ready to start data acquisition. When this request is acknowledged in the real-time CPU, the FPGA program runs.

In the second frame of the flat sequence, the data acquisition loops are placed. The acquisition loops are while loop structures which executes the loop content continuously at a desired rate or as fast as possible and stops when a specified stop incident is called. This may be either user control or error messages from the code. Normally, the FPGA while loops are left unstopped as the reference to the FPGA VI will be closed upon stop-action or error messages in the RT VI. The loops read data from the connected modules and write them to the designated data buffer. Multiple channels may be read in one single loop. Every time a loop runs and executes its tasks, the number of samples is determined by the number of channels being read in the loop, or by configuration of functionality special for the cModule in use. The loop rate is decisive for the sampling rate from the channels being read in the loop.

The loops are implemented such that the writing to the FIFO memory buffer is not executed in the first loop iteration. This is mainly because the write method node may execute and write the data from the previous loop iteration simultaneously as new data is acquired. This increases loop efficiency. Another aspect is to avoid that the values of the initialization of the shift register is written to the buffer and thereby make sure that all values being written to the buffer are sampled data from the cModule channels. The concept is termed pipe-lined data acquisition.

The write to FIFO method node writes one single value to the buffer, such that the write method must be executed the same number of times as there are channels being sampled in every iteration of the while loop. The values are then put in

the FIFO buffer in the same order as they are inserted in the sample array. The data is then interleaved in the FIFO buffer in labVIEW terminology and must be decimated when the buffer is read. The size of the buffer is determined in the RT VI.

A feedback-node is implemented at the timeout of the write method node. This is to let the user know that the FIFO buffer has been full and the write method has not written data to the buffer. This is considered as data loss and should be avoided and sets some requirements with regard to the buffer size and acquisition rate. The feedback node keeps the value from the previous loop iteration and will in this way make sure that the FIFO - buffer full warning is continuously on after a timeout of the buffer.

The implemented functionality is shown in the two labVIEW block diagrams in Figures C.2 and C.3 in Appendix C. Figure 5.1 illustrates by a flowchart/block diagram how the FPGA runs its loops simultaneously after the initiation.
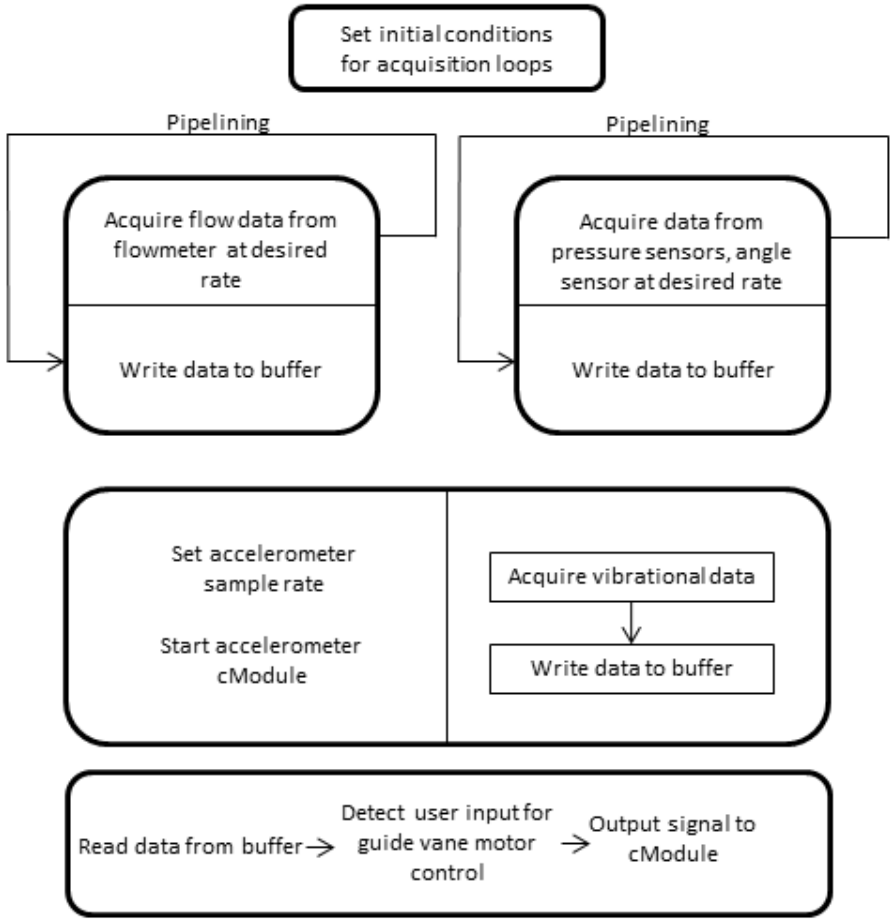
Figure 5.1: Flow chart describing the sequential structure of the FPGA VI and the concept of pipelined while loops. Each box is an individual step or loop in the VI.

5.3 Real time target VI

The real time target VI is implemented using the same methodology as the FPGA programming. However, due to its OS based operation, the function library is extended to include more complex operations and functions. Amongst other, the real-time target can handle networking and a wider range of data types and operations.

As mentioned before, the Real-Time main VI was implemented with some extra functionality to be able to operate the system without the creation of a superior Host VI. This implies that this system is not a true stand-alone embedded system. However, simple modifications and stable working network queues would allow the system to be deployed to stand-alone standard. Figure 5.2 show how the user interface were implemented. White boxes are for user input while the grey boxes are indicators which display relevant values and figures.

The first task of the real time main VI is to call the FPGA VI and run it. Then all variables in the FPGA Vi is configured and initialized. Controls are assigned to variables where user input is required. The sample rate is a typical user input to such programs while FIFO memory depth time-outs are typical constants given in the code in the block diagram. These commands are included in a single flat sequence structure to be sure that all configuration is completed before any further execution is performed. The run command sent to the FPGA VI initiates the IRQ-call. When all configurations are completed, the IRQ-call is acknowledged. This initiates the data acquisition at FPGA level.

Next, the global stop action button described in Section 5.4.3 is initialized. This button is an important and useful tool when the program and all loops should be terminated simultaneously. This initiation is placed in the first frame of a flat sequence structure. In the second frame, all data handling and processing are performed. This frame consists of seven different loops, all with a specific set of executeables. The different loops are presented in Section 5.3.1.

Finally, all FIFO buffers are stopped, queues are released and the error handles are collected from the loops and processed before the FPGA reference is closed.

5.3.1 Loop structures

There are four main different kind of loops; the producer loops, the consumer loops, the write loops and the event handler loops.

Producer and consumer loops

The producer loop read data from the assigned DMA-FIFO, decimates the data into the individual channels, convert the resulting arrays of data into waveforms with information of the time increment and the first time of the data set (t_0).

Figure 5.2: Front panel of Real-Time main VI.

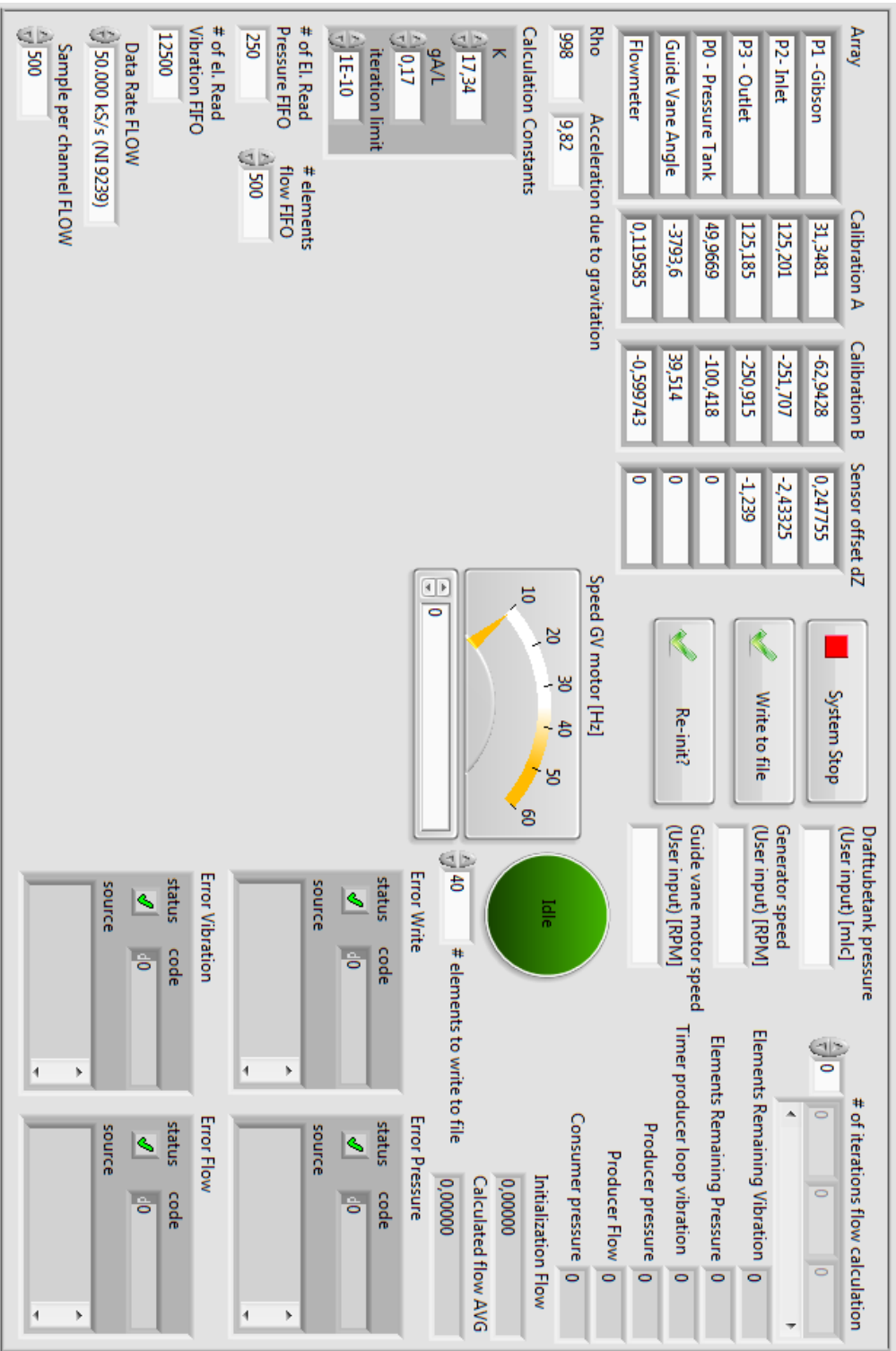An invoke method node is keeping track of the number of elements in the FIFO buffer such that the loop do not read elements from the buffer unless there is enough data to meet the requirement in number of samples per channel given by the user. The waveform is a convenient way to handle data in LabVIEW as all information is carried in one package. The channel waveforms are inserted into an array with dimension of the number of channels written to the FIFO memory. The length of each waveform is depending on the sampling rate and the total number of samples read from the FIFO. The array of waveforms is then inserted into a queue. All queues must be configured before the loops are executed the first time and necessary input to the obtain queue block is element data type, queue name and the number of pre-allocated memory blocks for the queue. If the size of the queue is inadequate, the producer loop will not be able to write new elements to the queue until elements have been read in the consumer loop, or any other loop reading the queue. This will result in a filling of the DMA-FIFO buffer and finally a loss of data. Three producer loops handle the data sent from the FPGA VI loops for acquisition of flowmeter, vibration and pressure and guide vane data.

The consumer loops contains handling and post processing of data acquired in the previous steps described in Section 5.3. The queued elements from the producer loops are dequeued here. The functionality of the consumer loops depends on what the desired output is. In this project, there are two consumer loops which handle all the acquired data. Different queues from the producer loops deliver the data in the desired format to the executables in the consumer loops.

In the consumer loop implemented for pressure, flow and guide vane angle data, two data processing sub-VIs are placed. These are described in Section 5.4. The processed data is once again queued for use in other loops, in this case the write to file loop. The derived data from the sampled data set is inserted into waveforms and finally into the output queue.

The consumer loop for vibration data is not doing any processing other than queuing data for the write to file loop. Data could be sent directly from the producer loop to the write to file loop, but for later expansion of the code and for implementation of real time post processing of vibrational data, the producer/consumer loop structure is maintained.

In the development process, the loop execution time per iteration is an interesting parameter to observe whether the loop is able to run stable and execute all its content within the limited time or not. This is implemented using a millisecond count and a feedback node in the time critical loops for surveillance.

Writer loop and event handler loop

The content of different loops may be controlled by an event handler loop. Upon user input, the event handler queues the information and send it to the receiver loop. In this case, the event handler of the writer loop initiate the writing process by queuing the case *Create File* to the writer loop upon user input. This is detected

by the writer loop which execute the *Create File* command and queues the *Write to File* command. This is in turn read in the next loop iteration and the loop writes until the specific requirement of written samples are met. Finally, the *Close File* event is queued and the file is closed in the next iteration. The writer loop writes data to TDMS-files and the use of waveforms speeds up the process as larger sets of data may be written at the same time. The different channels must be named and the channels are divided into categories such that post processing of data is simpler and that the data presentation is well-structured. The TDMS-files are read by DIAdem or excel or may be converted and imported to Matlab.

Guide vane motor frequency control

The guide vane motor is, as discussed in Chapter 4.2, controlled by a frequency converter which in turn are controlled by a $0 - 10\ V$ signal output from the NI9263 cModule (see Table 3.2). The module is controlled from the RT-VI by user input. The user declares the required rotational speed of the guide vane motor and the VI converts this value to the required voltage output by interpolation. The interpolant is then sent to the FPGA by a property read/write control as the update time requirement is not high. The FPGA then direct the output to the correct channel. This is not requiring lots of resources, such that this procedure is placed in the producer loop for vibrational data.
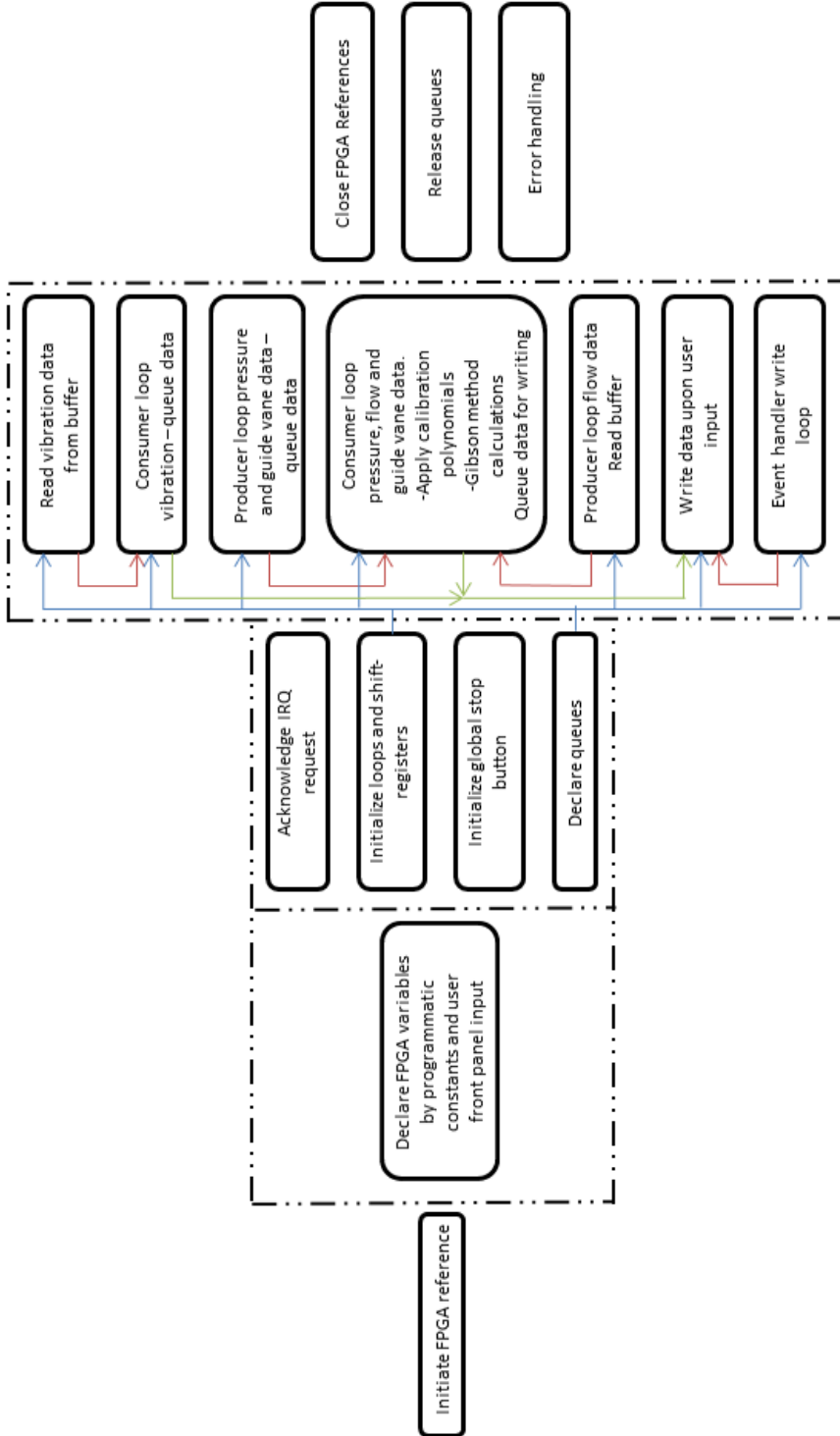
Figure 5.3: Flowchart for real time program execution.

5.4   SUB-VIs

The sub-VIs implemented for use in this program are essential. Together they make up the real time and post processing analysis of the acquired data. Sub-VIs are implemented where a specific procedure with standard input and output is applied such that the method may be used again without implementing it once more.

5.4.1   Calibration and signal scaling

In the consumer loop for pressure, flow and guide vane angle data, the sub-VI Signal Scaling and Correction is placed. This VI applies the calibration polynomials to the acquired signals. The VI behaves differently for the different types of signals. The calibration polynomials require that the signal is in volts due to the equipment used for calibration in the laboratory, while pressure sensors deliver a current signal. The 4-20 mA channels are converted to a voltage signal using a internal resistor. The cModule used for data acquisition in this project do not do any signal processing in the hardware. This is corrected for using Ohm's Law 5.1 The 4-20 mA signal is converted to the required 2-10 Volt signal by multiplication with a 500 Ohm resistor. When all signals are in the required format, the polynomial constants are applied. The polynomial is on the form $Y = AX + B$ where Y is the output in the desired units and A and B are constants from the calibration process. The pressure calibration is made to obtain the output in kPa. This need to be scaled in order to yield the desired output in meters of liquid column, and is handled in the proper case. The signals from the guide vane angle measurements and the flowmeter is in the correct units after application of the calibration polynomial and require no further scaling.
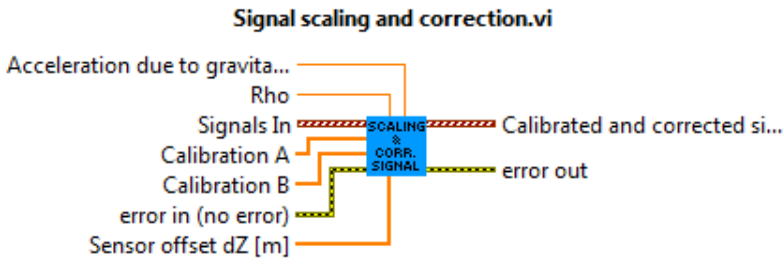
Figure 5.4: Sub-VI block diagram icon with explanation of nodes.

$$U = RI \tag{5.1}$$

5.4.2 Gibsons method in Real time analysis

The modified Gibsons method is implemented according to the discussion in Section 2.4. The logic of the method is displayed in Figure 5.5. The dashlined box represent the initiation of the method and one second of flow and head loss data are sampled and averaged to obtain the k-value in Equation A.7. Then the rest of the procedure is repeated for all values of sampled pressure data. The iteration process is repeated until the implicit equation (eq. 2.10) is valid. The LabVIEW environment is suitable for such processes were iterations are performed and there is a high requirement for reliability. Figure 5.6 illustrates the VI icon with input and output nodes.
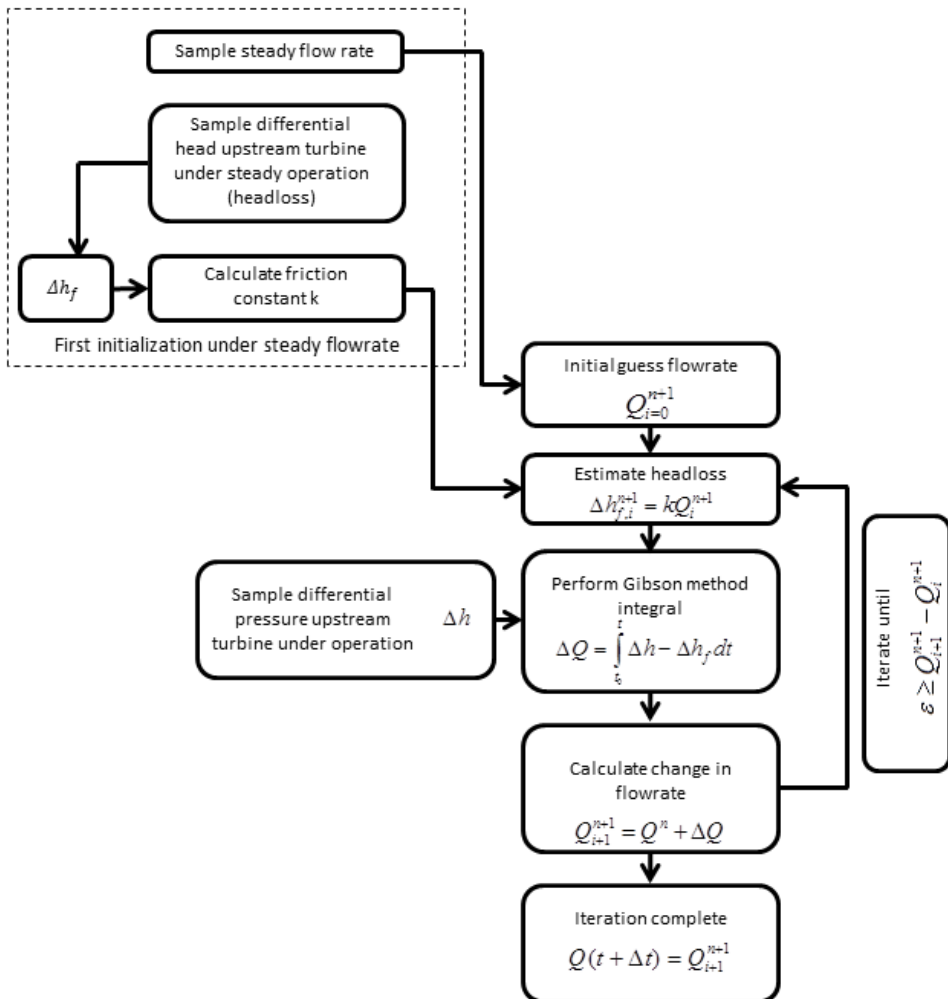
Figure 5.5: Logic of gibsons method in real time.
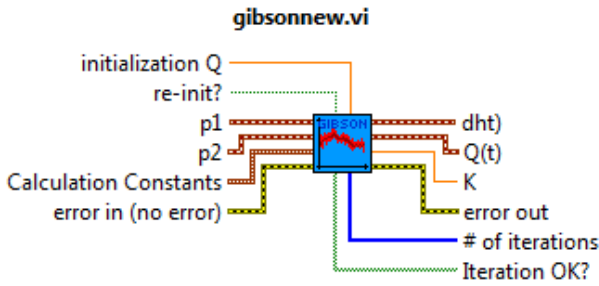
Figure 5.6: Sub-VI block digram icon with node designation.

5.4.3   Global stop action

It is a challenge in parallel loop structured VIs that the loops are not stopped simultaneously upon errors or stop commands, as data may not be passed from one running loop to another. Therefore a Global stop action sub-VI was constructed to receive stop commands from user input or upon error statements. The Sub-VI utilizes that uninitialized shift registers stores the last value sent to the shift register, and makes the value accessible in the next loop iteration. All VIs are executed in an non-re-entrant manner by default. This means that when the sub-VI are called from several different locations in the main VI, the sub-VI are executed one at the time and the data from the previous executions are passed on to the next execution of the sub-VI. Then, if user input or error handling throws a *set to true* statement in the first execution of the sub-VI, the remaining sub-VIs will access the value sent to the shift register in the order they are called. The sub-VI is initialized before all loops start to execute and the output is false by default. The block diagram of the sub-VI is included as Figure C.7 in Appendix C. The *Set* command is given to the sub-VI in one of the consumer loops as this is adequate to stop all loops in this application. The sub-VI could be placed in a dedicated loop, to better control the update time of the stop-action.
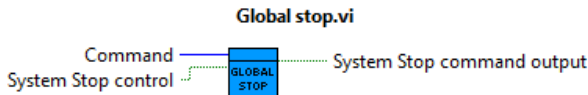
Figure 5.7: Sub-VI block diagram icon with node designation.

5.4.4   Post processing of acquired data

The acquired data is used to calculate further derived quantities. The net head, H_e, the available and required suction head, $NPSH_A$ and $NPSH_R$ and the Thoma

cavitation number σ_{pl}, are important variables to investigate the pressure conditions in the runner. In addition, the factors of speed and flow, n_{ED} and Q_{ED}, determines the operational point of the turbine. All these variables were investigated in the project thesis by Ruud (2013) [22] and it may be useful to compare the measured data from the experiments in this thesis qualitatively to those from simulations performed in the thesis by Ruud.

Sub-VIs are established for calculation of these derived quantities. Then the Sub-VIs may be used again where these calculations are to be performed. In this thesis, these calculations are not done in real-time, because it was found convenient to do the processing afterwards to maintain control of the calculations. The sub-VIs may easily be implemented into the consumer loops of the real-time main VI to do Real-Time analysis of the data. In an embedded system, this kind of post processing may be used to initiate different processes such at writing to file or other post processing of data. The systems then become more like a surveillance system than demonstrated in this thesis where user interaction and supervision was important.
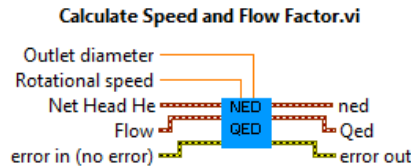
Figure 5.8: Block diagram icon for speed and flow factor calculations sub-VI with input and output nodes specified.
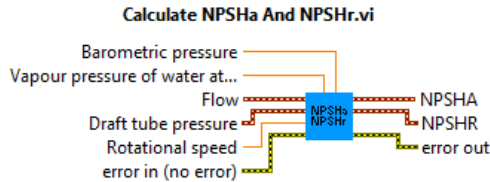
Figure 5.9: Block diagram icon for net pressure suction head calculations sub-VI with input and output nodes specified.
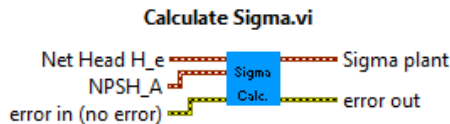
Figure 5.10: Block diagram icon for Thoma cavitation number calculations sub-VI with input and output nodes specified.

Chapter 6

Results

The results obtained during the performed experiments are presented in this chapter. The goal is to highlight the hydraulic transients in the hydropower system and how they influence the pressure conditions in the conduit system and the inception of cavitation. Another main part is the functionality of the surveillance program created for performing continuous measurements in an embedded system.

6.1 Savitzky-Golay filtering of data

The Savitzky-Golay filter in the LabVIEW software smooths the noisy data according to the discussion in Section 2.6.2. Figure 6.1 illustrates the effect of the filter to the unfiltered raw data from the measurements.
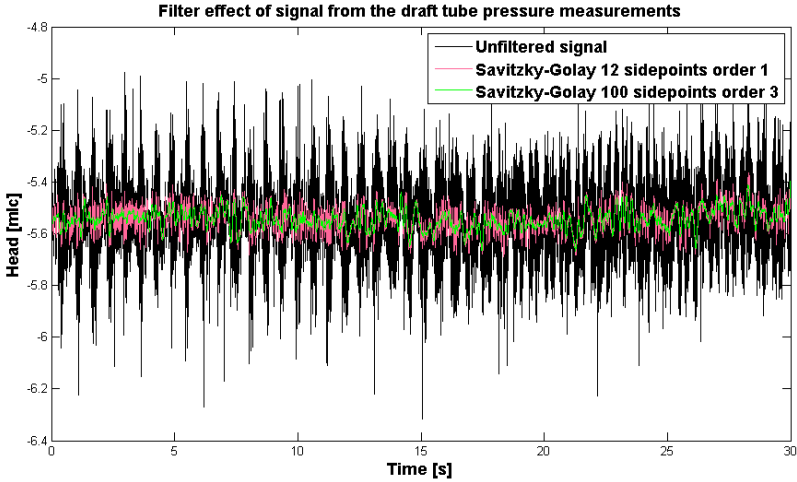
Figure 6.1: A comparison of the different signals before and after applying the Savitzky-Golay filtering method. Different input parameters are applied.

6.2   Stationary operation

The experiments performed under steady operation investigate the effect of submergence of the runner. The effect of lowering the pressure in the draft tube tank is qualitatively the same as reducing the tail water surface level. In this section the influence of reduced draft tube pressure will be presented.

6.2.1   Head and Flow

The net head over the turbine are presented in Figure 6.2. It is evident that at $-7,0$ mlc pressure in the draft tube tank, the head were not stationary and a transient were present in the system. Therefore, $-7,5$ mlc are included and used where stationary effects are important. Figure 6.3 show flow rate measurements and results from the Gibson method calculations. Notice how the flowrate changes more for the case where the draft tube tank pressure are $-7,0$ mlc. Notice also the offset of the calculated data series from the measured data series.
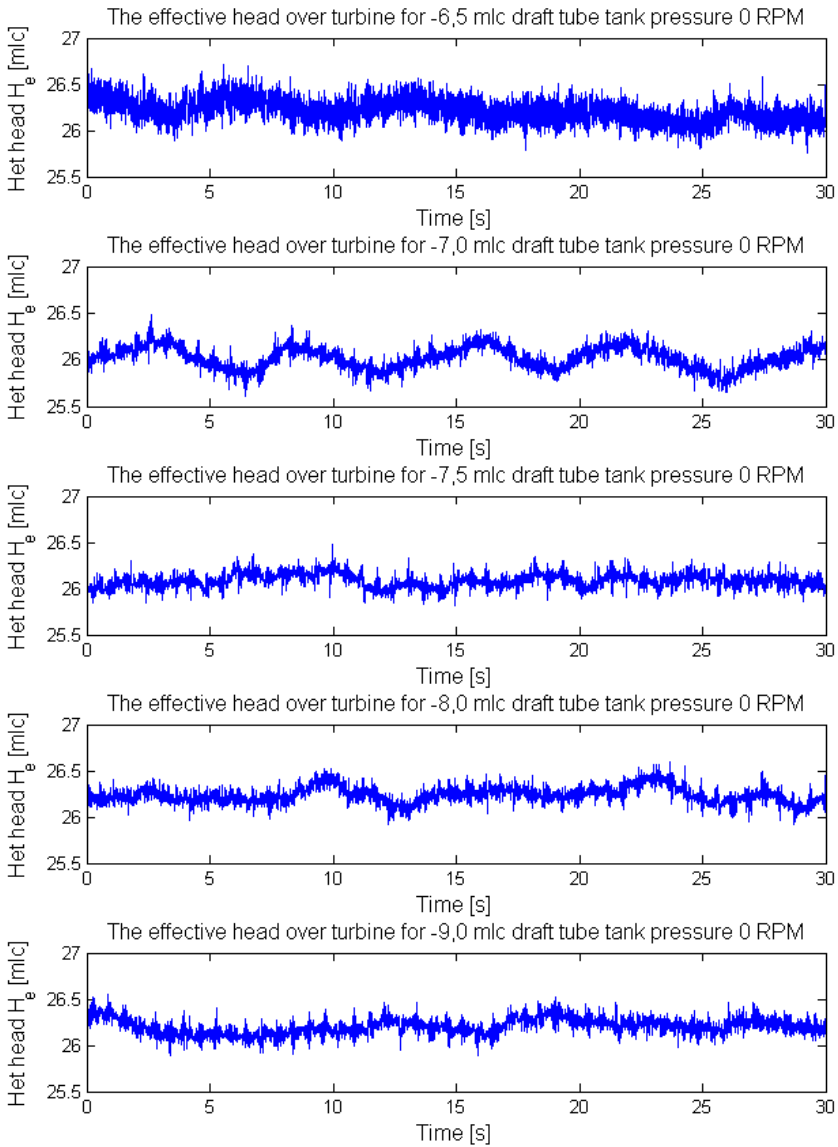
Figure 6.2: Figure presenting the net head H_e for steady turbine operation for a range of different submergence settings ($\Delta\alpha = 0$).
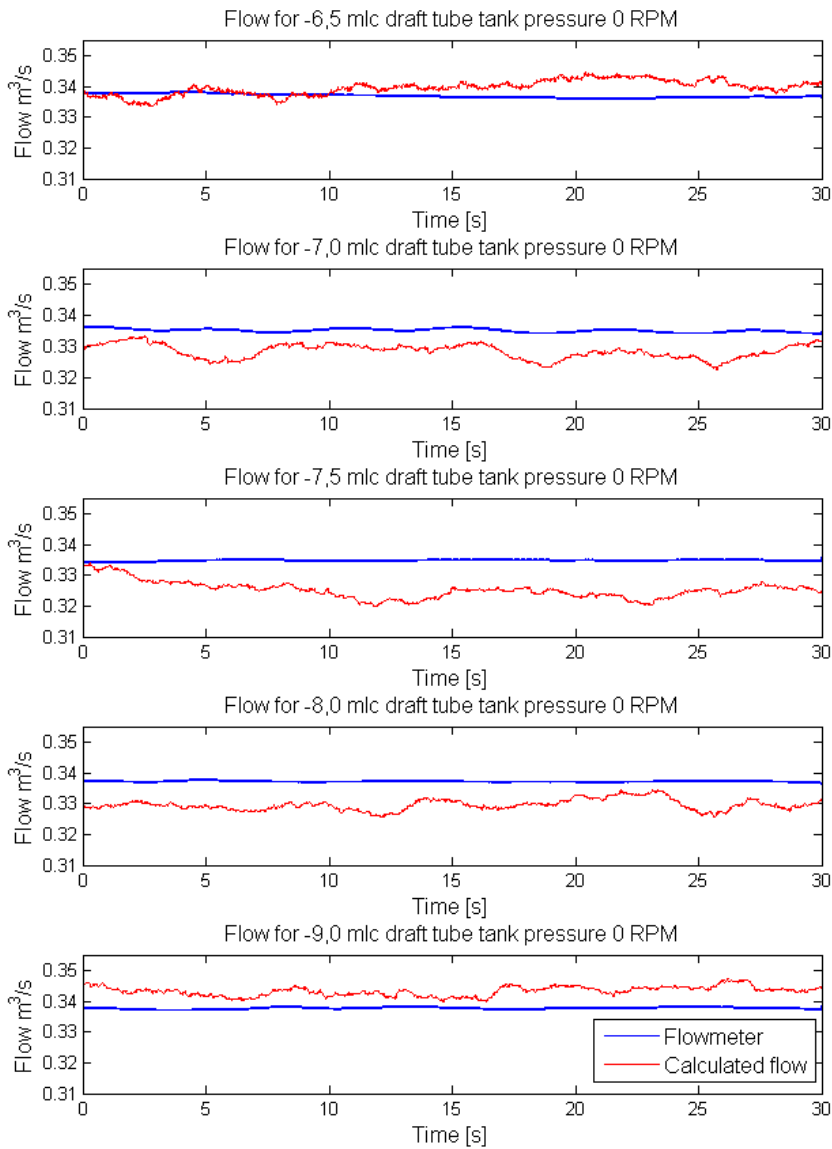
Figure 6.3: Comparison of the flowrate measured by the flowmeter in the francis rig and the calculated flowrate using Gibsons pressure-time method.

Table 6.1: *The relative deviation of calculated flow using Gibsons method to the flowrate measured by the flowmeter. (Averaged values for whole data series). The table displays data for both cyclic movement of guide vanes and stationary operation.*

| | Flow deviation [%] | | | | |
| | Guidevane RPM | | | | |
Pressure	0	60	45	30	15
-6,0	-2,891	0,911	-2,147	-1,517	-3,081
-6,5	-0,781	2,299	-2,045	0,505	2,485
-7,0	2,005	-0,549	-0,853	-5,960	1,281
-7,5	2,860	-0,710	-1,473	-0,179	-1,348
-8,0	2,274	-1,134	-2,955	-3,131	-4,753
-8,5	3,108	-6,302	-0,795	-0,997	-3,681
-9,0	-1,619	-3,051	-0,971	-1,373	0,139

Table 6.1 lists the deviation in percent of the average calculated flowrate and the measured flow rate.

Figure 6.4 demonstrate how the turbine operational point was taken from the best efficiency point towards full load operation conditions. The guide vane angle were increased in two increments from $\alpha = 10$ degrees via $\alpha = 10.5$ to $\alpha = 11$ degrees. Note that even when the guide vanes are kept at a constant opening degree, the operational points are not completely constant. n_{ED} and Q_{ED} are calculated from the acquired and calculated data. The curves (dots) are parametric with time as the parameter.
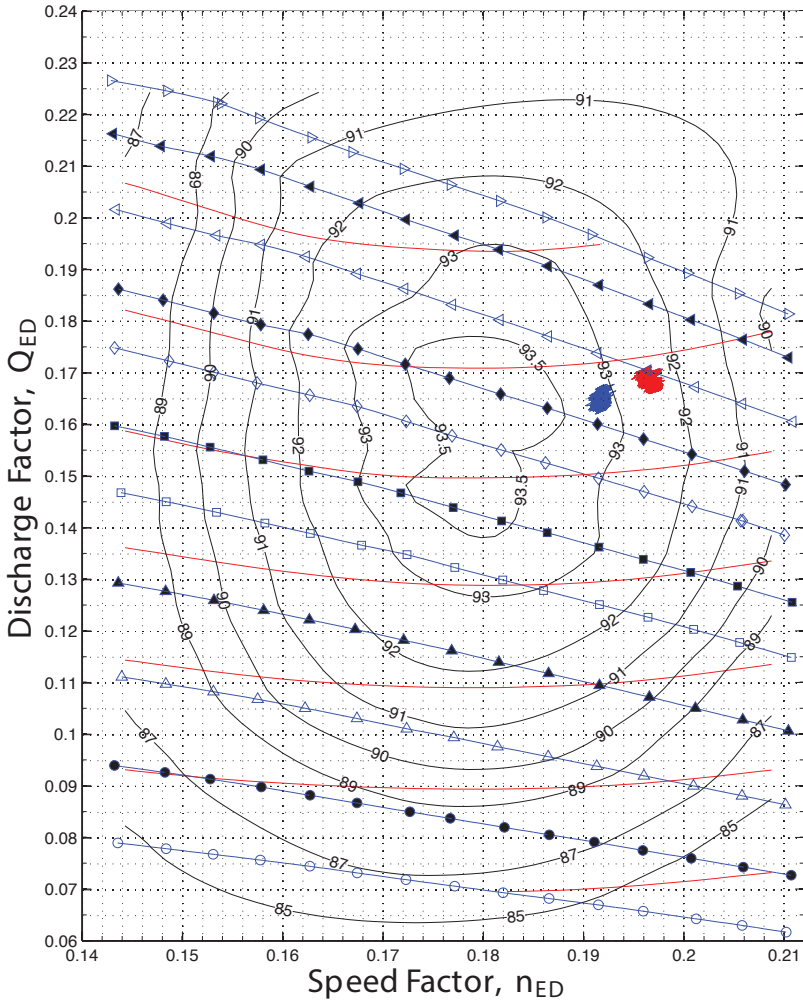
Figure 6.4: Hill diagram trace for steady operation at $-6, 0$ (blue) and (-9,0) mlc draft tube tank pressure.

6.2.2 Influence to the global cavitation parameters in steady state operation

The net positive suction head and the cavitation number are of great importance to investigate the influence from the different external input. In this section, the draft tube pressure is the only external varied parameter, and Figure 6.5 show how the cavitation number are lowered as the draft tube pressure are lowered. The selected data series display steady behavior, except for some slow low amplitude transients originating from slow pressure transients in the closed loop configuration. Notice how the decrements in draft tube pressure are not equidistant, and that the cavitation number are changed accordingly.
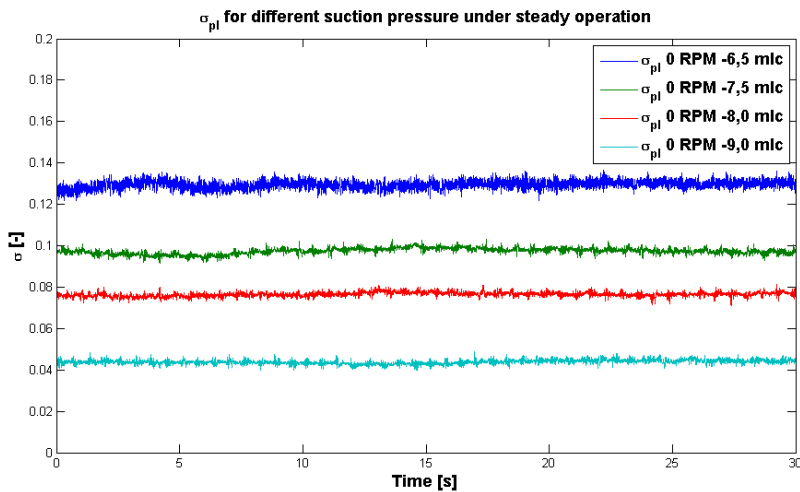
Figure 6.5: Plot of the thoma cavitation number for different turbine submergence settings for steady operation ($\Delta \alpha = 0$).

Figure 6.6 display the same influence to the net positive suction head. The available suction head are reduced while the required suction head is not affected as much and only slightly increased as the flowrate is increased. Notice how the available suction head are not lower than the required suction head at any of the turbine settings. The draft tube tank surface pressure could not be lowered further than $-9,0$ mlc.
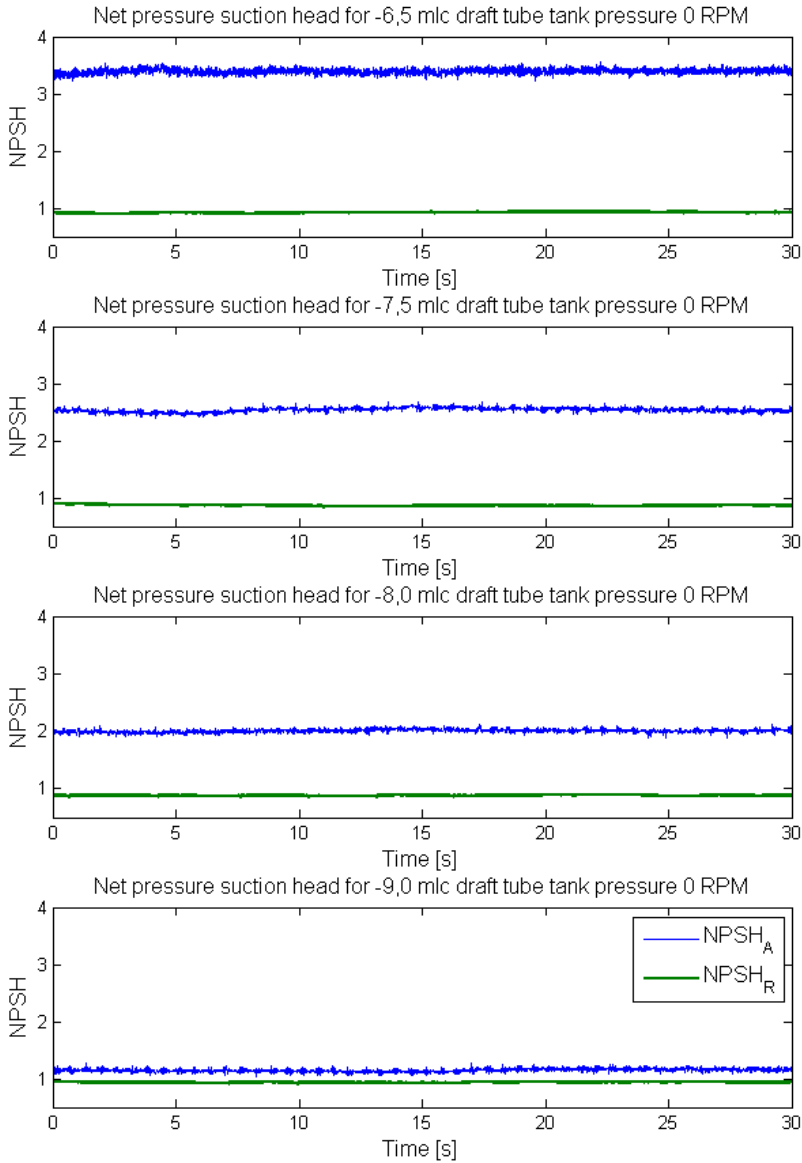
Figure 6.6: A comparison of $NPSH_A$ and $NPSH_R$ for different turbine submergence settings for steady operation ($\Delta\alpha = 0$).

6.2.3 Vibration measurements and analysis for steady operation

Vibrational data are collected for all operational settings. The frequency analysis of these data are presented in this section. The acquired signal is not calibrated. The data is only used for frequency analysis and not for amplitudes such that raw data are found sufficient. Some of the graphs are obtained from the LabVIEW analysis program. The waterfall plots are difficult to configure and are therefore without legends and third axis (applicate) label.

There are a few known frequencies that may be calculated in a Francis turbine. These are the blade passing frequency, the runner frequency and the guide vane passing frequency.

Table 6.2: *Known frequencies in francis turbine for operation at* 540 RPM.

Frequency origin	value [Hz]
Runner frequency	9
Guide vane passing frequency	252
Blade passing frequency	270
Three phase rectifier for generator	300

A representative interval of the frequency analysis from guide vane arm is presented in Figure 6.7. The known frequencies are all present in the plot along with several others. The amplitude of the guide vane passing frequency and the runner frequency are relatively low.
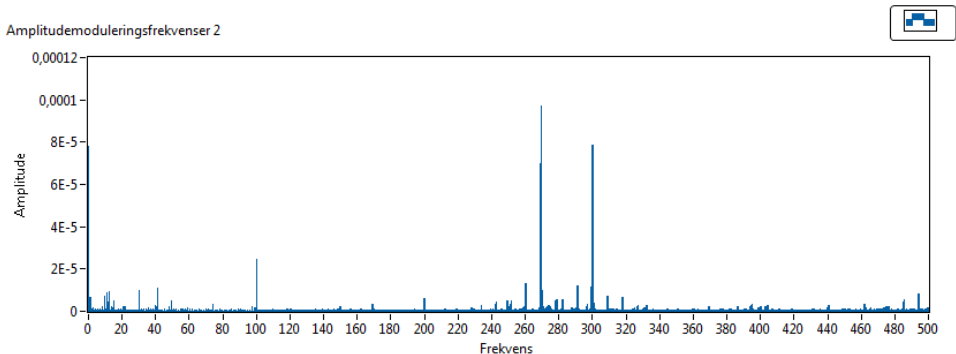
Figure 6.7: frequency-amplitude plot for the low frequency spectrum at 0 RPM and $-6, 0$ mlc.

Data from the accelerometer mounted at the friction torque bearing were also analyzed. There were a noticeable increase in amplitudes in the interval between $0-1000$ Hz when the draft tube tank pressure were decreased. This is an indication that there are more pressure induced vibration at low draft tube pressures.
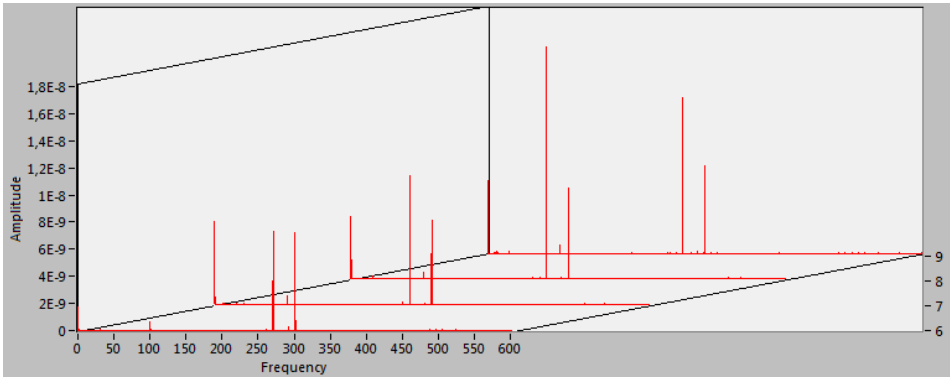
Figure 6.8: A waterfall plot of the frequency spectrum at the different draft tube tank pressures for stationary guide vanes. The draft tube pressure is indicated at the right labeled axis. Data from guide vane arm accelerometer.
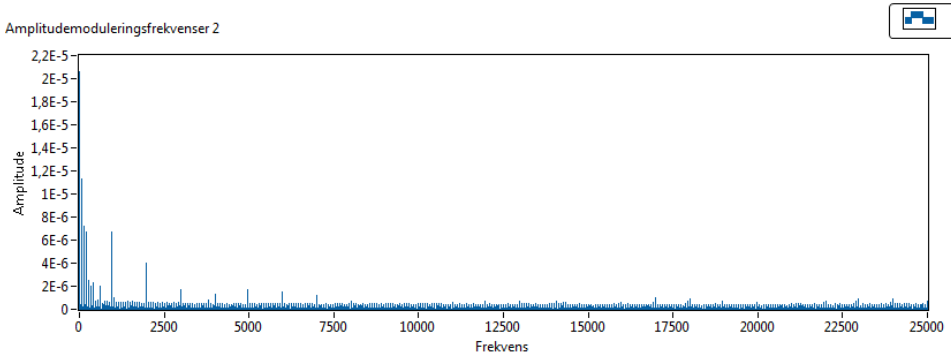
Figure 6.9: Frequency spectrum of stationary guide vanes with the turbine out of operation and emptied for water.

There are no frequencies the higher spectrum in the data series from the stationary guide vane operation and the amplitudes are zero from approximately 600 Hz and above.

An investigation was performed in conditions where the runner was inoperated, while the guide vane speed were changed between $0 - 60$ RPM. The stationary case of 0 RPM are displayed in the spectrum below. The turbine was completely emptied for water during these experiments to exclude the hydraulic effects.

6.3 Cyclic variation in guide vane angle setting

When the guide vanes are operated in a cyclic manner, the operational point of the turbine is changed correspondingly. These results are the main focus of this thesis, as the cyclic guide vane operation introduces transients into the system. The transients are measured by means of the pressure and the flow at different locations in the Francis rig, according to the presentation in Chapter 4. The guide vane movement is also recorded to verify that the external input to the system is as expected.

6.3.1 Guide vane angle measurements

The guide vane angle movement is presented in Figure 6.10. The first line is the unfiltered signal from the angular measurement sensor and the second is a calculated non-parametrical spline that is calculated using the DIAdem (Section 3.2) software from National Instruments. The method using splines is described in Section 2.6.3. Table 6.3 lists the input and output data from guide vane control and measurements.

Table 6.3: *Difference in measured and expected guide vane angle for operation at different guide vane motor speeds.*

RPM	GV motor period time[s]	$T = \Delta t$ [s]	f_{meas} [Hz]	f_{input} [Hz]	Deviation [%]
0	0	0	0	0	0
15	4,0	3,870	0,258	0,25	3,4
30	2,0	1,936	0,517	0,5	3,3
45	1,33	1,280	0,781	0,75	4,2
60	1,0	0,940	1,064	1	6,4

6.3.2 Head and flow

Figure 6.11 displays how the effective head is influenced by the regular guide vane movement. The courses are qualitatively equal for all different turbine level settings. Therefore, only the case of $-7,0$ mlc are included here. Note how the influence to the net head is more distinct for faster guide vane movement. Also note that the average head is approximately constant for all variation, which also applies to all other periodic data and turbine level settings.

In Figures 6.13 and 6.14 the pressure in the air cushion in the pressure tank is displayed. Notice that in Figure 6.13, the pressure seem to vary periodically for the case where the guide vane motor is set to zero RPM. The corresponding guide vane angle is displayed in the uppermost plot of Figure 6.10.
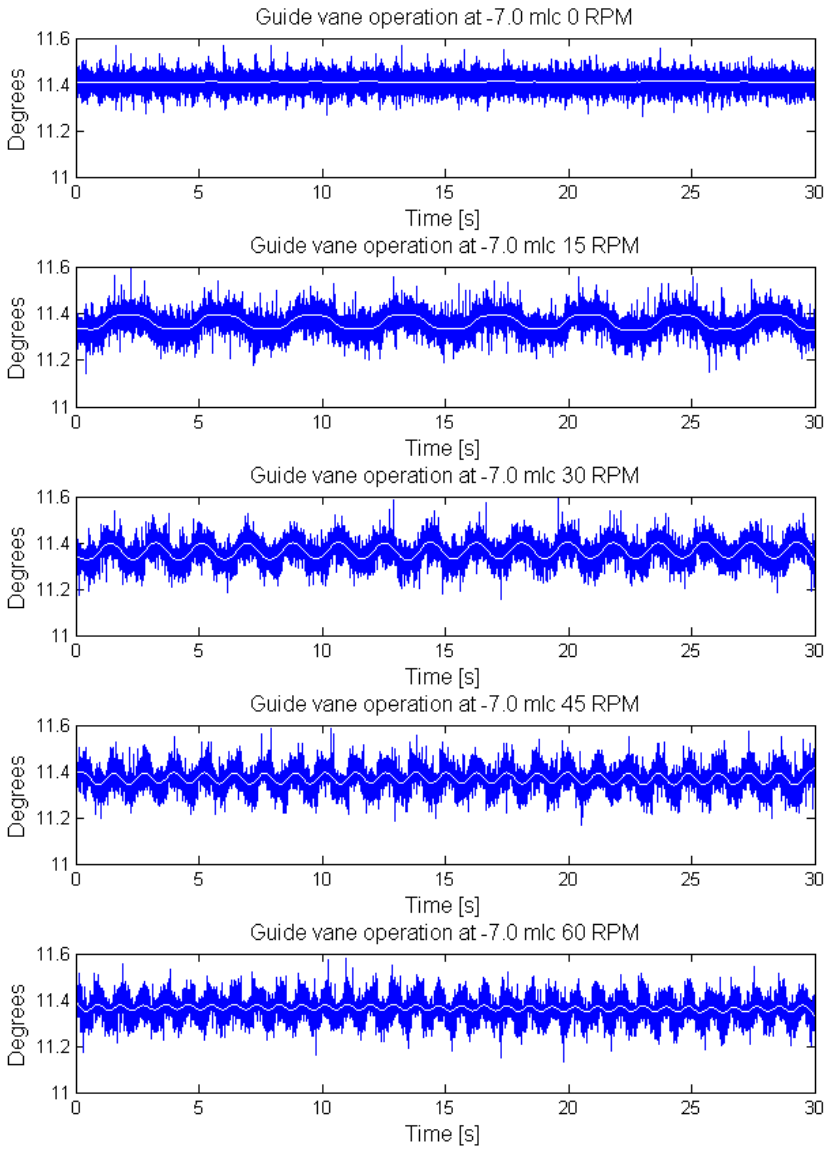
Figure 6.10: Guide vane variation at different speeds of rotation on guide vane motor. The white line in the figure represents the non-parametric splines calculated for the noisy signal.
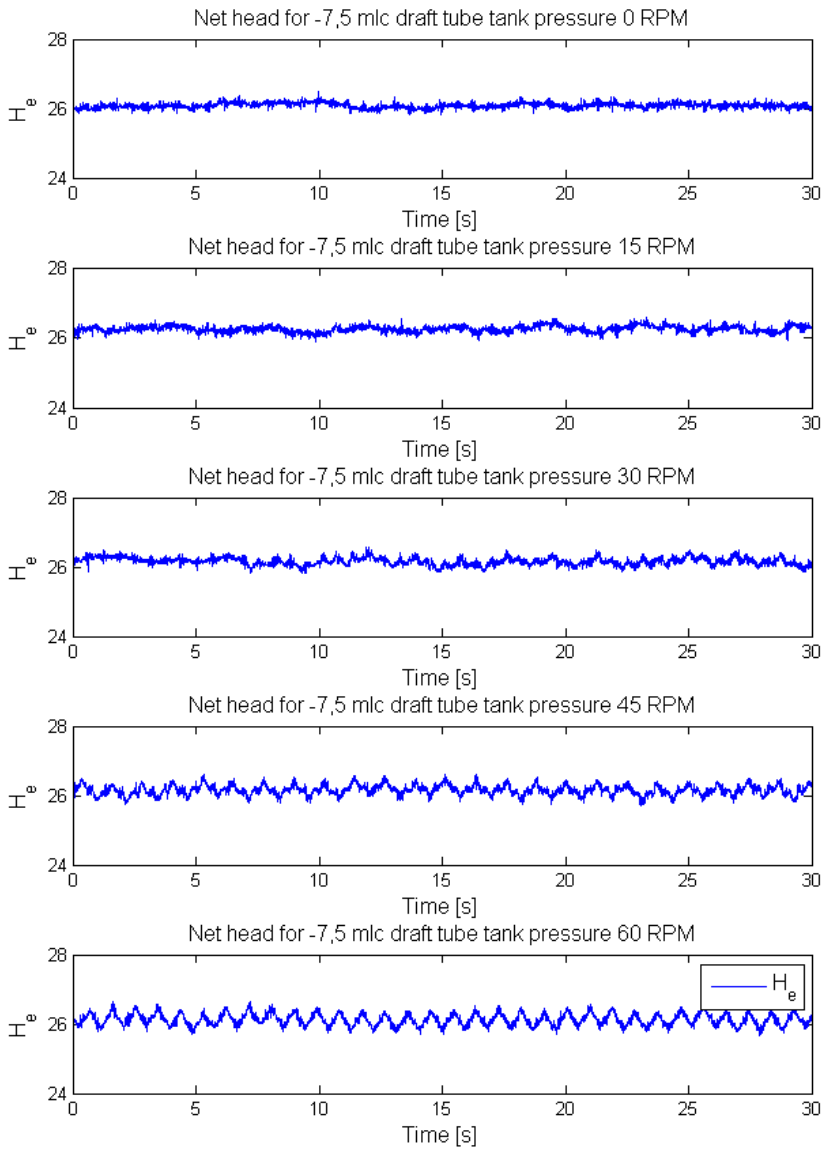
Figure 6.11: Graphs showing the influence of guide vane variation to the effective head.

Some simple calculations were made assuming that the pump may be seen as the source of pressure head equivalent to the geodetic head of a reservoir to find the "traditional" U-tube surge frequency. The equations of Section 2.1 were applied.

Table 6.4: *Calculation of theoretical surge frequency in closed loop operation.*

Property	Value	Unit
Tunnel length L_t	$19,068$	$[m]$
Initial Air volume V_0	$1,4632$	$[m^3]$
Surge chamber area $A_{chamber}$	$3,80$	$[m^2]$
Tunnel area A_t	$0,073$	$[m^2]$
Initial chamber pressure h_0	$18,5$	$[mlc]$
Equivalent chamber area A_s	$0,05567$	$[m^2]$
Surge frequency ω_s	$0,819$	$[s^{-1}]$
Period time T_s	$1,22$	$[s]$

The surge frequency presented in Table 6.4 is remarkable as it is far off the value that represent the physical system. A frequency analysis of the pressure data from the pressure tank (the surge chamber) show that the natural frequency lies close to $0,135$ Hz.

Further, note that in Figures 6.13 and 6.14, the head in the pressure tank is lower for decreasing draft tube tank pressure. This is as expected due to the fact that the net head is kept constant by adjusting the pump delivered head as the downstream pressure is lowered.

Tables 6.5 and 6.6 compares the surge frequency conditions at different operational speeds. The frequencies are obtained by finding the period time of the signal in DIAdem (see Section 3.2) for a range of periods and then averaged. It was a difficult task to separate the noise from the signal and different methods such as the non-parametrical splines and the Savitzky-Golay filter were applied and compared to extract the best approximation of the period time from the signals. The frequencies were very little distinct for all but the case shown in Figure 6.12.
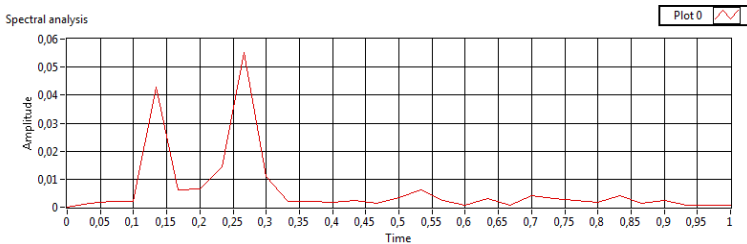
Figure 6.12: Simple plot of the frequency analysis of the pressure signal for the pressure tank at 15 RPM and $-7,0$ mlc draft tube tank pressure.

Note that the surge frequency in the last column deviates only slightly from the
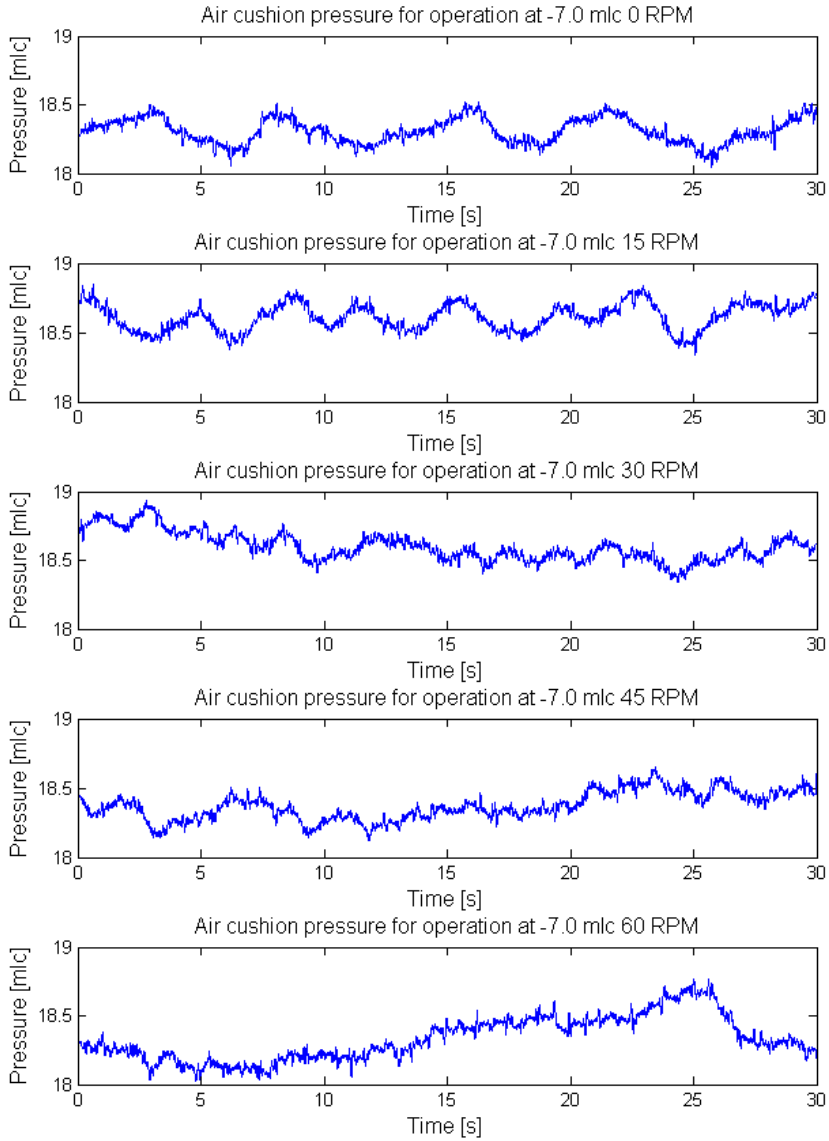
Figure 6.13: Figure displaying the pressure in the pressure in the pressure tank for the different guide vane operation settings.

imposed frequency by the guide vanes given in Table 6.3. Additionally, if the measured frequency of the guide vanes and the surges are compared in Table 6.3 and Table 6.5, it is evident that the frequency of the surges are less than the imposed frequency of the guide vanes. This indicates that the imposed frequency is not equal to the natural frequency and that the losses and inertia of water are influencing the frequency of the surges.

Table 6.5: *Approximated frequencies and period times for surges in the pressure tank in the francis rig. Operation at suction pressure of $-7,0$ mlc and different guide vane motor speeds.*

GV motor [RPM]	GV motor freq. [Hz]	Surge period [s]	Surge freq. [Hz]
0	0	4,85	0,216
15	0,25	3,94	0,254
30	0,5	2,13	0,4695
45	0,75	1,21	0,826
60	1	1,21	0,826

Table 6.6: *Approximated frequencies and period times for surges in the pressure tank in the francis rig. Operation at suction pressure of -9,0 mlc and different guide vane motor speeds.*

GV motor [RPM]	GV motor freq. [Hz]	Surge period [s]	Surge freq. [Hz]
0	0	0	0
15	0,25	4,14	0,244
30	0,5	2,12	0,472
45	0,75	1,21	0,826
60	1	0,91	1,099

Figures 6.15 and 6.16 present how the Gibson method flowrate was estimated compared to the flow rate from the flowmeter. Figure 6.15 represent the data series where the deviation between the calculated and measured flowrate are small. Figure 6.16 demonstrate the opposite scenario where the calculated flowrate poorly represent the measured flowrate. The causes and implications of this will be discussed further in Chapter 7. Notice how the amplitude of the periodic operation is large in the calculated series while the flowmeter yield small flowrate variation. An estimate of the periodicity of the calculated flowrate is in the range of the actual frequency of the guide vanes presented in Table 6.3.

Figure 6.17 show how the the operational point of the turbine wanders in the hill diagram as the guide vane angle alternates. Q_{ED} varies considerably more for the settings displayed in Figure 6.17 than the steady operation in Figure 6.4. The wandering is more stretched out vertically, which corresponds to the increased
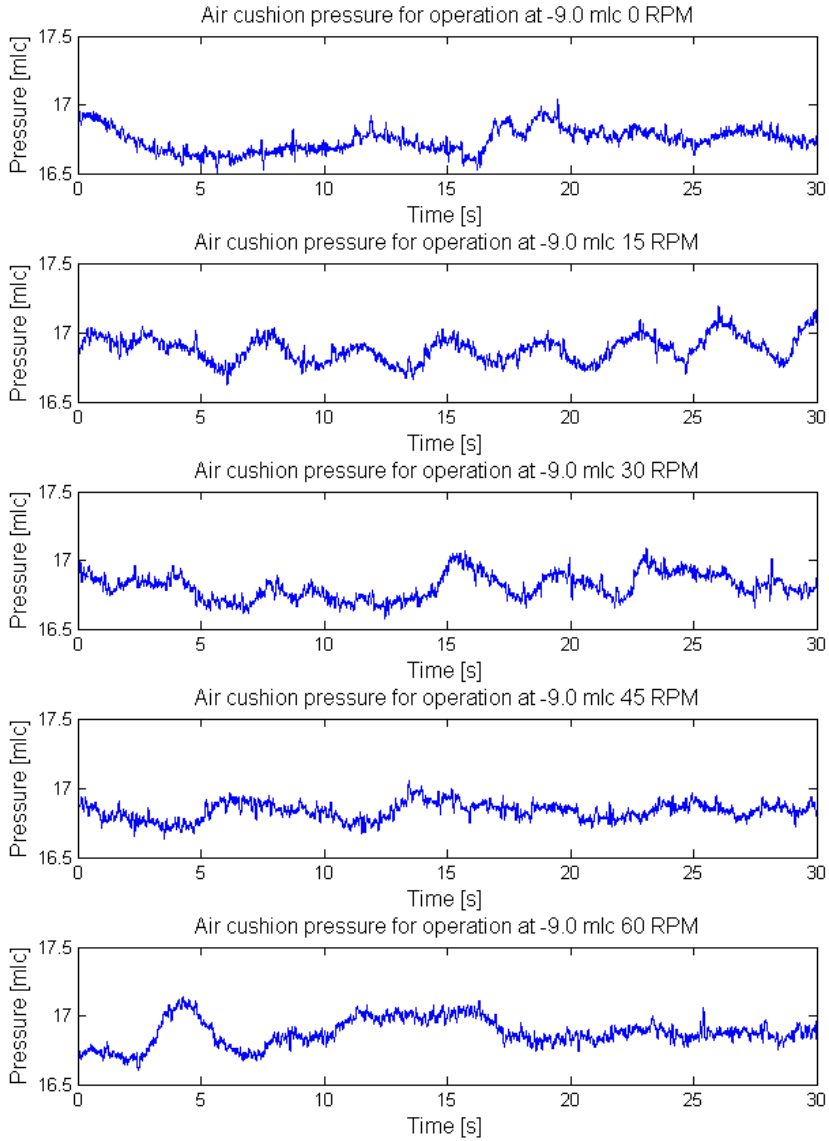
Figure 6.14: Figure displaying the pressure in the pressure tank for the different guide vane operation settings. (the signal is filtered using the Savitzky-Golay filter).
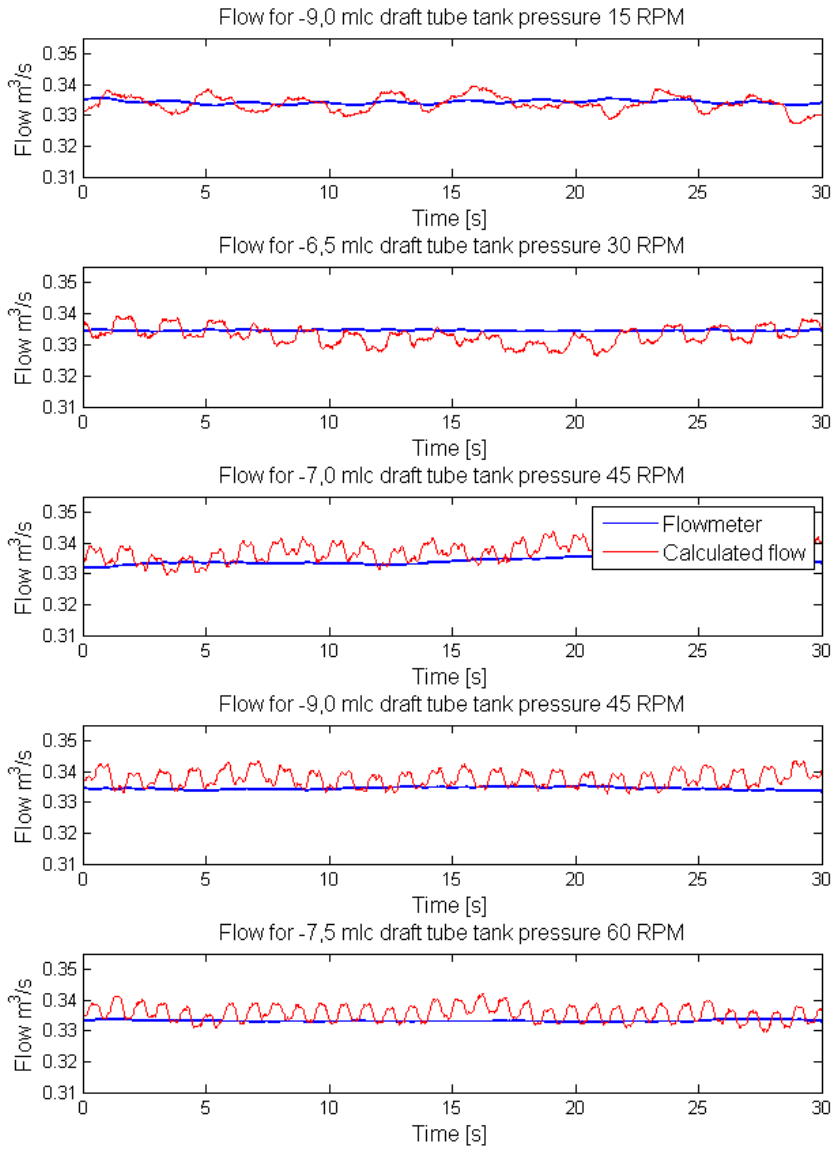
Figure 6.15: Stack of plot showing the comparison between the measured and Gibson method calculated flowrate for different RPM guide vane periodic operation. Set of good quality data series.
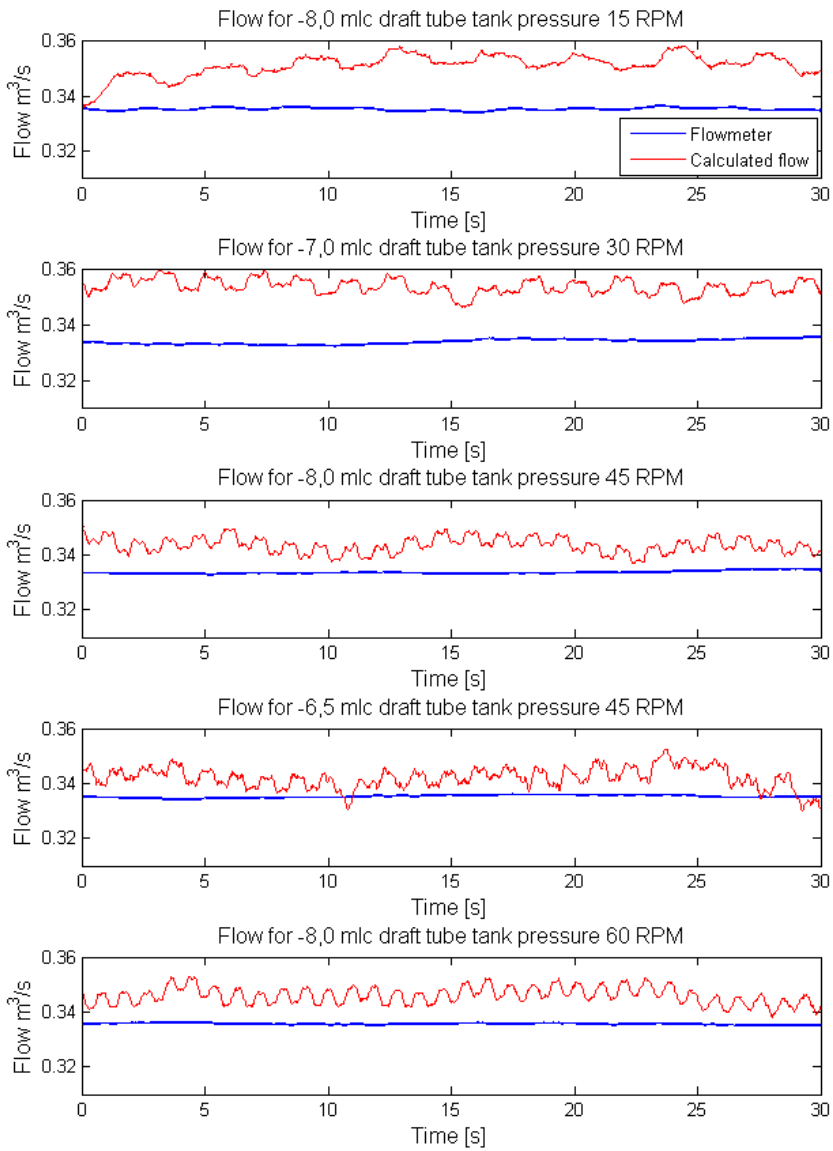
Figure 6.16: Stack of plot showing the comparison between the measured and Gibson method calculated flowrate for different guide vane periodic operation. Set of poorly estimated flowrate.
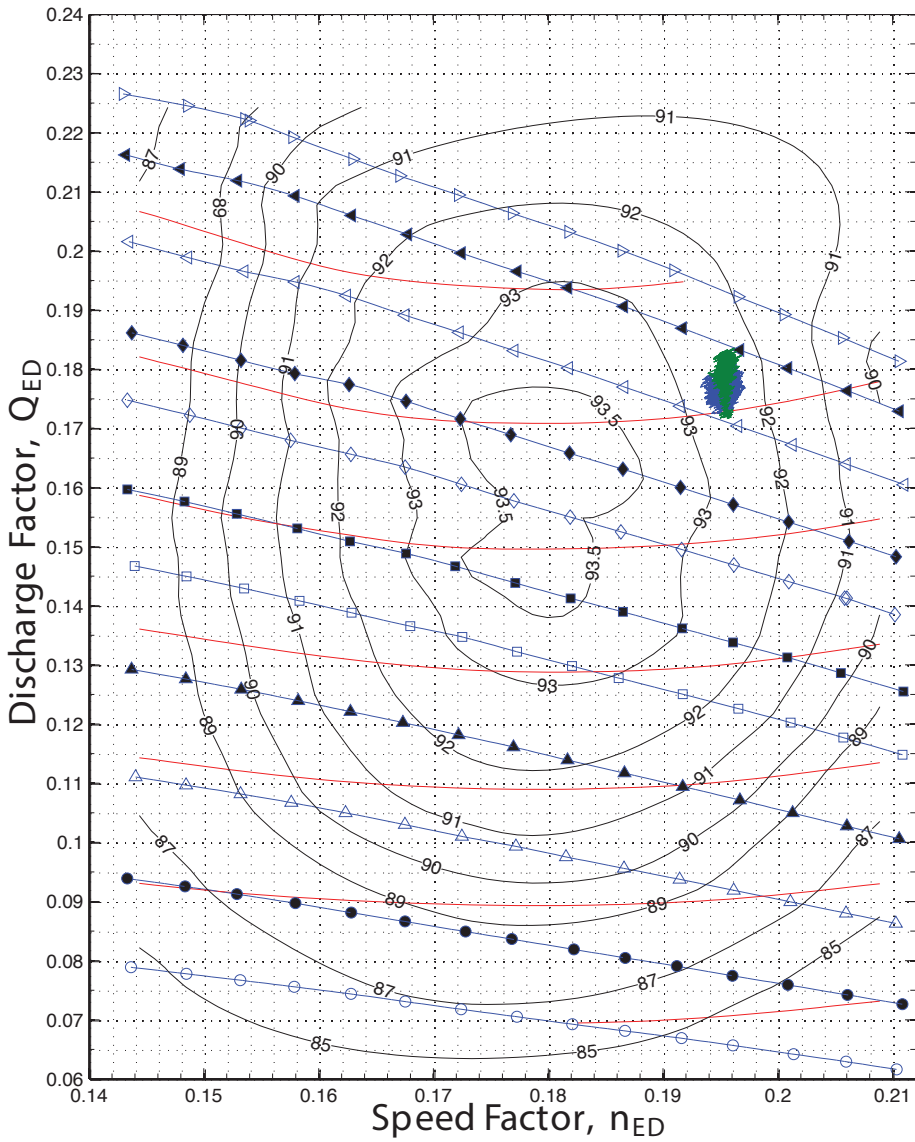
Figure 6.17: Hill diagram wandering trace for cyclic guide vane movement. The blue graph is for 15 RPM and $-8,0$ mlc in the draft tube tank. The green is 60 RPM and $-9,0$ mlc. The initial minimum angle is at 11 degrees.

guide vane angle and thereby increased flow rate. Notice also that the variation in n_{ED} is reduced as the guide vane angle rate of change is increased.

6.3.3 Influence to the global cavitation parameters in cyclic guide vane operation

Figures 6.18 and 6.19 display how the available and required net positive suction head are influenced by the pressure in the draft tube tank. The submergence of the turbine is lowered along with the tank pressure. Successive, the available suction head is lowered. The required suction head is also lowered but is less sensitive to the submergence as it depends on the outlet flow velocity and the runners rotational speed (see Equation 2.7). $NPSH_R$ is only slightly increased because of the increased fluid velocity at the outlet. $NPSH_A$ is directly influenced by the submergence and varies relatively more. The available suction head is never less than the required suction head. This may be due to the design of the runner, but is also likely to be the result of uncertain determination of the constants in Equation 2.7.
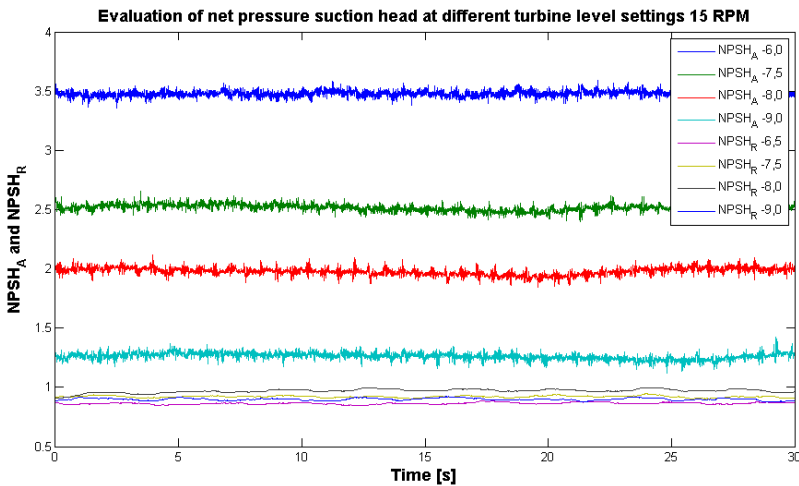
Figure 6.18: Comparison of the net positive suction head at different turbine level settings.

The Thoma cavitation number is best presented by numerical tables. The graphs of the data for σ_{pl} are very difficult to investigate for influence from the dynamic operation. Therefore, the data in Tables 6.7 and 6.8 is obtained using the built in fast Fourier transform tool of DIAdem, with the rectangular transform window applied. The amplitudes are distinct in the frequency analysis and easily detected in the Amplitude diagrams. The change in the cavitation number, σ_{pl}, due to the
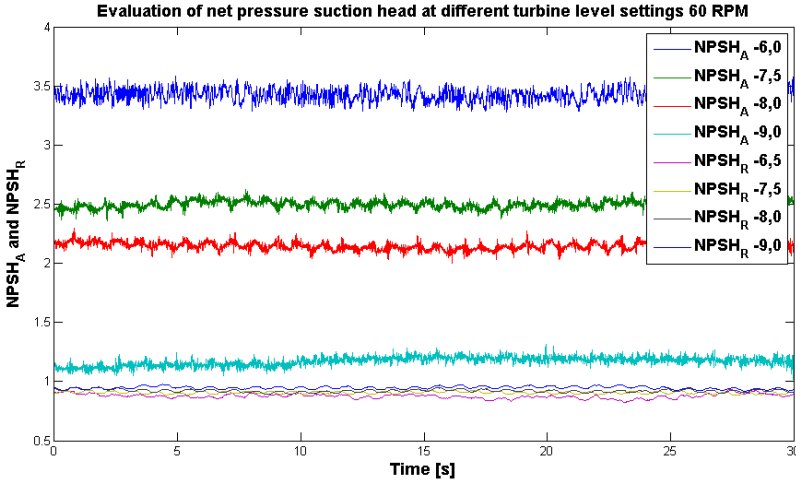
Figure 6.19: Comparison of the net positive suction head at different turbine level settings.

dynamic operation of the guide vanes is small and in the range of $0 - 10, 6 \cdot 10^{-3}$. Very similar results were obtained for all different draft tube tank pressures, and data for $-6, 5$ mlc and $-9, 0$ mlc is presented here.

Table 6.7: *Analysis of Thoma cavitation number variation for operation at a constant draft tube tank pressure of $-6, 5$ mlc.*

RPM	Mean cav.number [-]	$f_{\Delta\sigma}$ [Hz]	$A_{\Delta\sigma}$ [-]	relative change [$^o/_{oo}$]
0	0,130	*No significant frequency*		
15	0,133	0,267	$6, 10 \cdot 10^{-4}$	4,59
30	0,132	0,53	$6, 33 \cdot 10^{-4}$	4,80
45	0,290	0,80	$8, 07 \cdot 10^{-4}$	2,78
60	0,130	1,07	$9, 09 \cdot 10^{-4}$	6,99

Notice that the frequency at which the σ_{pl} occurs for the operation point of 15 RPM and $-9, 0$ mlc in Table 6.8. The frequency deviates from the trend at the other operational points as it then should lie close to $0, 25$ Hz. The cause of this is not known. However, in all other data-series, a frequency peak was visible at approximately $0, 135$ Hz and it may be this frequency that occurs in this data series at greater amplitude. This other frequency is assumed to be the natural frequency of surges in the Francis rig, as most measured signals contain this frequency at some level.

Table 6.8: *Analysis of Thoma cavitation number for operation at a constant draft tube tank pressure of $-9,0$ mlc.*

RPM	Mean cav.number [-]	f_σ [Hz]	$A_{\Delta\sigma}$ [-]	relative change [$^o/_{oo}$]
0	0,0439	*No significant frequency*		
15	0,0481	0,133	$2,69 \cdot 10^{-4}$	5,59
30	0,0464	0,533	$4,93 \cdot 10^{-4}$	10,6
45	0,0479	0,80	$4,53 \cdot 10^{-4}$	9,45
60	0,0445	1,07	$2,74 \cdot 10^{-4}$	6,15
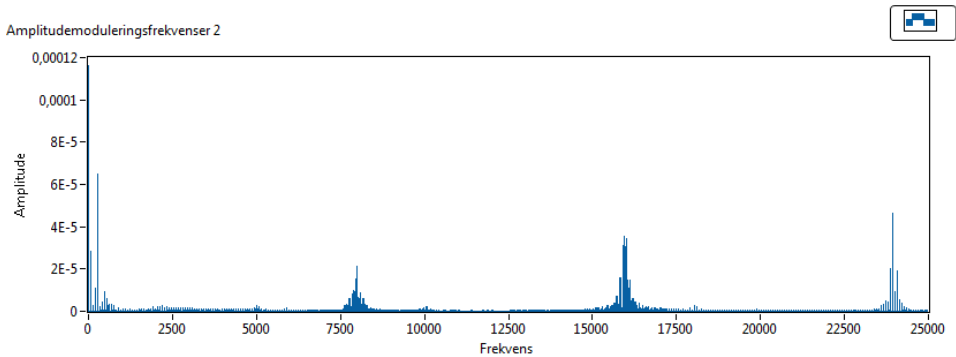
Figure 6.20: Frequency spectrum of vibration measurement at guide vane arm under cyclic movement of guide vane at 15 RPM.

6.3.4 Vibration measurements and analysis

The guide vane arm mounted accelerometer yields some interesting results when the guide vane motor is initiated. Distinct peaks occur in the high frequency band from 7500 Hz and above. The low frequency spectrum are relatively unaffected by the guide vane movement, except for an increase at the frequency of the guide vanes itself. The phenomenon are presented in Figure 6.20. The frequency analysis of data from the accelerometer at the friction torque bearing yields no significant results in the high frequency spectrum where cavitation is expected to occur. Figure 6.21 is an example of the results from this analysis. The results are qualitatively equal for all test data series.

The variation of these frequencies are displayed in the waterfall plot in Figure 6.22.

Notice that the frequencies shown in Figure 6.22 are spread out and the amplitude lowered for increasing guide vane movement speed. Also notice the 0 RPM case where there are no such effects. This is valid for all draft tube pressures and the graphs for the other series are qualitatively equal.

Figure 6.23 show how the frequency spectrum of the data inqured from the ac-
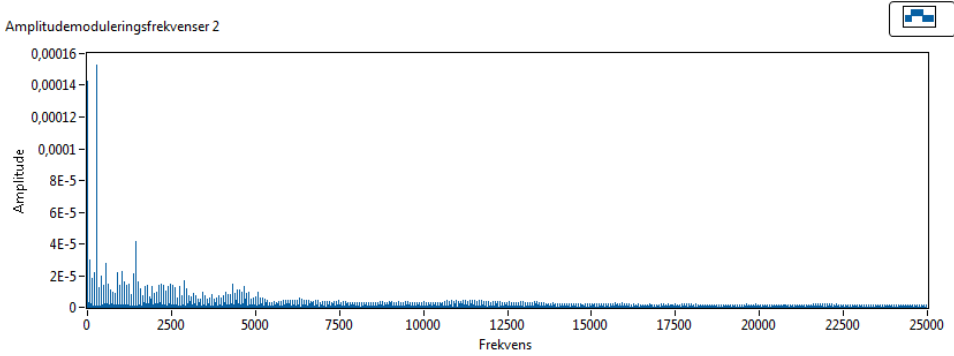
Figure 6.21: Frequency spectrum of vibration measurement at friction torque bearing under cyclic movement of guide vane at 15 RPM.
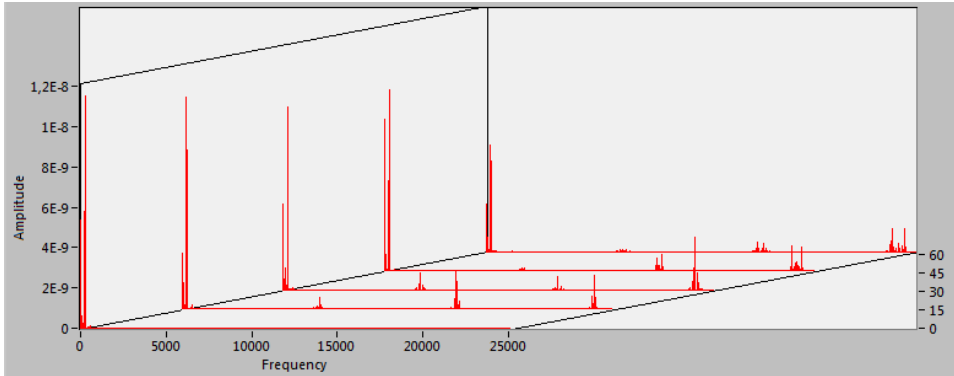
Figure 6.22: Evolution of frequency spectrum from $0 - 60$ RPM at constant draft tube tank pressure (-9.0 mlc). Data from accelerometer located at the guide vane arm.
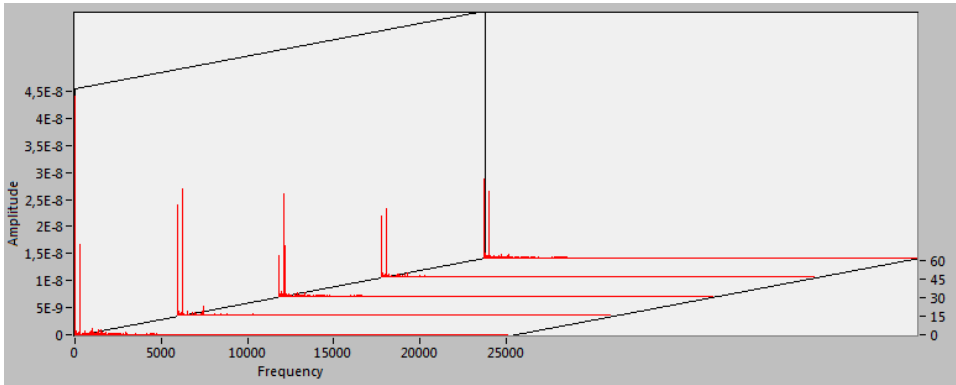
Figure 6.23: Evolution of frequency spectrum from $0-60$ RPM at constant draft tube tank pressure (-9.0 mlc). Data from accelerometer located at the friction Torque bearing.
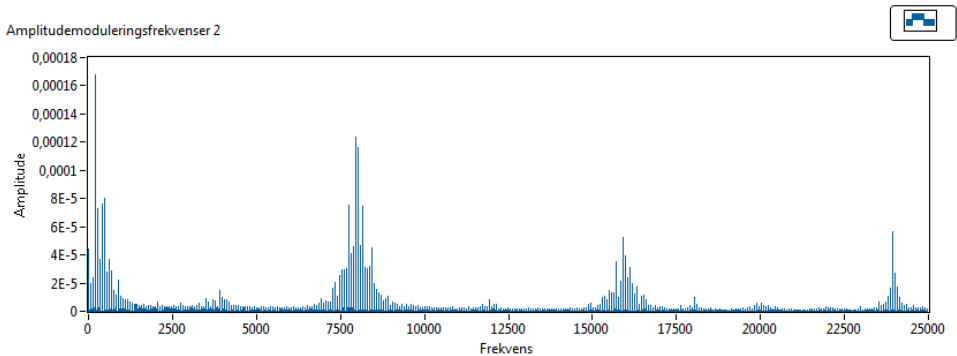
Figure 6.24: Frequency spectrum of operated guide vanes at 15 RPM without water in the turbine. Guide vane accelerometer.

celerometer mounted on the friction torque bearing. The spectrum show no indications of increased amplitudes in the interval indicated in Section 2.3.

A test were performed to investigate the frequencies visible in the high frequency spectrum of Figure 6.20. As these frequencies are not present when the guide vanes are stationary at constant angle, the main suspect was the movement of the guide vanes. The rig were therefore emptied for water and experiments were carried out for all rotational speeds from $0-60$ RPM. The results are presented in Figures 6.24 and 6.25. Notice how the amplitudes are higher in the low guide vane rate of change. The higher frequencies are dampened more than the low at 60 RPM. Also notice the increased level in the low frequency range compared to that of Figure 6.20. The amplitudes have shifted from the higher to the lower frequency spectrum.
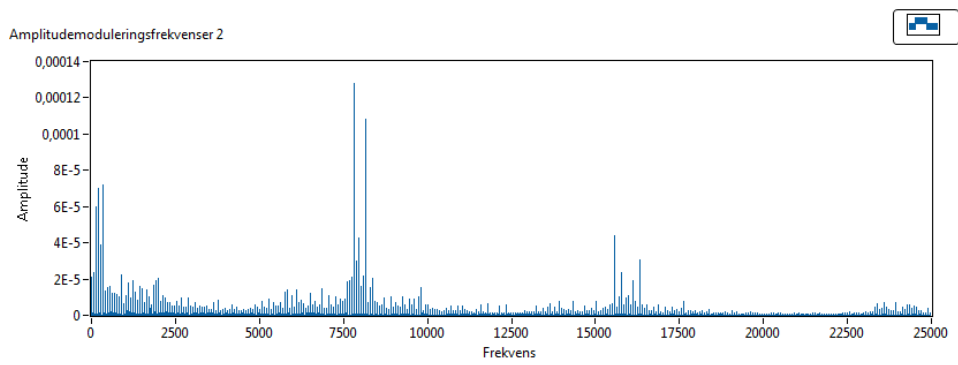
Figure 6.25: Frequency spectrum of operated guide vanes at 60 RPM without water in the turbine. Guide vane accelerometer.

Chapter 7

Discussion

For this thesis, an embedded surveillance program has been developed in the software LabVIEW. The surveillance program has been used in experiments in the laboratory to test hardware and software and to investigate the hypothesis that pressure transients influence the cavitation conditions. The results acquired with the embedded surveillance program will be discussed in this chapter. The surveillance program itself will also be evaluated along with the development process. The results from the autors project thesis, Ruud (2013) are qualitative comparative to the results obtained here. However, the dynamics of the closed loop configuration are very different from the case simulated in named thesis due to the pump regulator and pressure tank.

7.1 Measurements from experiments

In this section the obtained results for the different modes of operation will be discussed.

7.1.1 Instrumentation

There is no need to hide the fact that some of the choices with regard to instrumentation should be improved. Especially the choice of two different sensors for the two cross-sections used to measure the differential pressure may have lead to greater sample errors than necessary. In addition, the lack of proper shaft bearing, one of the accelerometers was placed on the torque friction bearing, which is unlikely to propagate the vibrations in the desired manner. The age of the compactRIO introduced some difficulties with regard to available resources and configuration. However, the sensors, National Instrument hardware and cables were well func-

tioning. Experiments were conducted with only minor difficulties, which speak for well-planned and constructed experiments.

7.1.2 Savitszky-Golay filtered data

The filtered data obtained using the built in Savitzky-Golay filter in LabVIEW, are found adequately accurate and no significant data is lost in the filtering process. It has not been possible for the author to investigate the complete influence of the filtering to the amplitude variation in the signal. However comparisons made between frequency and amplitude analysis of the raw data signal and the filtered signal reveals that the information is preserved in the filtered signal. The plots of these investigations are left out of the report as they only were used to verify the validity of the filtered signal. The reduction in noise was beneficial as the variations became more distinct and comparison between two signals was easier.

7.1.3 Stationary turbine operation

Stationary turbine operation means that the head, flow, speed, guide vane angle and power is kept constant. The measurements carried out for different turbine submergence level settings are presented in Section 6.2. The net head is displayed in Figure 6.2. The effective head is slightly higher for the -6,5 mlc case. This is because the pump delivering the pressure were adjusted to much when the draft tube tank pressure were lowered from the initial -6,0 mlc setting. There is some variation in the data series for the different settings. Some noise is present, but also present are slow changing pressure transients. Especially notice the case of -7,0 mlc, where periodic transients are evident. The upper graph in Figure 6.10 show how the guide vanes are inoperated for this case. The period-time of these transients are recognizable in several of the data series. Amplitudes of these transients are also quite large, such that operation may not be considered to be completely steady with regards to effective head and flow. The origin of these transients may be remaining of the induced transients in previous experiments, and the period time indicates that it is a natural frequency of the water in the turbine rig. This suggest that the time between two measurement series were inadequate and more time should be added between series to let the transients dampen out.

Figure 6.3 present a comparison between the flow rate measured by the installed flowmeter and the calculated flow rate from the modified Gibson's method. The flowmeter measure a nearly steady flowrate only influenced by the pressure transients. The calculated flow rate is deviating from the measured data. The flowmeter are considered to be accurate at stationary flow rates and the deviation seen in the calculated flow is therefore erroneous. However, the error is quite small. The use of one 2,5 bar and one 10 bar gauge pressure sensors may influence the pressure difference since the resolution of the 10 bar sensor is poorer than for the 2,5 bar sensor. This could affect the differential pressure and propagate the error to the

calculation method. The friction factor constant k could have been logged for all measurements such that a sensitivity analysis could be performed. The deviation between the two methods at $t = 0$, indicates that the method is very sensitive to the value of k. Two series in Figure 6.3 starts from the same point as the flowmeter while the three other do not. The average offset is however quite constant and indicates that the initial value of k influence the calculations and the development. Table 6.1 present the relative difference between the average flow measured by the flowmeter and the one calculated. The deviation ranges from approximately -3 to 3 %. At flow rates around $0,335\ m^3/s$ this corresponds to a $\pm 10\ l/s$ deviation which is quite a lot. There is no correlation between the draft tube tank pressure and the deviation. The deviation should be minimized for stationary operation if the value of the friction factor could be determined accurately for the specific flowrate.

Figure 6.4 show how n_{ED} and Q_{ED} are changing and how the operational point, given by the coefficients for head and flow, is moving around in the hill diagram. The two points are at different guide vane angle to illustrate how the turbine moves in the diagram when different parameters are changed. The fact that the turbine operation point are not entirely steady even at constant guide vane angle, is an expected but interesting observation. It suggests that the efficiency of the turbine is changed and this affects the output. Some of the movement must be explained as noise in measured pressure data.

Influence to the global cavitation parameters

The results presented in Figure 6.5 show that the Thoma cavitation number for different turbine submergence setting varies as expected for reduced submergence (lowered draft tube tank pressure). The cavitation number is reduced when the draft tube tank pressure, and thereby the draft tube pressure is reduced. This validates the theory of submerged reaction turbines. Similarly, the influence of reduced draft tube pressure is quantified by the net positive suction head available and required in Figure 6.6. The required suction head is calculated using the Kværner formula, Equation 2.7, with the constants chosen in the lower part of the interval due to the fact that the runner is well designed with regard to cavitation [5]. The required suction head is not greatly influenced by the change of submergence as the flowrate and rotational speed is fairly constant. The available suction head is directly dependent on the submergence and is reduced as the effective turbine level setting is decreased. In the last graph in Figure 6.6, the available suction head is only slightly higher than the required suction head. A further decrease of the draft tube tank pressure, or an increase of flow through the turbine would lead to an cavitating regime when the two lines pass each other. The available head would then be insufficient to keep the turbine out of the cavitating regime.

Vibrational data

The vibrational data show little influence from the changes of draft tube pressure. The waterfall plot of Figure 6.8 indicates that the vibrations at the guide vane arm are approximately constant for all draft tube pressures measured here. The calculated frequencies in Table 6.2 of the system are all detectable in the frequency spectrum of Figure 6.7. There are some other distinct frequencies than the calculated ones. These are at 100, 200 and 300. The two first do not have a known source but might originate from the grid frequency (50 Hz). The last is known in the laboratory to originate from the three phase rectifier for the generator. The frequency spectrum for the whole range up to 25 kHz in Figure 6.9 show a different spectrum for low frequencies than the case with operated turbine with water. This is not considered in this thesis as the figure is included to investigate the origin of the frequency peaks of Figure 6.20.

7.1.4   Periodic operation of guidevanes

The periodic movement imposed to the guide vanes serves as an external input to the system. The purpose of this input is to create a periodic hydraulic transient and by that investigate the influence of these transients to the cavitation parameters. Figure 6.10 display how the guide vane angle was changed for one of the measurement series. The upper figure show how the guide vanes are stationary and the other four how the guide vane motor impose the cyclic movement. The white line in the figure is to investigate the frequency of the cyclic movement. This line is produced using the non-parametrical spline interpolation method. It is evident from the figure that the splines do not represent the amplitude of the signal in a good manner and the result is poorer for higher frequencies. However, additional investigations show that the period of the signal are well represented. This method needs to be tuned to achieve the best fit with regard to amplitude. The splines need to be corrected using a weighing factor to represent the real measured quantity. This is easy to detect in periodic signals like the guide vane angle, but might be harder to detect in more random signals and care should be taken if this method is applied to such signals. However, the frequency of the parametric spline curve should represent the measured quantity in a good manner. Table 6.3 show numerically how the measured angle variation deviates from the frequency set in the guide vane motor. There is quite some deviation and the cause of this is not fully known, but the suspect of this variation is the frequency converter. The non-linear relation mentioned in Section 4.3.5 between signal input and output frequency at low frequencies may have contaminated the expected output. Error increases as the frequency increases such that it may also be a certain inertia that causes this error, which may cause the movement to be unsymmetrical.

Figure 6.11 present how the net head changes for the different operational settings. The guide vane movement is clearly visible in the graphs and the rate of change is faster for the faster guide vane movement. The amplitude of the variation is

increasing for increased rate of change of the guide vane position. This indicates that the inlet pressure is changed more for faster movement. This is in accordance with the Joukowsky equation for pressure change in fluids where the velocity is changed. The net head is also at a constant average level as desired, for best representation of the phenomenon under investigation. The average net head is actually deviating less than the corresponding data for stationary operation of the guide vanes. This indicates that the guide vane movement stabilizes the pressure about an average value.

Figures 6.13 and 6.14 show how the pressure in the air cushion above the free water surface in the upstream pressure tank varies in the different scenarios. The lack of periodicity in most of the graphs indicates that the guide vane movement on a general basis influence the pressure in the tank in little degree for such low amplitudes of external input. However, for 15 RPM (0, 25 Hz), there are distinct periodic behavior for all scenarios. This is an indication that this kind of operation lies close to a natural frequency of the water in the conduit system. Also, as treated before, the same periodic behavior is detected for at least one case where the guide vanes are not dynamically operated (upper graph in Figure 6.13). That is an interesting observation as larges amplitudes may be produced near this frequency and may have implications for further investigations in this subject in the laboratory. An frequency analysis of these transients revealed that the natural frequency probably lies lower than 0, 25 Hz as Figure 6.12 indicates. This frequency of approximately 0, 135 Hz is visible in many of the measurement series and is as before assumed to be a natural frequency of the water in the conduit system. The calculated value for the surge frequency between the pump and the pressure tank presented in Table 6.4 are not the same frequency as observed in the measurements. The conduit length to obtain this frequency by calculations are above 500 meters. The frequency from Table 6.4 are visible for some operational points in the net head but not for all. That means that the natural frequency origins from somewhere else in the system. The origin is not known to the author but one plausible explanation is that there is an U-tube oscillation between the surge chamber and the draft tube tank, but this is an difficult parameter to calculate due to the effect of the turbine which lies in between. A survey using the software LV-Trans, developed in a cooperation between Statkraft and Sintef Energy, and a model of the governed turbine could look into this (see [24]).

The surge frequencies of the pressure surges in the pressure tank (Fig. 6.13 and 6.14) presented in Table 6.5 and 6.6 do show some relation to movement of the guide vanes. However, as the amplitudes are small, the influence of these surges to cavitation inception is small and greater amplitudes should be introduced to do a closer investigation of the phenomenon. This may explain the small variation in the Thoma cavitation number and net positive suction head (see Section 7.1.4)

Figures 6.15 and 6.16 compares the calculated and measured flow rate for the cyclic operated guide vanes. For this scenario the flowmeter were not expected to yield as accurate results as for stationary operation. This may seem validated as there is very little variation in the measured flow rate. The derived flowrate from the

modified Gibsons pressure time method seem to vary more and the estimated period time of the flow rate corresponds well with the frequencies from Table 6.3. The graphs of the calculated flowrate in Figure 6.15 represent the expected average flowrate that the flowmeter would yield under transients while Figure 6.16 demonstrate the opposite. The difference between accurate data in Figure 6.15 and the deviating data in Figure 6.16 are suspected to originate from uncertain determination of the friction factor of Equation 2.11. As this value is not stored, an closer investigation of this is not performed in this thesis.

The Hill diagram wandering is increased upon cyclic external disturbances compared to the stationary case discussed in Section 7.1.3. This wandering is presented in Figure 6.17. The flow is variating more and more vertical movement is the result. The head varies less under increased guide vane rate of change as observed in Figure 6.11 and discussed in Section 6.3.2. The result is less variation in n_{ED} and a narrower vertical trace in the hill diagram. The increase in vertical movement increase the likeliness of cavitation occurrence as the flowrate increases more than the speed factor and the pressure are decreased.

Influence to the global cavitation parameters

Figures 6.18 and 6.19 show the variation in net positive suction head available and required. The influence of the guide vane variation is relatively small compared to the influence of the reduced submergence of the runner. The flowrate variation clearly influence the $NPSH_R$ but the amplitudes are limited (see Section 7.1.4).

The relation between the net head and the Thoma cavitation number is evident and the Tables 6.7 and 6.8 show that the frequency of σ_{pl} is approximately the same as the guide vane variation frequency. The net head variation is then directly influencing the cavitation number. The variation in sigma is so small (see A in Tables 6.7 and 6.8) under the current transient conditions that it is unlikely to induce periodically inception of cavitation based on this variation. The amplitudes will probably have to increase in order for this to occur. Equation 2.9 show that the variation of σ_{pl} depends on the net positive suction head available and the effective head. That means that the variation in the cavitation number originates from changes in the inlet or outlet head, the flow, and the variation in the surface level downstream the turbine. Unfavorable conditions where the downstream surface level is at a minimum and the inlet pressure is at a maximum in transients will increase the amplitude of the changing cavitation number. It is therefore important to limit these effects when operating under such conditions.

Frequency analysis of vibration measurements

The investigation of the frequency response of the rig with moving guide vanes detected that the external input created some sort of vibration or noise in the system. At least, one may rule out that the frequencies are hydraulic effects. This

makes the frequency analysis of the vibration data unreliable and discarded as invalid. The frequency analysis of data from the friction torque bearing location are valid, but show no indications of an increase in amplitudes in the interval between $5 - 25$ kHz (see Figure 6.23). Therefore, no cavitation detection could be performed by analysis of accelerometer data.

No cavitation detection is made from analysis of the data obtained in the experiments. However, influence to the draft tube swirl and the free stream cavities were visually detected and recorded on film. Very few cavitation bubbles were detected on the runner vanes by visual inspection, but the most stable bubbles were visible at the lowest draft tube pressures. The lack of periodicity and pressure pulse amplitudes may cause the occurrence to be difficult to detect.

7.2 Embedded surveillance program

The surveillance program functionality are satisfactory. During the experiments the program did not malfunction at any time. The francis system were continuously under surveillance by the program. All queues were of sufficient size and it is not known to the author that any data were lost during the experiment. Some of the post processing of the acquired data was not implemented into the program. Especially the vibration analysis was expected to require too large parts of the available RAM such that these data were written to file as raw data. There is also some issues with regard to what kind of information the user want from the frequency analysis. There is limited storage capacity such that full sets of frequency analysis cannot be stored in the memory of the cRIO. The study by PhD. Jarle Vikør Ekanger will hopefully yield some results with regard to finding efficient methods for Real-Time analysis of data from accelerometers.

Some of the post processing of the pressure and guide vane angle data was also excluded to make sure the system did not overload. However, with more accessible RAM, these tasks may without difficulties be implemented into the consumer loops of the Real-Time VI. The VIs for the pressure post processing are implemented such that they easily can be included in the RT-application with only minor adjustments to the block diagrams and code writing to file.

The program was running stable, and both acquisition, writing to file and error handling worked properly. No errors occurred during experiments but the system were tested for some failures initially which all were handled as desired by aborting the program and error-statement display.

The embedded system was operated in Scan-Mode which means that the unit is accessible from the host computer. This was necessary due to the lack of a networked host VI. If the host Vi was implemented, the cRIO should be operated in FPGA mode and user input and information should be handled by network queues. This would be the obvious choice if the application was installed to do prototype investigations.

Chapter 8

Conclusion

External input impressed to the guide vanes of a Francis model turbines has been confirmed to impact the required conditions for cavitation to occur. This is confirmed by measuring the influence to relevant parameters such as the required net positive head. The investigation performed, demonstrate how the flow in governed turbines are affected by continuous influence from moving guide vanes. This experimental study suggests that hydraulic transients influence the flow conditions through the turbine and that these effects may be observed and recorded by real-time surveillance applications. During the work on this experimental investigation, a thoroughly prepared embedded surveillance application has been developed. General theory and information of hardware and software are presented in Chapter 3.

The embedded application was built using the LabVIEW software and hardware from National Instruments. Implementation is done using both built in library functionality of LabVIEW, as well as self-made functionality for use in specific range of applications. Quite some effort was put into the work of the development process to really understand the subtlety and functionability of the Real-Time module of LabVIEW. Networking, binary data, unit power supply and circuit analysis are wider area of knowledge that were necessary to address and understand to be able to build the application from basic components. A modified Gibsons method were derived and implemented to demonstrate the ability to do real time processing of acquired data along with several other tasks. The true parallel nature of the hardware were demonstrated and utilized by performing data acquisition from multiple sensors and devices simultaneously.

An experiment was planned and executed in the laboratory to congregate information on hydraulic transients, cavitation conditions and flow rate determination using the developed real-time application. The results are compiled, analyzed and presented in Chapter 6. The external input proved to generate hydraulic transient in measures of head and flowrate. These effects introduced pressure fluctuation in the turbine which influenced the general cavitation parameters. Different input

frequencies resulted in corresponding influence to other parameters such as speed and flow factor, net positive suction head, Thoma number etc. The transients introduce undsteady operation of the turbine and the trace in the hill diagram is demonstrated. This also indicates how the efficiency and power are influenced by transients induced by load changes in the turbine. Transient cavitation occurrence was visually confirmed without being detected in the measured quantities. Therefore, no deduction can be made with regard to cavitation detection by vibration analysis with basis in the experiments presented in this thesis.

The experimental set up could be improved to yield better result with regard to vibration measurements. The flow rate may, by proper tuning of the model parameters, be determined using Gibsons pressure-time method. Transient friction should be addressed to yield more accurate results. The uncertainty of the measurements is not determined. Measurements of transient behavior lead to large uncertainties and are not always representative for the uncertainty of the measurements. Therefore, little weight is put on uncertainty analysis in this thesis. The experimental survey confirms previous numerical simulation of the same subject.

Chapter 9

Further work

An experimental survey of the subject presented in this thesis build a foundation for further development. To obtain further experience with both Real-Time surveillance and investigation of cavitation inception in turbines, there are still tasks to carry out. At first, the pressure and vibration data post processing should be implemented in the Real-Time analysis. The work of Jarle Vikør Ekanger is advancing in this subject. Power plants that are equipped with networked communication would allow remote access to stand-alone systems. A creation of HOST-VIs that can be used from another location for supervision of the embedded system would increase the applicability of the total system.

To increase the accuracy of the modified Gibson method, a Kalman-filter methodology could be useful to obtain better modeling of transient friction factor and head loss. A uncertainty analysis could be performed, and later implemented into the embedded system for higher reliability.

The motor that regulate the guide vanes in a periodic manner may be utilized for other applications, e.g. an investigation of the frequency response of the turbine with runner and generator. The sinusoidal external input will then work as the disturbance to excite the system. The range of motor speed settings might be a limitation with regard to such studies. The motor could also be used to investigate the natural response of the surges in the system. The range from 0,10 to 0,25 Hz should be addressed to obtain larger amplitudes in the pressure chamber.

References

[1] Anders Peter Andersen and Knud Aage Mørch. *Tensile Strength of Water Exposed to Pressure Pulses*, pages 540–545. CAV2012, 2012.

[2] Prof. Hermod Brekke. *Grunnkurs i hydrauliske strømningsmaskiner*. Vannkraftlaboratoriet, NTNU, 2001.

[3] Prof. Hermod Brekke. *Hydraulisk Måleteknikk*, volume 2. Vannkraftlaboratoriet, NTNU, 2003.

[4] Professor Emiritus Hermod Brekke. Personal communication fall and spring, 2013 and 2014.

[5] Professor Ole G. Dahlhaug. Personal communication fall, 2013.

[6] X. Escaler, M. Farhat, F. Avellan, and E. Egusquiza. Cavitation erosion tests on a 2d hydrofoil using surface-mounted obstacles. *Wear*, 254:441–449, 2003.

[7] X. Escaler, E. Egusquiza, M. Farhat, F. Avellan, and M. Coussirat. Detection of cavitation in hydraulic turbines. *Mechanical Systems and Signal Processing*, 20:983–1007, 2006.

[8] J.P. Franc and J.M. Michel. *Fundamentals of Cavitation*. Fluid Mechanics and Its Applications. Springer, 2011.

[9] Stud. Techn. Håkon Hjort Francke. Virkningsgradsmålinger på lavtrykks francisturbiner. Masters thesis, Norwegian University of Science and Technology, Trondheim, june 2006.

[10] Håkon Hjort Francke FDB AS. Personal communication spring, 2014.

[11] IEC. Hydraulic turbines, storage pumps and pump-turbines - model acceptance tests. Technical Report IEC 60193, The International Electrotechnical Commission, 3, rue de Varembé, Case postale 131, CH-1211 Genève 20, Switzerland, 1999.

[12] National Instruments. www.ni.com. Product descriptions, 2014.

[13] Morten Kjeldsen CEO FDB AS. Personal communication fall, 2013.

[14] E. Kreyszig. *Advanced Engineering Mathematics 9th Edition*. Wiley Plus Products. John Wiley & Sons Canada, Limited, 2006.

[15] M.J. Moran and H.N. Shapiro. *Fundamentals of Engineering Thermodynamics: With Appendices*. John Wiley & Sons Canada, Limited, 2010.

[16] Professor Knud Åge Mørch. Guest lecture NTNU, June, 2014.

[17] Professor Torbjørn K. Nielsen. Personal communication spring, 2014.

[18] Torbjørn Nielsen. Dynamisk dimensjonering av vannkraftverk, 1990.

[19] Morgan Pickering. *FFT for partial differential equations*. Electronic and electrical engineering research studies, Applied and engineering mathematics series; 4. Letchworth: Research Studies Press, 1986.

[20] Francis 99 project. Francis 99, luleå university of technology/ntnu, June, 2014. URL `http://www.ltu.se/research/subjects/Stromningslara/Konferenser/Francis-99?l=en`.

[21] Stud. Techn. Bjørn Winther Solemslie. Optimalisering av ringledning for peltonturbin. Master thesis, Norwegian University of Science and Technology, Trondheim, June 2010.

[22] Stud. Techn. Kjetil Guddal Ruud. Modulated cavitation in hydro turbines. Project thesis, Norwegian University of Science and Technology, Trondheim, December 2013.

[23] Abraham. Savitzky and M. J. E. Golay. Smoothing and differentiation of data by simplified least squares procedures. *Analytical Chemistry*, 36(8):1627–1639, 1964.

[24] Dr. ing. Bjørnar Svingen. Application of labview for dynamic simulation of hydraulic piping systems, 2005. URL `http://www.scansims.org/sims2005/SIMS2005_42.pdf`.

[25] Jeffrey Travis and Jim Kring. *LabVIEW for Everyone: Graphical Programming Made Easy and Fun (3rd Edition) (National Instruments Virtual Instrumentation Series)*. Prentice Hall PTR, Upper Saddle River, NJ, USA, 2006. ISBN 0131856723.

[26] Ronald E. Walpole, Raymond H. Myers, Sharon L. Myers, and Keying Ye. *Probability & statistics for engineers and scientists*. Pearson Education, 8th edition, 2007.

[27] A.J. Wheeler and A.R. Ganji. *Introduction to Engineering Experimentation*. Pearson/Prentice Hall, 2004.

[28] F.M. White. *Fluid Mechanics*. McGraw-Hill series in mechanical engineering. McGraw-Hill Higher Education, 2008. ISBN 9780071286466.

[29] www.grabcad.com user pseudonyme: Doxyde. motorredutor, May 2012. URL `https://grabcad.com/library/motorredutor`.

Appendix A

Gibsons Method

For a pipe segment, Newtons 2nd law may be applied to investigate the acceleration and deceleration of fluid flow.

$$F = ma \tag{A.1}$$

the forces acting on the fluid mass is

$$F_{p1} = p_1 A_1 \qquad F_{p2} = p_2 A_2 \qquad F_f = \tau \pi D L.$$

The pipe segment is assumed horisontal such that there is no difference in geodetic potential.

The mass of the fluid in the pipe is given by $m = \rho A L$ and the acceleration is the rate of change in bulk fluid velocity $a = \frac{dV}{dt}$. The acceleration of the mass is defined positive in the direction of the flow such that $ma = -\rho A L \frac{dV}{dt}$ Applied to equation A.1 this yields

$$p_1 A_1 - p_2 A_2 - \tau \pi D L = -\rho A L \frac{dV}{dt} \tag{A.2}$$

The downstream pressure force and the friction force works in the opposite direction of the flow and is therefore subtracted from the upstream pressure force.

For a pipe where the cross section is uniform, $A_1 = A_2$ and $V = \frac{Q}{A}$ such that:

$$(p_1 - p2)A - \tau \pi D L = -\rho L \frac{dQ}{dt}$$

The Darcy-Weisbach friction factor can be applied to express τ in terms of the fluid velocity:

$$\tau = \frac{f}{8} \rho V^2 \tag{A.3}$$

Since $F_f = A\Delta p_f$, Newtons 2nd law now reads

$$A(\Delta p - \Delta p_f) = -\rho L \frac{dQ}{dt}.$$

rearrange and integrate to solve for the volumetric flow rate:

$$\int_{Q_0}^{Q} dQ = \frac{A}{\rho L} \int_{t_0}^{t} (\Delta p - \Delta p_f) dt. \tag{A.4}$$

This equation may also of course be rewritten using the more common pressure head in *mlc* by applying $p = \rho g h$, which also apply to the head loss.

The pressure difference due to friction is

$$\Delta p_f = \frac{F_f}{A} = \frac{\tau \pi D L}{\frac{\pi D^2}{4}} = \rho \frac{fL}{2D} \frac{Q^2}{A^2}. \tag{A.5}$$

Further:

$$k = \frac{fL}{2gDA^2}. \tag{A.6}$$

such that

$$\Delta h_f = kQ^2 \tag{A.7}$$

And the final result yields an implict equation for the change in flowrate over an increment in time.

$$\Delta Q = Q - Q_0 = \frac{gA}{L} \int_{t_0}^{t} (\Delta h - \Delta h_f) dt. \tag{A.8}$$

In both equation A.4 and A.8 there is dependency between the pressure/head loss due to friction and the flow rate according to equation A.5 and equation A.7. This dependency yields some problems with regard to solving for the flowrate numerically and an iteration process must be performed to obtain an adequately accurate flow rate for this application.

Appendix B

The chapter "Cavitation" by Ruud (2013)

The content of this appendix is in its whole included from the thesis by Ruud (2013) [22]

Cavitation is a phenomenon occurring in liquid flow. In this study, only hydrodynamic cavitation is considered. The phenomenon can be defined as *"the breakdown of a liquid medium under very low pressures"* [8]. Cavitation can occur if the local pressure decrease below the vapor pressure of the liquid. Vapor bubbles will then grow from "weak spots" in the flow named nuclei and form a cavity in the liquid. The nuclei can be either a particle or air trapped in the flow, or existing vapor bubbles of the micro scale in the free flow or trapped in roughnesses at the material surface that constrain the liquid. It is common to divide cavitation into two regimes. One where the vapor bubbles are attached to a material surface in the system, and one regime where the nuclei are in the free flow [8]. When these bubbles are brought into an area of high pressure or the pressure at the position of the bubble is increased, the bubble can collapse, or implode, under influence of the increased pressure it is exposed to. The whole process of bubble inception, growth and implosion is what is termed cavitation.

B.1   Types of cavitation

In the Francis turbine, Escaler et al. [7] describes five types of cavitation from which mainly the two first are considered in this study.

B.1.1 Leading Edge Cavitation

Cavitation due to operation outside the best efficiency point. Highly erosive cavitation if fully developed.

B.1.2 Traveling Bubble Cavitation

This form of cavitation is due to a low thoma cavitation number, i.e. not sufficient suction head. These cavitation bubbles occur at the outlet of the runner and might be carried along the flow to implode in the draft tube rather than on the runner vane surface. Nevertheless, this type of cavitation may reduce the efficiency of the runner.

B.1.3 Draft Tube Swirl

String of cavitation bubbles originating from the hub of the runner and is a function of $NPSH_A$. This vortex rope might induce powerful pressure pulses in the draft tube.

B.1.4 Inter-blade Vortex Cavitation

Due to the diverging channel that the hub and ring make up between the runner vanes, the flow will separate and create secondary flow patterns and cavitation bubbles. The occurrence of these vortexes are limited to part load operation [7].

B.1.5 Von Karman Vortex Cavitation

Near the leading edge, vortex shedding, as described in section B, may be present.

B.2 Thoma cavitation number

The vapor pressure of a fluid can be defined as the pressure at which the phase change from liquid to vapor occurs. The vapor pressure p_v varies as a function of the temperature and is tabulated for water [15]. The Thoma cavitation number is defined by [8] where pressure is given in $[Pa]$

$$\sigma_v = \frac{p_\infty - p_v(T)}{\Delta p} \tag{B.1}$$

p_∞ is a reference pressure, measured close to where cavitation inception is expected. This number describes how likely the flow is to cavitate at a particular point. At

any point of cavitation inception, the cavitation number $\sigma_v = \sigma_{vi}$. It is obvious that cavitation will occur either because the reference pressure is lowered, or that the pressure difference is increased. The varying pressure due to surges or water hammers in the system will clearly affect the cavitation number by means of the reference pressure p_∞, and is of major importance in this study. In hydro power applications, this parameter is often given by the available NPSH and is then defined

$$\sigma_{pl} = \frac{NPSH}{H_e} \tag{B.2}$$

If the efficient head H_e is a function of time, then the cavitation number will also be a function of time.

B.3   Water quality

The water quality is a measure of the ratio between the mass of vapor to the total mass of fluid in the control volume looked upon [15]

$$x = \frac{m_{vapor}}{m_{liquid} + m_{vapor}} \tag{B.3}$$

A water quality ratio of 0 corresponds to saturated liquid and a ratio of unity correspond to saturated vapor.
In the context of a hydro power plant, sediments in the water may also play a key part in cavitation as they introduce more nuclei in the flow [13]. In water with quality value close to zero, attached cavitation is dominant. In the presence of gas nuclei in the water, bubbles traveling with the free flow are present as well [8].

B.4   Henry's law

Henry's law connects the partial pressure of a gas over a liquid to the concentration of the gas in the liquid at the point of saturation [8].

$$C_{si} = H_i p_i \tag{B.4}$$

In equation B.4, H_i is Henry's constant which is a function of the temperature of the gas. If the gas is atmospheric air, the partial pressure of oxygen and nitrogen must be taken into account [8].

B.5   Spherical bubble dynamics

In order to describe the development of nucleus in the flow, the Rayleigh-Plesset equation is established with a set of assumptions found applicable for this thesis. The main parameter in this equation is the bubble radius and its first and second derivatives. From the Navier-Stokes equation in the axial flow direction and by applying boundary conditions the equation may be expressed as [8]

$$\rho \left[R\ddot{R} + \frac{3}{2}\dot{R}^2 \right] = p_v - p_\infty(t) + p_{g0}\left(\frac{R_0}{R}\right)^{3\gamma} - \frac{2S}{R} - 4\mu\frac{\dot{R}}{R} \tag{B.5}$$

This equation is developed assuming that the bubble is a sphere and that the bubble center is stationary. The equation can be used as an approximation to cases where the bubble center is traveling in the flow like the case is in a hydro power turbine [8].

If a bubble in equilibrium to its surroundings is exposed to a pressure greater than the vapor pressure, the bubble will collapse. The time it takes from the initiation of the collapse until the bubble is completely imploded is called the Rayleigh time τ [8]. By integration of equation B.5 and rewrite using that the terms in the bracket on the left hand side can be rewritten to describe the kinetic energy of the liquid, the Rayleigh time can be determined.

$$\tau \cong 0.915 R_0 \sqrt{\frac{\rho}{p_\infty - p_v}} \tag{B.6}$$

The full development of these equations can be found in the book Fundamentals of Cavitation by J. P. Franc and J. M. Michel (2011) [8] and will not be explored here. A bubble at equilibrium with radius 0.1 *cm* exposed to an external pressure of 0.1 *bar* collapses in 0.3 *milliseconds*.

B.5.1   Effect of water properties

The bubble dynamics are affected by viscosity, tensile strength of the water and the content of non condensable gas in the bubble. Viscosity slows down both growth and collapse of the bubble. It will also work as a damping factor if the bubble size is oscillating under oscillating pressures. The tensile strength of water under very low pressure increases the growth speed of the bubble, but decreases the velocity of the surface of a collapsing bubble. The amount of non-condensable gas will also affect the rate of change in radius because it will take some longer time to condense the vapor in the bubble [8].

Appendix C

Block diagrams for surveillance program

Some of the block diagrams of the RT surveillance program are added here to improve the documentation. Be aware that where case structures are included, one or more cases are not presented.
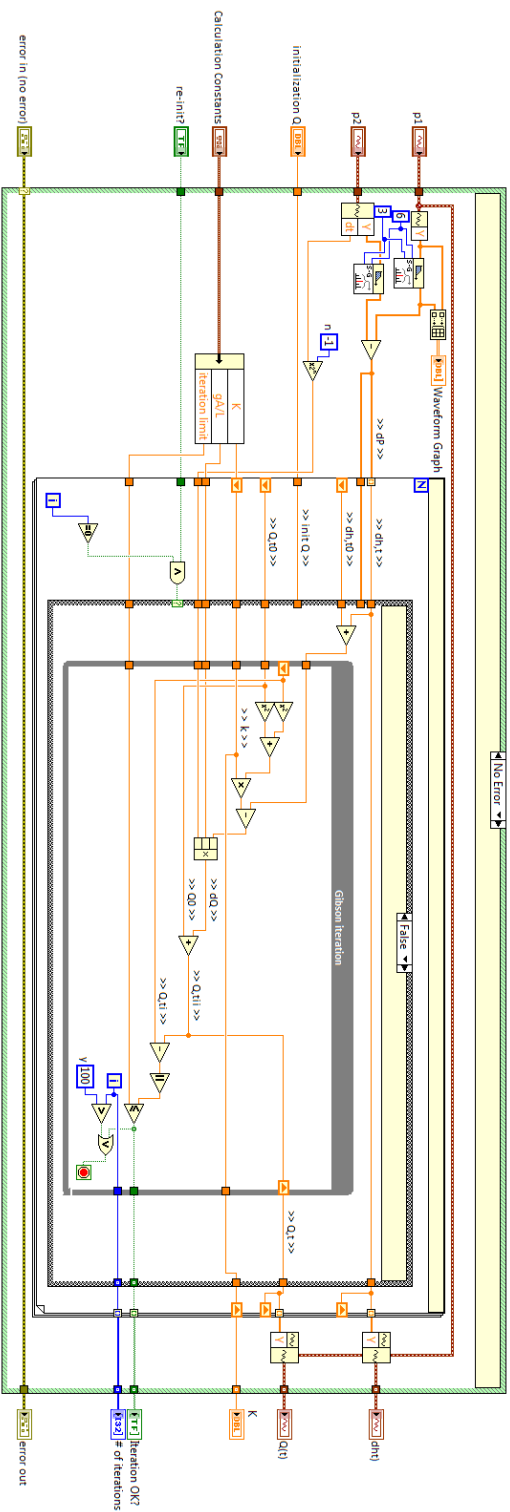
Figure C.1: Block diagram for Gibson Method sub-VI.
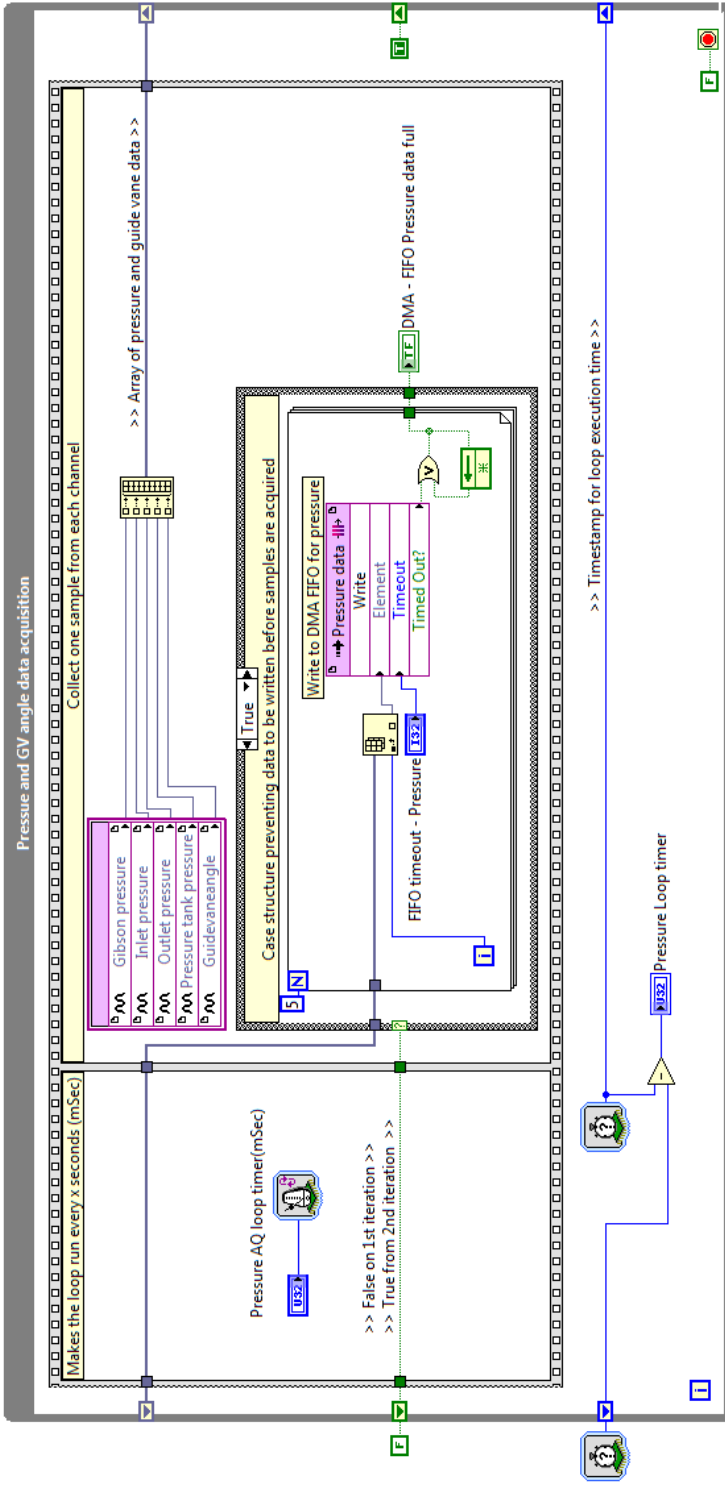
Figure C.2: Block diagram showing the acquisition loop for pressure and guide vane angle data.
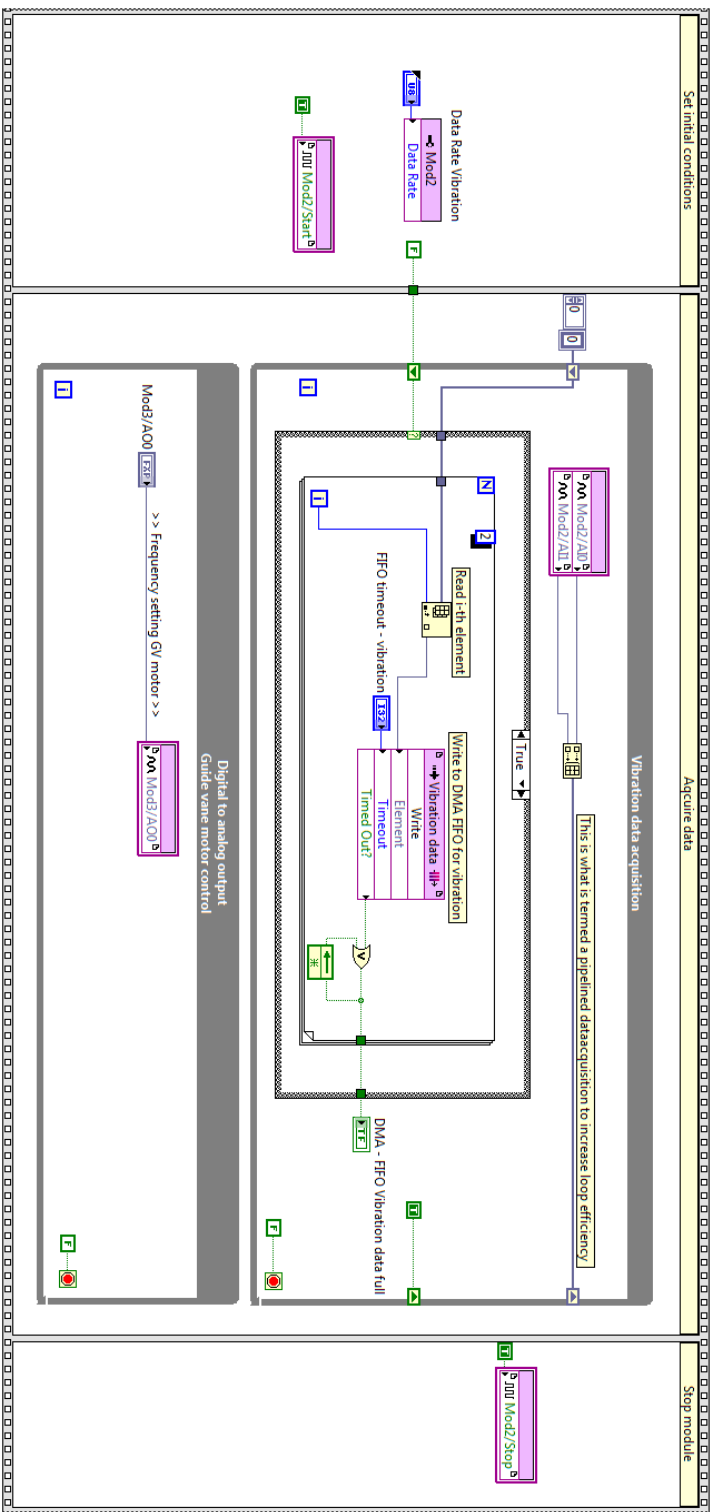
Figure C.3: Block diagram showing the acquisition loop for vibration data.
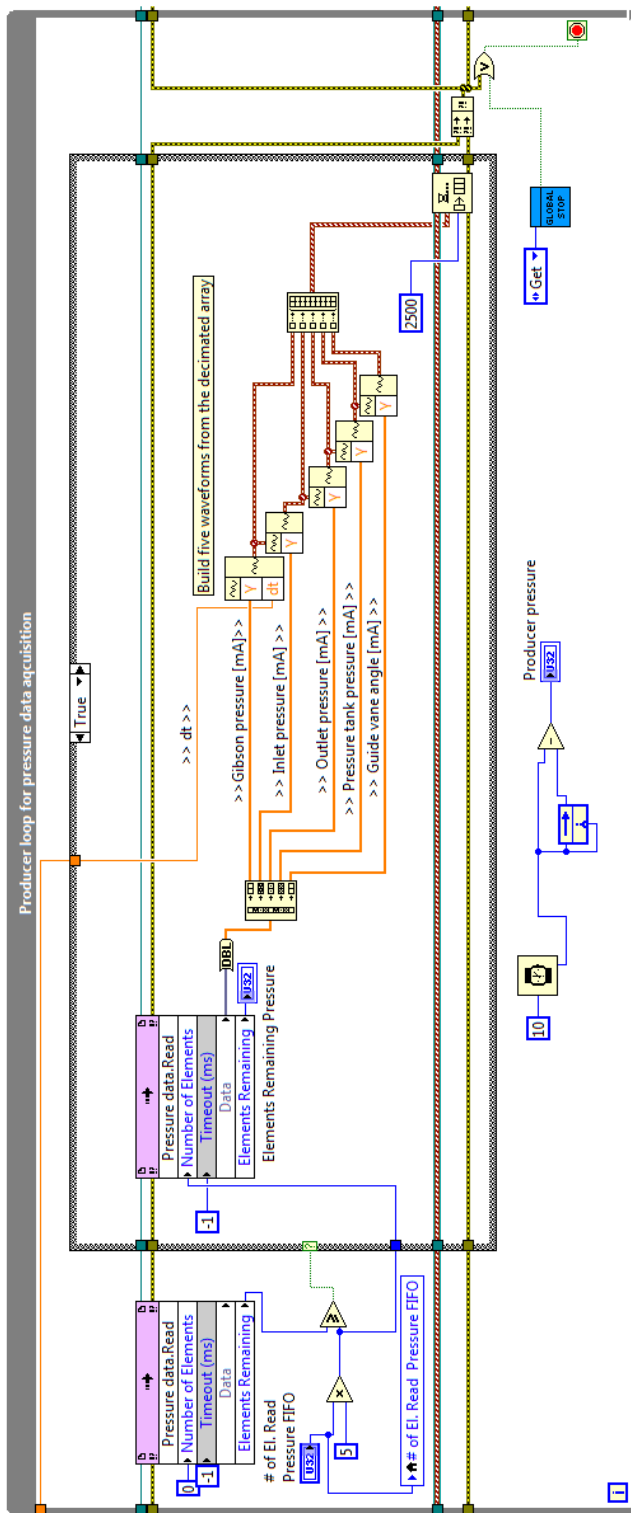
Figure C.4: Example of producer loop for reading FIFO and distributing data to consumer loops.
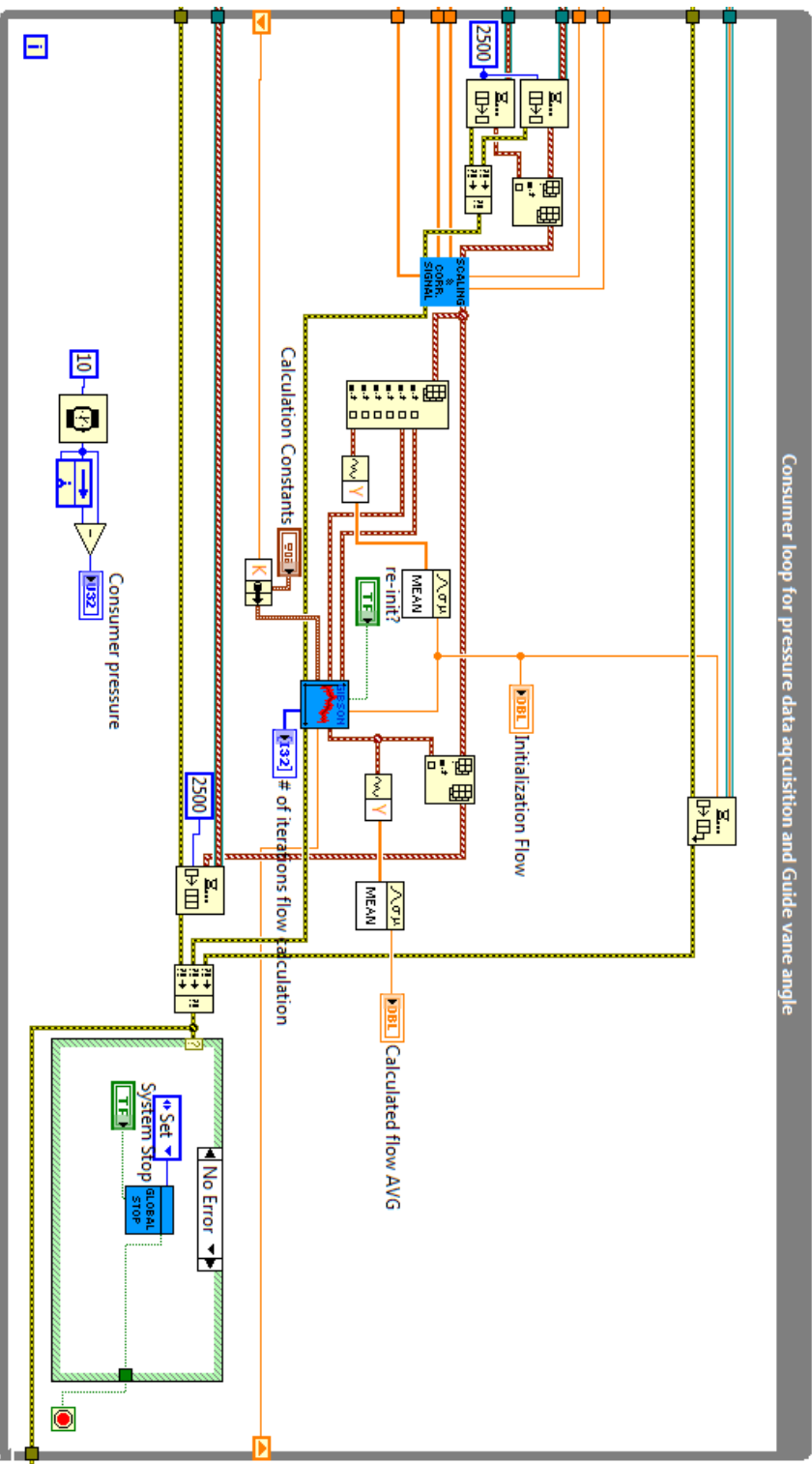
Figure C.5: Example of producer loop for rerecieving queued elements from producer loops.
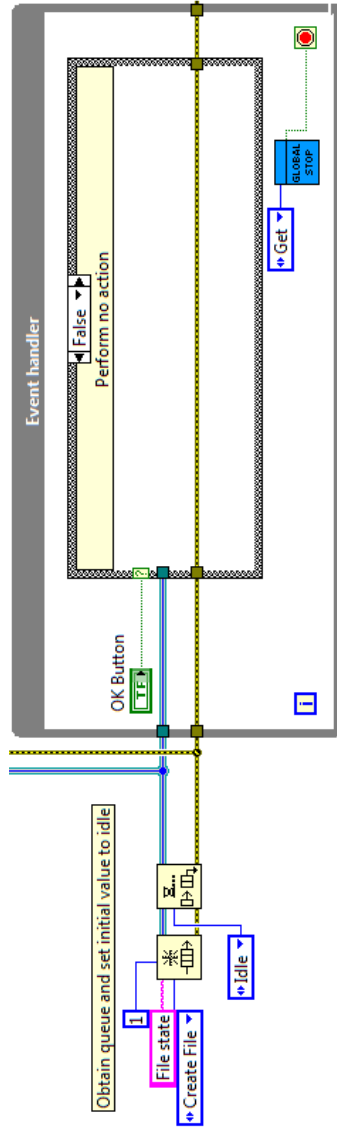
Figure C.6: Event handler loop with initialization for writer loop control.
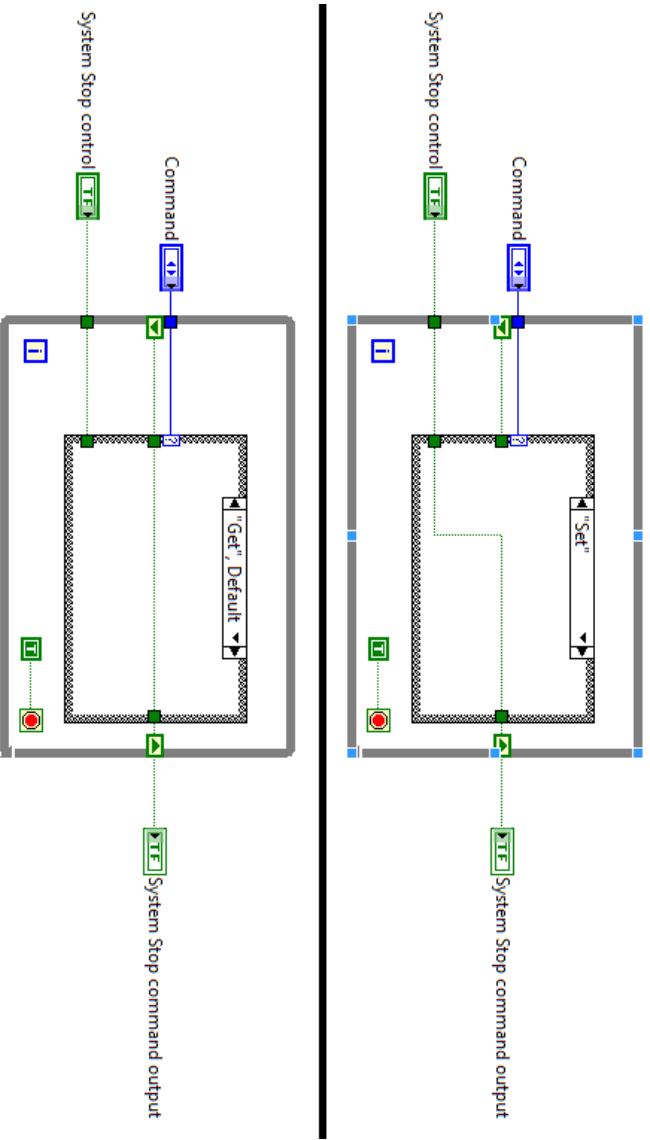
Figure C.7: Block diagram for global stop action sub-VI. The Set case is shown above the line and the default Get case is shown below.

Appendix D

Configuration of RT-Target on a network

Always make sure that the latest (or proper) cRIO driver and NI-MAX software is installed on the host computer before setting up a embedded system. When the Real Time target shall be configured, it is important that the target and the host is on the same subnet mask. That means that the target should be configured in a local connection before it is connected to a network hub. The procedure applied by the author is to put SAFE MODE and IP RESET switches on the target to on and connect the target to the host computer by an ethernet cable. Then the target should appear under the Remote Systems header in NI-MAX with the default settings, which is an IP-adress of 0.0.0.0 for older targets, and by default DHCP or Link Local configuration on later units. If the unit is booted with 0.0.0.0, the unit must be found with NI-MAX, wired directly to the computer using and ethernet cable and in the network settings tab, DHCP - Link Local should be selected and saved. Then the unit must be restarted to apply the new settings. When the unit is restarted, and the status in the system settings tab is "Running", the ethernet cable can be disconnected and both the host computer and the target may be connected to a switch at which the internet cable is connected. In this thesis, the cRIO is connected to the local network and is set up with DHCP and is therefor available from every computer on the same subnet. This is beneficial with regards to the availabilty and flexibility that this solution introduces. Support is then possible for any person on the same network with the access password. For the author of this thesis, this implied that the target was accessible both in the laboratory and from the office. Cat5 ethernet cables were used along with a switch that connected all devices to the network.

Appendix E

Calibration charts

All calibration charts are included in this appendix.

- Guide vane angle sensor calibration
- Pressure sensor P2 inlet calibration and values
- Pressure sensor P3 outlet calibration and values
- Pressure sensor P1 Gibson pressure calibration and values
- Pressure sensor P0 Pressure tank calibration and values
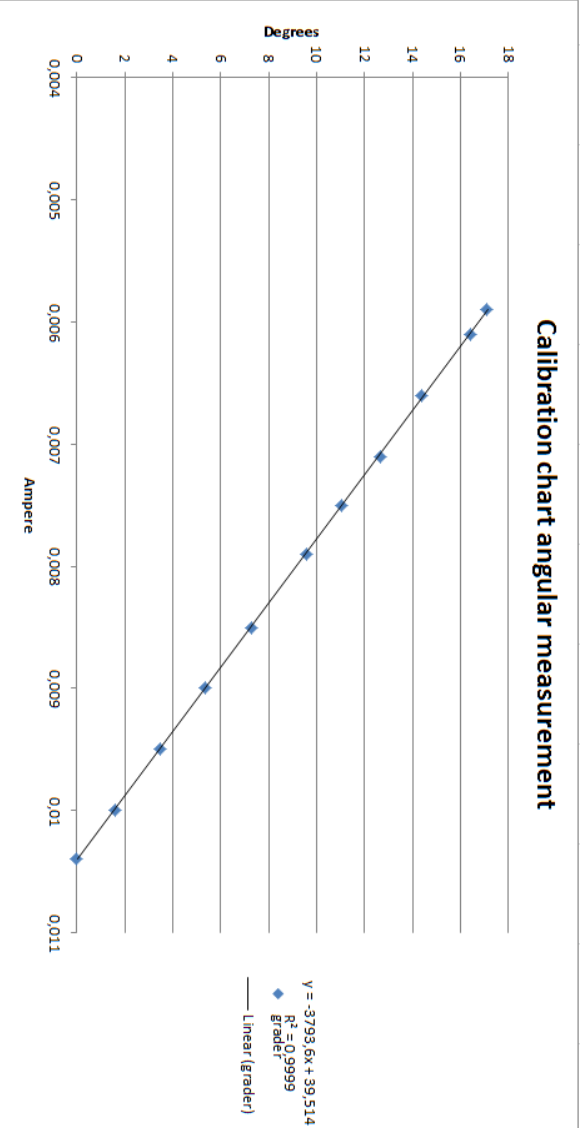
Figure E.1: Calibration chart for angular converter

CALIBRATION REPORT

CALIBRATION PROPERTIES
Calibrated by: Sigurd Haga
Type/Producer: Druck PTX1400
SN: Y21674/07
Range: 0-10 bar g
Unit: kPa

CALIBRATION SOURCE PROPERTIES
Type/Producer: Pressurements deadweight tester P3223-1
SN: 66256
Uncertainty [%]: 0,01

POLY FIT EQUATION:
Y= -251.70683147E+0X^0 + 125.20071257E+0X^1

CALIBRATION SUMARY:
Max Uncertainty   : Inf [%]
Max Uncertainty   : 0.041295 [kPa]
RSQ   : 1.000000
Calibration points : 30
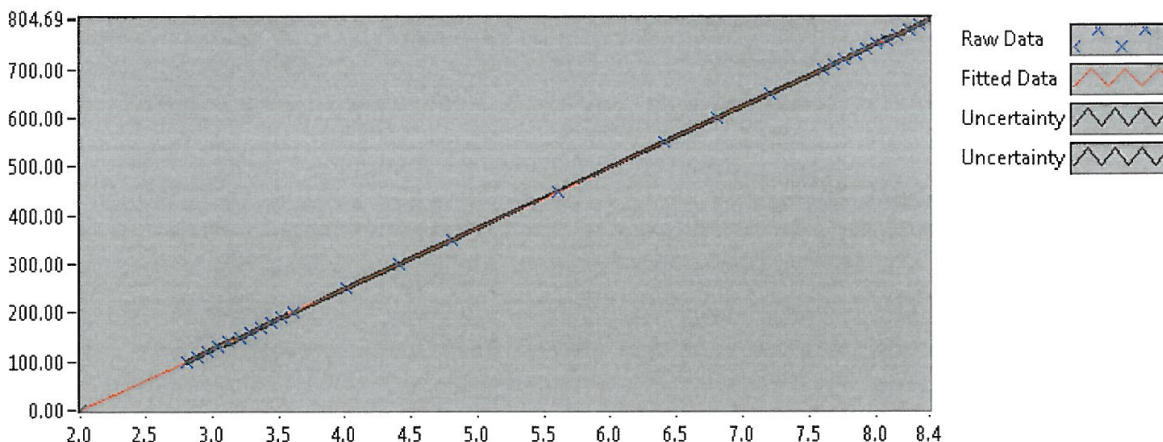
Figure 1 : Calibration chart (The uncertainty band is multiplied by 100)

Sigurd Haga

CALIBRATION VALUES

Value [kPa]	Voltage [V]	Best Poly Fit [kPa]	Deviation [kPa]	Uncertainty [%]	Uncertainty [kPa]
0.000000	2.011169	0.092931	-0.092931	Inf	NaN
99.415864	2.805229	99.509837	-0.093973	0.039400	0.039169
109.430971	2.885031	109.501155	-0.070184	0.035169	0.038486
119.446078	2.964944	119.506332	-0.060254	0.031654	0.037810
129.461185	3.044922	129.519614	-0.058429	0.028690	0.037143
139.476293	3.124689	139.506450	-0.030157	0.026160	0.036488
149.491400	3.204719	149.526257	-0.034858	0.023975	0.035841
159.506507	3.284417	159.504564	0.001942	0.022073	0.035207
169.521614	3.364449	169.524633	-0.003019	0.020400	0.034583
179.536721	3.444246	179.515229	0.021492	0.018923	0.033974
189.551828	3.524062	189.508202	0.043626	0.017609	0.033378
199.566935	3.603703	199.479328	0.087607	0.016435	0.032799
249.642471	4.003693	249.558330	0.084141	0.012059	0.030105
299.718006	4.403813	299.653673	0.064333	0.009300	0.027872
349.793541	4.803577	349.704463	0.089078	0.007500	0.026235
449.944612	5.602959	449.787613	0.156999	0.005587	0.025139
550.095683	6.403160	549.973410	0.122273	0.004935	0.027145
600.171219	6.803189	600.057219	0.114000	0.004857	0.029149
650.246754	7.203735	650.205901	0.040853	0.004871	0.031675
700.322290	7.604032	700.323337	-0.001048	0.004939	0.034587
710.337397	7.684037	710.340088	-0.002692	0.004958	0.035219
720.352504	7.764219	720.378959	-0.026456	0.004977	0.035854
730.367611	7.844151	730.386501	-0.018890	0.004997	0.036498
740.382718	7.924500	740.446277	-0.063559	0.005019	0.037159
750.397825	8.004477	750.459415	-0.061590	0.005041	0.037828
760.412932	8.084452	760.472328	-0.059396	0.005064	0.038506
770.428039	8.163878	770.416465	0.011574	0.005086	0.039181
780.443146	8.244222	780.475657	-0.032511	0.005109	0.039876
790.458254	8.324299	790.501372	-0.043118	0.005136	0.040595
800.473361	8.404625	800.558217	-0.084856	0.005159	0.041295

COMMENTS:

The uncertainty is calculated with 95% confidence. The uncertainty includes the randomness in the calibrated instrument during the calibration, systematic uncertainty in the instrument or property which the instrument under calibration is compared with (dead weight manometer, calibrated weights etc.), and due to regression analysis to fit the calibration points to a linear calibration equation. The calculated uncertainty can be used as the total systematic uncertianty of the calibrated instrument with the given calibration equation.

CALIBRATION REPORT

CALIBRATION PROPERTIES
Calibrated by: Sigurd Haga
Type/Producer: Druck PTX1400
SN: D20661/04/2011
Range: 0-10 bar g
Unit: kPa

CALIBRATION SOURCE PROPERTIES
Type/Producer: Pressurements deadweight tester P3223-1
SN: 66256
Uncertainty [%]: 0,01

POLY FIT EQUATION:
Y= -250.91547257E+0X^0 + 125.18474835E+0X^1

CALIBRATION SUMARY:
Max Uncertainty   : Inf [%]
Max Uncertainty   : 0.036732 [kPa]
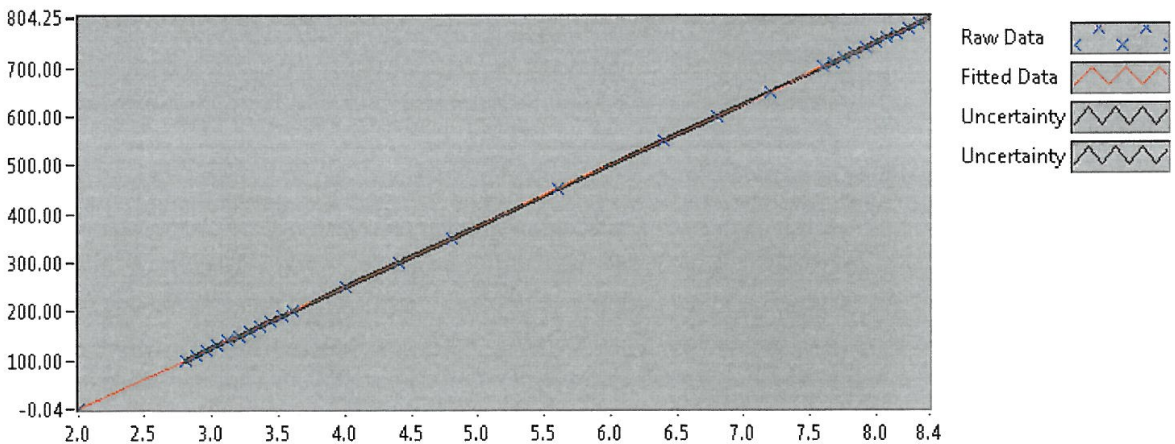RSQ   : 1.000000
Calibration points : 30

Figure 1 : Calibration chart (The uncertainty band is multiplied by 100)

Sigurd Haga

CALIBRATION VALUES

Value [kPa]	Voltage [V]	Best Poly Fit [kPa]	Deviation [kPa]	Uncertainty [%]	Uncertainty [kPa]
0.000000	2.004067	-0.036839	0.036839	Inf	NaN
99.415864	2.797695	99.313294	0.102570	0.035048	0.034844
109.430971	2.878049	109.372396	0.058575	0.031281	0.034232
119.446078	2.958511	119.444976	0.001102	0.028153	0.033628
129.461185	3.038730	129.487224	-0.026039	0.025516	0.033033
139.476293	3.118577	139.482812	-0.006519	0.023266	0.032450
149.491400	3.198913	149.539687	-0.048287	0.021321	0.031874
159.506507	3.278927	159.556150	-0.049643	0.019627	0.031307
169.521614	3.359178	169.602432	-0.080819	0.018140	0.030751
179.536721	3.439146	179.613178	-0.076457	0.016825	0.030207
189.551828	3.519165	189.630271	-0.078443	0.015655	0.029675
199.566935	3.598926	199.615207	-0.048272	0.014609	0.029155
249.642471	3.998583	249.646179	-0.003709	0.010721	0.026765
299.718006	4.398473	299.706296	0.011710	0.008270	0.024786
349.793541	4.797999	349.720871	0.072670	0.006670	0.023331
449.944612	5.597755	449.838134	0.106479	0.004969	0.022359
550.095683	6.398159	550.036443	0.059240	0.004390	0.024146
600.171219	6.797914	600.079637	0.091582	0.004320	0.025926
650.246754	7.198177	650.186546	0.060208	0.004331	0.028160
700.322290	7.598640	700.318362	0.003928	0.004393	0.030763
710.337397	7.678699	710.340535	-0.003138	0.004410	0.031325
720.352504	7.758745	720.361007	-0.008503	0.004427	0.031890
730.367611	7.838548	730.351140	0.016471	0.004444	0.032454
740.382718	7.918889	740.408616	-0.025898	0.004463	0.033047
750.397825	7.997820	750.289668	0.108157	0.004481	0.033626
760.412932	8.078768	760.423119	-0.010186	0.004503	0.034238
770.428039	8.158853	770.448531	-0.020492	0.004524	0.034851
780.443146	8.239067	780.489997	-0.046850	0.004545	0.035467
790.458254	8.319413	790.548207	-0.089953	0.004568	0.036109
800.473361	8.399547	800.579684	-0.106323	0.004589	0.036732

COMMENTS:

The uncertainty is calculated with 95% confidence. The uncertainty includes the randomness in the calibrated instrument during the calibration, systematic uncertainty in the instrument or property which the instrument under calibration is compared with (dead weight manometer, calibrated weights etc.), and due to regression analysis to fit the calibration points to a linear calibration equation.The calculated uncertainty can be used as the total systematic uncertianty of the calibrated instrument with the given calibration equation.

CALIBRATION REPORT

CALIBRATION PROPERTIES
Calibrated by: Sigurd Haga
Type/Producer: Druck PTX1400
SN: Z00227/07
Range: 0-4 bar g
Unit: kPa

CALIBRATION SOURCE PROPERTIES
Type/Producer: Pressurements deadweight tester P3223-1
SN: 66256
Uncertainty [%]: 0,01

POLY FIT EQUATION:
$Y= -100.41820358E+0X^0 + 49.96688477E+0X^1$

CALIBRATION SUMARY:
Max Uncertainty   : Inf [%]
Max Uncertainty   : 0.044186 [kPa]
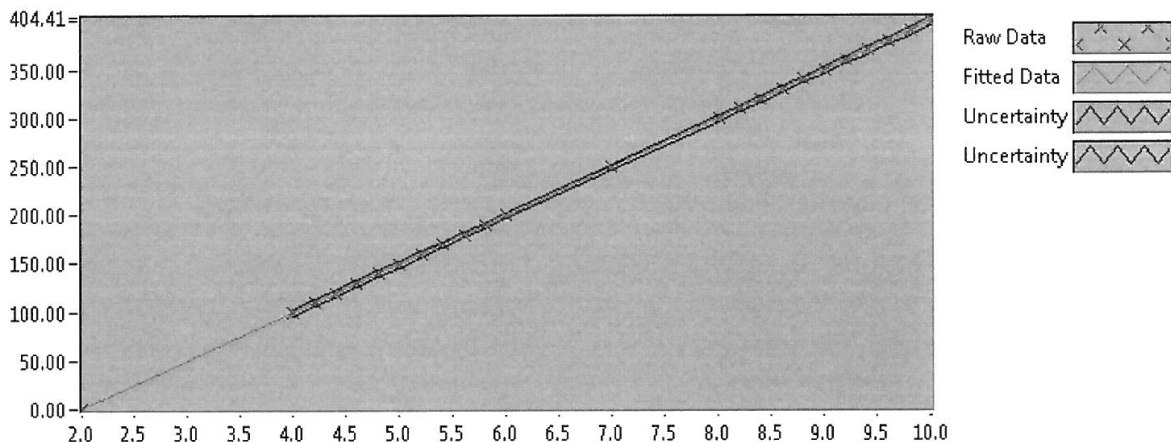RSQ   : 1.000000
Calibration points : 24

Figure 1 : Calibration chart (The uncertainty band is multiplied by 100)

Sigurd Haga

CALIBRATION VALUES

Value [kPa]	Voltage [V]	Best Poly Fit [kPa]	Deviation [kPa]	Uncertainty [%]	Uncertainty [kPa]
0.000000	2.012470	0.138675	-0.138675	Inf	NaN
99.415864	3.999243	99.411494	0.004370	0.040645	0.040408
109.430971	4.200290	109.457181	-0.026210	0.035337	0.038669
119.446078	4.401184	119.495226	-0.049148	0.030966	0.036988
129.461185	4.601059	129.482380	-0.021195	0.027329	0.035380
139.476293	4.801165	139.481032	-0.004739	0.024265	0.033844
149.491400	5.000907	149.461528	0.029871	0.021669	0.032393
159.506507	5.201620	159.490552	0.015955	0.019455	0.031031
169.521614	5.402217	169.513742	0.007872	0.017568	0.029781
179.536721	5.602288	179.510661	0.026060	0.015962	0.028657
189.551828	5.801537	189.466505	0.085323	0.014599	0.027673
199.566935	6.001874	199.476747	0.090188	0.013448	0.026838
249.642471	7.004300	249.564850	0.077620	0.010177	0.025406
299.718006	8.006613	299.647304	0.070702	0.009585	0.028729
309.733113	8.207218	309.670897	0.062216	0.009642	0.029865
319.748220	8.407960	319.701378	0.046842	0.009735	0.031128
329.763327	8.608415	329.717492	0.045835	0.009854	0.032495
339.778434	8.809336	339.756860	0.021575	0.009995	0.033962
349.793541	9.010762	349.821523	-0.027982	0.010153	0.035514
359.808649	9.210883	359.820914	-0.012266	0.010319	0.037127
369.823756	9.411952	369.867704	-0.043949	0.010496	0.038815
379.838863	9.612487	379.887836	-0.048973	0.010677	0.040556
389.853970	9.813714	389.942494	-0.088524	0.010863	0.042350
399.869077	10.014834	399.991847	-0.122770	0.011050	0.044186

COMMENTS:

The uncertainty is calculated with 95% confidence. The uncertainty includes the randomness in the calibrated instrument during the calibration, systematic uncertainty in the instrument or property which the instrument under calibration is compared with (dead weight manometer, calibrated weights etc.), and due to regression analysis to fit the calibration points to a linear calibration equation. The calculated uncertainty can be used as the total systematic uncertianty of the calibrated instrument with the given calibration equation.

CALIBRATION REPORT

CALIBRATION PROPERTIES
Calibrated by: Sigurd Haga
Type/Producer: Druck PTX1400
SN: Z00580/02
Range: 0-2,5 bar g
Unit: kPa

CALIBRATION SOURCE PROPERTIES
Type/Producer: Pressurements deadweight tester P3223-1
SN: 66256
Uncertainty [%]: 0,01

POLY FIT EQUATION:
Y= -62.94281179E+0X^0 + 31.34806609E+0X^1

CALIBRATION SUMARY:
Max Uncertainty   : Inf [%]
Max Uncertainty   : 0.016306 [kPa]
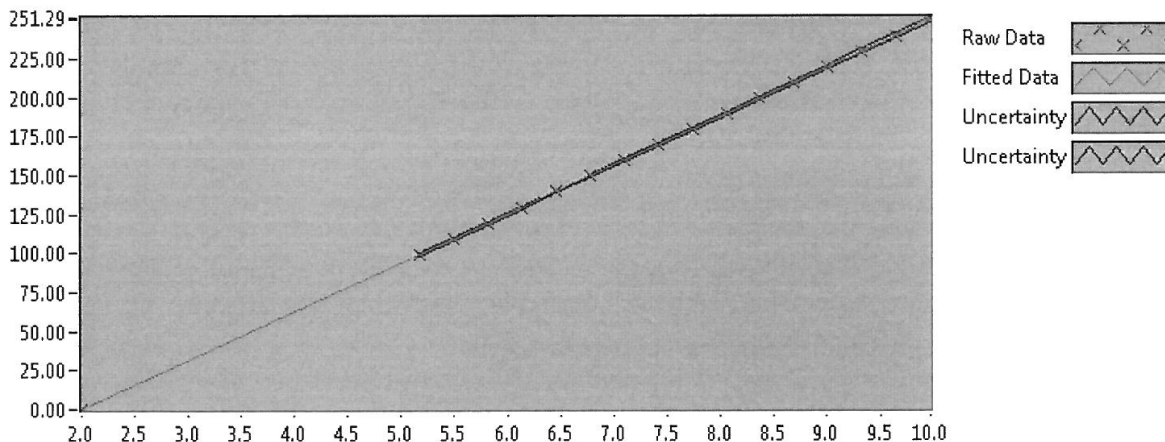RSQ   : 1.000000
Calibration points : 17

Figure 1 : Calibration chart (The uncertainty band is multiplied by 100)

Sigurd Haga

CALIBRATION VALUES

Value [kPa]	Voltage [V]	Best Poly Fit [kPa]	Deviation [kPa]	Uncertainty [%]	Uncertainty [kPa]
0.000000	2.009170	0.040768	-0.040768	Inf	NaN
99.415864	5.179483	99.423951	-0.008087	0.013903	0.013822
109.430971	5.498190	109.414805	0.016166	0.011636	0.012734
119.446078	5.817696	119.430701	0.015378	0.009834	0.011747
129.461185	6.137583	129.458531	0.002654	0.008414	0.010893
139.476293	6.456885	139.468040	0.008252	0.007321	0.010211
149.491400	6.775547	149.457469	0.033931	0.006509	0.009731
159.506507	7.095612	159.490895	0.015611	0.005946	0.009484
169.521614	7.415071	169.505309	0.016305	0.005598	0.009490
179.536721	7.734466	179.517728	0.018993	0.005429	0.009747
189.551828	8.054542	189.551501	0.000327	0.005402	0.010240
199.566935	8.373961	199.564681	0.002254	0.005478	0.010931
209.582042	8.693828	209.591877	-0.009835	0.005628	0.011796
219.597149	9.013899	219.625484	-0.028334	0.005824	0.012789
229.612256	9.333073	229.630978	-0.018721	0.006046	0.013883
239.627363	9.652167	239.633960	-0.006596	0.006285	0.015060
249.642471	9.971997	249.660001	-0.017530	0.006532	0.016306

COMMENTS:

The uncertainty is calculated with 95% confidence. The uncertainty includes the randomness in the calibrated instrument during the calibration, systematic uncertainty in the instrument or property which the instrument under calibration is compared with (dead weight manometer, calibrated weights etc.), and due to regression analysis to fit the calibration points to a linear calibration equation. The calculated uncertainty can be used as the total systematic uncertianty of the calibrated instrument with the given calibration equation.

Appendix F

Risk assessment

- Risk assessment for laboratory tests
- Risk assessment for field trip
- Risk assessment report for laboratory in norwegian

NTNU		Risikovurdering	utarbeidet av	Nummer	Dato	
			HMS-avd.	HMSRV2603	04.02.2011	
◨			godkjent av	side	Erstatter	
HMS/KS			Rektor	1 av 2	9.2.2010	

Enhet: Institutt for energi og prosessteknikk   **Dato: 07.06.2014**
Linjeleder:
Deltakere ved risikovurderingen (m/ funksjon): Kjetil Guddal Ruud, Student

ID nr	Aktivitet fra kartleggings-skjemaet	Mulig uønsket hendelse/ belastning	Vurdering av sannsyn-lighet (1-5)	Vurdering av konsekvens:				Risiko-verdi	Kommentarer/status Forslag til tiltak
				Menneske (A-E)	Ytre miljø (A-E)	Øk/ materiell (A-E)	Om-dømme (A-E)		
1	Lekkasje fra trykk-satt utstyr	Fysisk skade ved treff av stråle	2	E	A	B	A	E2	Jevnlig sjekk av trykkutsatte og/eller trykksatte deler utsatt for vibrasjon/store materialspenninger. Utføres av ansvarlig person
2	Bevegelse i laboratoriet	Fall, klemfare, elektrisk støt, fallende objekter	1	D	A	A	B	D1	Følge henvisninger og oppmerking. Benytte nødvendig verneutstyr. Følge gjeldende HMS-regelverk og prosedyrer
3	Montering av instumenter og måleutstyr	Elektrisk støt - lav spenning, klemfare.	2	A	A	B	A	A2	Jording av instrumenter, bruke hansker og isolert verktøy.

Sannsynlighet
1. Svært liten
2. Liten
3. Middels
4. Stor

Konsekvens
A. Svært liten
B. Liten
C. Moderat
D. Alvorlig

Risikoverdi (beregnes hver for seg):
Menneske = Sannsynlighet x Konsekvens Menneske
Ytre miljø = Sannsynlighet x Konsekvens Ytre miljø
Økonomi/materiell = Sannsynlighet x Konsekvens Øk/matriell
Omdømme = Sannsynlighet x Konsekvens Omdømme

NTNU		Risikovurdering	utarbeidet av	Nummer	Dato	
			HMS-avd.	HMSRV2603	04.02.2011	
			godkjent av	side	Erstatter	
HMS/KS			Rektor	1 av 2	9.2.2010	

Enhet: Institutt for energi og prosessteknikk   **Dato: 17.02.2014**

Linjeleder:

Deltakere ved risikovurderingen (m/ funksjon): Kjetil Guddal Ruud, Student

ID nr	Aktivitet fra kartleggings-skjemaet	Mulig uønsket hendelse/ belastning	Vurdering av sannsyn-lighet (1-5)	Vurdering av konsekvens:				Risiko-verdi	Kommentarer/status Forslag til tiltak
				Menneske (A-E)	Ytre miljø (A-E)	Øk/ materiell (A-E)	Om-dømme (A-E)		
1	Transport med bil	Kollisjon, utforkjøring	3	E	A	C	A	E3	Uthvilt sjåfør, stopp ved tretthet. Inneha gyldig norsk førerkort. Kontrollere tilstand på kjøretøy
2	Bevegelse i kraftstasjon	Fall, klemfare, elektrisk støt	1	D	A	A	B	D1	Følge henvisninger og oppmerking. Benytte nødvendig verneutstyr.
3	Inspeksjon av løpehjul	Oversvømmelse av inspeksjonssted	1	E	A	B	E	E1	Kontrollere stengeorgan og sørge for tilstrekkelig merking av operatørpanel.
4	Montering av instumenter og måleutstyr	Elektrisk støt - lav spenning, klemfare.	2	A	A	B	A	A2	Jording av instrumenter, bruke hansker.

Sannsynlighet
1. Svært liten
2. Liten
3. Middels
4. Stor
5. Svært stor

Konsekvens
A. Svært liten
B. Liten
C. Moderat
D. Alvorlig
E. Svært alvorlig

Risikoverdi (beregnes hver for seg):
Menneske = Sannsynlighet x Konsekvens Menneske
Ytre miljø = Sannsynlighet x Konsekvens Ytre miljø
Økonomi/materiell = Sannsynlighet x Konsekvens Øk/matriell
Omdømme = Sannsynlighet x Konsekvens Omdømme

NTNU		Risikovurdering	utarbeidet av	Nummer	Dato
			HMS-avd.	HMSRV2603	04.02.2011
			godkjent av	side	Erstatter
HMS/KS			Rektor	2 av 2	9.2.2010

5. Svært stor   *E. Svært alvorlig*

Sannsynlighet vurderes etter følgende kriterier:

Svært liten 1	Liten 2	Middels 3	Stor 4	Svært stor 5
1 gang pr 50 år eller sjeldnere	1 gang pr 10 år eller sjeldnere	1 gang pr år eller sjeldnere	1 gang pr måned eller sjeldnere	Skjer ukentlig

Konsekvens vurderes etter følgende kriterier:

Gradering	Menneske	Ytre miljø Vann, jord og luft	Øk/materiell	Omdømme
E Svært Alvorlig	Død	Svært langvarig og ikke reversibel skade	Drifts- eller aktivitetsstans >1 år.	Troverdighet og respekt betydelig og varig svekket
D Alvorlig	Alvorlig personskade. Mulig uførhet.	Langvarig skade. Lang restitusjonstid	Driftsstans > ½ år Aktivitetsstans i opp til 1 år	Troverdighet og respekt betydelig svekket
C Moderat	Alvorlig personskade.	Mindre skade og lang restitusjonstid	Drifts- eller aktivitetsstans < 1 mnd	Troverdighet og respekt svekket
B Liten	Skade som krever medisinsk behandling	Mindre skade og kort restitusjonstid	Drifts- eller aktivitetsstans < 1uke	Negativ påvirkning på troverdighet og respekt
A Svært liten	Skade som krever førstehjelp	Ubetydelig skade og kort restitusjonstid	Drifts- eller aktivitetsstans < 1dag	Liten påvirkning på troverdighet og respekt

Risikoverdi = Sannsynlighet x Konsekvens
Beregn risikoverdi for Menneske. Enheten vurderer selv om de i tillegg vil beregne risikoverdi for Ytre miljø, Økonomi/materiell og Omdømme. I så fall beregnes disse hver for seg.

Til kolonnen "Kommentarer/status, forslag til forebyggende og korrigerende tiltak":
Tiltak kan påvirke både sannsynlighet og konsekvens. Prioriter tiltak som kan forhindre at hendelsen inntreffer, dvs. sannsynlighetsreduserende tiltak foran skjerpet beredskap, dvs. konsekvensreduserende tiltak.

Risikovurderingsrapport

Francisrigg; Reversibel Pumpeturbin(RPT)

Prosjekttittel	Generell operasjon av Francis-riggen ved VKL
Prosjektleder	Torbjørn Nielsen
Enhet	NTNU
HMS-koordinator	Morten Grønli
Linjeleder	Olav Bolland
Riggnavn	Francis turbin/pumpeturbin-rigg ved VKL
Plassering	Vannkraftlab
Romnummer	42
Riggansvarlig	Bård Aslak Brandåstrø
Risikovurdering utført av	Bård Aslak Brandåstrø

INNHOLDSFORTEGNELSE

1 INNLEDNING

Riggen står i hovedrommet til vannkraftlaboratoriet. Formålet med riggen er å gjøre modelltester på løpehjul av typen Francis eller pumpeturbin. Riggen har vært i bruk i lang tid. De aktuelle målingene skal kunne vise virkningsgradsdiagram og karakteristikker for turbiner.

2 ORGANISERING

Rolle	NTNU	Sintef
Lab Ansvarlig:	Morten Grønli	Harald Mæhlum
Linjeleder:	Olav Bolland	Mona J. Mølnvik
HMS ansvarlig:	Olav Bolland	Mona J. Mølnvik
HMS koordinator	Morten Grønli	Harald Mæhlum
HMS koordinator	Per Bjørnås	
Romansvarlig:	Bård Brandåstrø	
Prosjekt leder:	Torbjørn Nielsen	
Ansvarlig riggoperatører:	Bård Brandåstrø, Joar Grilstad, Ole dahlhaug	

3 RISIKOSTYRING AV PROSJEKTET

Hovedaktiviteter risikostyring	Nødvendige tiltak, dokumentasjon	DTG
Prosjekt initiering	Prosjekt initiering mal	
Veiledningsmøte	Skjema for Veiledningsmøte med pre-risikovurdering	X
Innledende risikovurdering	Fareidentifikasjon – HAZID Skjema grovanalyse	X
Vurdering av teknisk sikkerhet	Prosess-HAZOP Tekniske dokumentasjoner	X
Vurdering av operasjonell sikkerhet	Prosedyre-HAZOP Opplæringsplan for operatører	X
Sluttvurdering, kvalitetssikring	Uavhengig kontroll Utstedelse av apparaturkort Utstedelse av forsøk pågår kort	X

4 TEGNINGER, FOTO, BESKRIVELSER AV FORSØKSOPPSETT

Vedlegg:
Prosess og Instrumenterings Diagram, (PID)
Komponentliste med spesifikasjoner
Tegninger og bilder som beskriver forsøksoppsetningen.

5 EVAKUERING FRA FORSØKSOPPSETNINGEN

Se kapittel 14 "Veiledning til rapport mal.
Evakuering skjer på signal fra alarmklokker eller lokale gassalarmstasjon med egen lokal varsling med lyd og lys utenfor aktuelle rom, se 6.2

Evakuering fra rigg området foregår igjennom merkede nødutganger.

6   VARSLING

6.1   Før forsøkskjøring

Varsling per e-post, med opplysning om forsøkskjøringens varighet og involverte til:
- HMS koordinator NTNU/SINTEF
  HaraldStein.S.Mahlum@sintef.no
  Erik.langorgen@ntnu.no
  Baard.brandaastro@ntnu.no
- *Prosjektledere på naborigger varsles for avklaring rundt bruk av avtrekksanlegget uten fare eller forstyrrelser av noen art, se rigg matrise.*

All forsøkskjøringen skal planlegges og legges inn i aktivitetskalender for lab. Forsøksleder må få bekreftelse på at forsøkene er klarert med øvrig labdrift før forsøk kan iverksettes.

6.2   Ved uønskede hendelser

BRANN
Ved brann en ikke selv er i stand til å slukke med rimelige lokalt tilgjengelige slukkemidler, skal nærmeste brannalarm utløses og arealet evakueres raskest mulig. En skal så være tilgjengelig for brannvesen/bygningsvaktmester for å påvise brannsted.
Om mulig varsles så:

NTNU	SINTEF
Labsjef Morten Grønli, tlf: 918 97 515	
HMS: Morten Grønli, tlf: 91897515	
Instituttleder: Olav Bolland: 91897209	

GASSALARM
Ved gassalarm skal gassflasker stenges umiddelbart og området ventileres. Klarer man ikke innen rimelig tid å få ned nivået på gasskonsentrasjonen så utløses brannalarm og laben evakueres. Dedikert personell og eller brannvesen sjekker så lekkasjested for å fastslå om det er mulig å tette lekkasje og lufte ut området på en forsvarlig måte.
Varslingsrekkefølge som i overstående punkt.

PERSONSKADE
- Førstehjelpsutstyr i Brann/førstehjelpsstasjoner,
- Rop på hjelp,
- Start livreddende førstehjelp
- **Ring 113** hvis det er eller det er tvil om det er alvorlig skade.

ANDRE UØNSKEDE HENDELSER (AVVIK)
NTNU:
Rapporteringsskjema for uønskede hendelser på
http://www.ntnu.no/hms/2007_Nettsider/HMSRV0401_avvik.doc

7   VURDERING AV TEKNISK SIKKERHET

7.1   Fareidentifikasjon, HAZOP

Se kapittel 14 "Veiledning til rapport mal.
Forsøksoppsetningen deles inn i følgende noder:

Node 1	Rørsystem med pumpe
Node 2	Roterende turbin
Node 3	Hydraulikkanlegg
Node 4	Energidreper

Vedlegg, skjema: Hazop_mal
Vurdering:
Node1:
-Overtrykksventil som slår ut dersom trykket i systemet blir for høyt.
-Rørelementer er eksternt levert og godkjent for aktuelt trykk.
Node2:
-Roterende utstyr står utilgjengelig for folk. Dvs det er innkapslet eller man må klatre for å nå opp til det.
Node3:
-Trykk i slanger og rør(olje vann) Hydraulikkslanger er ikke egenprodusert
-Trykksatt utstyr er sertifisert og kjøpt inn av eksterne leverandører
Node4:
-Fare for støy.

7.2   Brannfarlig, reaksjonsfarlig og trykksatt stoff og gass

Se kapittel 14 "Veiledning til rapport mal.
Inneholder forsøkene brannfarlig, reaksjonsfarlig og trykksatt stoff

Ja	Trykksatt hydraulikkolje, trykksatt vann

Vedlegg Ex-sonekart:
Vurdering: *Arbeidsmedium er vann. Alle rør er levert av eksternt firma med prøvesertifikat Hydraulikk til hydrostatisk lager. Hyllevare komponenter, de er dermed ikke egenprodusert.*

7.3   Trykkpåkjent utstyr

Inneholder forsøksoppsetningen trykkpåkjent utstyr:

JA Utstyret trykktestes i henhold til norm og dokumenteres

Trykkutsatt utstyr skal trykktestes med driftstrykk gange faktor 1.4,for utstyr som har usertifiserte sveiser er faktoren 1.8. Trykktesten skal dokumenteres skriftlig hvor fremgangsmåte framgår.
Vedlegg: Prøvesertifikat for trykktesting finnes i Lab.perm.
Vurdering:

7.4 Påvirkning av ytre miljø (utslipp til luft/vann, støy, temperatur, rystelser, lukt)

Se kapittel 14 "Veiledning til rapport mal..

NEI	

Vurdering: Det blir ingen utslipp til ytre miljø.

7.5 Stråling

Se kapittel 14 "Veiledning til rapport mal.

NEI	

Vedlegg:
Vurdering: Ingen strålekilder.

7.6 Bruk og behandling av kjemikalier

Se kapittel 14 "Veiledning til rapport mal.

Ja	

Vedlegg:
Vurdering: Hydraulikkolje, mineralsk olje. Datablad er vedlagt

7.7 El sikkerhet (behov for å avvike fra gjeldende forskrifter og normer)

NEI	

Her forstås montasje og bruk i forhold til normer og forskrifter med tanke på berøringsfare
Vedlegg:
Vurdering: Alt elektrisk utstyr er forsvarlig montert og står slik permanent.

8   VURDERING AV OPERASJONELL SIKKERHET

Sikrer at etablerte prosedyrer dekker alle identifiserte risikoforhold som må håndteres gjennom operasjonelle barrierer og at operatører og teknisk utførende har tilstrekkelig kompetanse.

8.1 Prosedyre HAZOP

Se kapittel 14 "Veiledning til rapport mal.
Metoden er en undersøkelse av operasjonsprosedyrer, og identifiserer årsaker og farekilder for operasjonelle problemer.
Vedlegg: HAZOP_MAL_Prosedyre
Vurdering: Operatør har et eget rom for å kjøre riggen.

8.2 Drifts og nødstopps prosedyre

Se kapittel 14 "Veiledning til rapport mal.
Nødstopp koordineres med labpersonell, for å unngå at man må ta en omvei via laben for nødstopp ved evakuering.
Vedlegg "Procedure for running experiments"

8.3 Opplæring av operatører

Dokument som viser Opplæringsplan for operatører utarbeides for alle forøksoppsetninger.
- *Kjøring av pumpesystem.*

Vedlegg*:* Opplæringsplan for operatører

8.4 Tekniske modifikasjoner

Vurdering: Modifikasjoner gjøres i samråd med Torbjørn Nielsen/Bård Brandåstrø

8.5 Personlig verneutstyr

- ▪ *Det er påbudt med vernebriller i sonen anlegget er plassert i.*

Vurdering: Vernebriller viktig, pga vann og hydraulikkolje under trykk.

8.6 Generelt

Vurdering: Alle forsøk kjøres med operatør til stede.

8.7 Sikkerhetsutrustning

- *Vernebriller*

8.8 Spesielle tiltak

9 TALLFESTING AV RESTRISIKO – RISIKOMATRISE

Se kapittel 14 "Veiledning til rapportmal.

Risikomatrisen vil gi en visualisering og en samlet oversikt over aktivitetens risikoforhold slik at ledelse og brukere får et mest mulig komplett bilde av risikoforhold.

IDnr	Aktivitet-hendelse	Frekv-Sans	Kons	RV
1	*Lekkasje i Hydraulikk,*	1	A	A1
2	*Fremmedlegemer i vannet*	1	A	A1
3	*Rørbrudd*	1	A	A1
4	*Roterende Aksling*	1	B	B1

Vurdering restrisiko: *Det er liten restrisiko ved forsøkene, foruten at trykksatt vann og olje fordrer bruk av vernebriller. Fremmedlegemer i vannet gir liten risiko for personskade, men kan føre til store skader på maskineri.*

10 KONKLUSJON

Riggen er bygget til god laboratorium praksis (GLP).

Hvilke tekniske endringer eller endringer av driftsparametere
vil kreve ny risikovurdering: Ingen

Apparaturkortet får en gyldighet på **4 måneder**
Forsøk pågår kort får en gyldighet på **4 måneder**

11   LOVER FORSKRIFTER OG PÅLEGG SOM GJELDER

Se http://www.arbeidstilsynet.no/regelverk/index.html
- Lov om tilsyn med elektriske anlegg og elektrisk utstyr (1929)
- Arbeidsmiljøloven
- Forskrift om systematisk helse-, miljø- og sikkerhetsarbeid (HMS Internkontrollforskrift)
- Forskrift om sikkerhet ved arbeid og drift av elektriske anlegg (FSE 2006)
- Forskrift om elektriske forsyningsanlegg (FEF 2006)
- Forskrift om utstyr og sikkerhetssystem til bruk i eksplosjonsfarlig område NEK 420
- Forskrift om håndtering av brannfarlig, reaksjonsfarlig og trykksatt stoff samt utstyr og anlegg som benyttes ved håndteringen
- Forskrift om Håndtering av eksplosjonsfarlig stoff
- Forskrift om bruk av arbeidsutstyr.
- Forskrift om Arbeidsplasser og arbeidslokaler
- Forskrift om Bruk av personlig verneutstyr på arbeidsplassen
- Forskrift om Helse og sikkerhet i eksplosjonsfarlige atmosfærer
- Forskrift om Høytrykksspyling
- Forskrift om Maskiner
- Forskrift om Sikkerhetsskilting og signalgivning på arbeidsplassen
- Forskrift om Stillaser, stiger og arbeid på tak m.m.
- Forskrift om Sveising, termisk skjæring, termisk sprøyting, kullbuemeisling, lodding og sliping (varmt arbeid)
- Forskrift om Tekniske innretninger
- Forskrift om Tungt og ensformig arbeid
- Forskrift om Vern mot eksponering for kjemikalier på arbeidsplassen (Kjemikalieforskriften)
- Forskrift om Vern mot kunstig optisk stråling på arbeidsplassen
- Forskrift om Vern mot mekaniske vibrasjoner
- Forskrift om Vern mot støy på arbeidsplassen

Veiledninger fra arbeidstilsynet
se: http://www.arbeidstilsynet.no/regelverk/veiledninger.html

12   VEDLEGG

13 DOKUMENTASJON

- Tegninger, foto, beskrivelser av forsøksoppsetningen
- Hazop_mal
- Sertifikat for trykkpåkjent utstyr
- Håndtering avfall i NTNU
- Sikker bruk av LASERE, retningslinje
- HAZOP_MAL_Prosedyre
- Forsøksprosedyre
- Opplæringsplan for operatører
- Skjema for sikker jobb analyse, (SJA)
- Apparaturkortet
- Forsøk pågår kort

14   VEILEDNING TIL RAPPORTMAL

Kap 5 Evakuering fra forsøksoppsetningen
Beskriv i hvilken tilstand riggen skal forlates ved en evakueringssituasjon.

Kap 7 Vurdering av teknisk sikkerhet
Sikre at design av apparatur er optimalisert i forhold til teknisk sikkerhet.
Identifisere risikoforhold knyttet til valgt design, og eventuelt å initiere re-design for å sikre at størst mulig andel av risiko elimineres gjennom teknisk sikkerhet.
Punktene skal beskrive hva forsøksoppsetningen faktisk er i stand til å tåle og aksept for utslipp.

7.1 Fareidentifikasjon, HAZOP
Forsøksoppsetningen deles inn i noder: (eks M*otorenhet, pumpeenhet, turbinenhet.)*
Ved hjelp av ledeord identifiseres årsak, konsekvens og sikkerhetstiltak. Konkluderes det med at tiltak er nødvendig anbefales disse på bakgrunn av dette. Tiltakene lukkes når de er utført og Hazop sluttføres.
(eks "No flow", årsak: rør er deformert, konsekvens: pumpe går varm, sikkerhetsforanstaltning: måling av flow med kobling opp mot nødstopp eller hvis konsekvensen ikke er kritisk benyttes manuell overvåkning og punktet legges inn i den operasjonelle prosedyren.)

7.2 Brannfarlig, reaksjonsfarlig og trykksatt stoff.
I henhold til Forskrift om håndtering av brannfarlig, reaksjonsfarlig og trykksatt stoff samt utstyr og anlegg som benyttes ved håndteringen

Brannfarlig stoff: Fast, flytende eller gassformig stoff, stoffblanding, samt stoff som forekommeri kombinasjoner av slike tilstander, som i kraft av sitt flammepunkt, kontakt med andre stoffer, trykk, temperatur eller andre kjemiske egenskaper representerer en fare for brann.
Reaksjonsfarlig stoff: Fast, flytende, eller gassformig stoff, stoffblanding, samt stoff som forekommer i kombinasjoner av slike tilstander, som ved kontakt med vann, ved sitt trykk, temperatur eller andre kjemiske forhold, representerer en fare for farlig reaksjon, eksplosjon eller utslipp av farlig gass, damp, støv eller tåke.
Trykksatt stoff: Annet fast, flytende eller gassformig stoff eller stoffblanding enn brann- eller reaksjonsfarlig stoff, som er under trykk, og som derved kan representere en fare ved ukontrollert utslipp.

Nærmere kriterier for klassifisering av brannfarlig, reaksjonsfarlig og trykksatt stoff er fastsatt i vedlegg 1 i veiledningen til forskriften "Brannfarlig, reaksjonsfarlig og trykksatt stoff"
http://www.dsb.no/Global/Publikasjoner/2009/Veiledning/Generell%20veiledning.pdf
http://www.dsb.no/Global/Publikasjoner/2010/Tema/Temaveiledning_bruk_av_farlig_stoff_Del_1.pdf

Rigg og areal skal gjennomgås med hensyn på vurdering av Ex sone

- Sone 0: Alltid eksplosiv atmosfære, for eksempel inne i tanker med gass, brennbar væske.
- Sone 1: Primær sone, tidvis eksplosiv atmosfære for eksempel et fylle tappe punkt
- Sone 2: Sekundert utslippssted, kan få eksplosiv atmosfære ved uhell, for eksempel ved flenser, ventiler og koblingspunkt

7.4 Påvirkning av ytre miljø

Med forurensning forstås: tilførsel av fast stoff, væske eller gass til luft, vann eller i grunnen støy og rystelser påvirkning av temperaturen som er eller kan være til skade eller ulempe for miljøet.

Regelverk: http://www.lovdata.no/all/hl-19810313-006.html#6

NTNU retningslinjer for avfall se: http://www.ntnu.no/hms/retningslinjer/HMSR18B.pdf

7.5 Stråling

Stråling defineres som

Ioniserende stråling: Elektromagnetisk stråling (i strålevernsammenheng med bølgelengde <100 nm) eller hurtige atomære partikler (f.eks alfa- og beta-partikler) som har evne til å ionisere atomer eller molekyler
Ikke-ioniserende stråling: Elektromagnetisk stråling (bølgelengde >100 nm), og ultralyd1, som har liten eller ingen evne til å ionisere.
Strålekilder: Alle ioniserende og sterke ikke-ioniserende strålekilder.
Ioniserende strålekilder: Kilder som avgir ioniserende stråling, f.eks alle typer radioaktive kilder, røntgenapparater, elektronmikroskop
Sterke ikke-ioniserende strålekilder: Kilder som avgir sterk ikke-ioniserende stråling som kan skade helse og/eller ytre miljø, f.eks laser klasse 3B og 4, MR2-systemer, UVC3-kilder, kraftige IR-kilder4
1 Ultralyd er akustisk stråling ("lyd") over det hørbare frekvensområdet (>20 kHz). I strålevernforskriften er ultralyd omtalt sammen med elektromagnetisk ikke-ioniserende stråling.
2 MR (eg. NMR) - kjernemagnetisk resonans, metode som nyttes til å «avbilde» indre strukturer i ulike materialer.
3 UVC er elektromagnetisk stråling i bølgelengdeområdet 100-280 nm.
4 IR er elektromagnetisk stråling i bølgelengdeområdet 700 nm – 1 mm.

For hver laser skal det finnes en informasjonsperm(HMSRV3404B) som skal inneholde:
- Generell informasjon
- Navn på instrumentansvarlig og stedfortreder, og lokal strålevernskoordinator
- Sentrale data om apparaturen
- Instrumentspesifikk dokumentasjon
- Referanser til (evt kopier av) datablader, strålevernbestemmelser, o.l.
- Vurderinger av risikomomenter
- Instruks for brukere
- Instruks for praktisk bruk; oppstart, drift, avstenging, sikkerhetsforholdsregler, loggføring, avlåsing, evt. bruk av strålingsmåler, osv.
- Nødprosedyrer

Se ellers retningslinjen til NTNU for laser: http://www.ntnu.no/hms/retningslinjer/HMSR34B.pdf

7.6 Bruk og behandling av kjemikalier.
Her forstås kjemikalier som grunnstoff som kan utgjøre en fare for arbeidstakers sikkerhet og helse.
Se ellers: http://www.lovdata.no/cgi-wift/ldles?doc=/sf/sf/sf-20010430-0443.html
Sikkerhetsdatablar skal være i forøkenes HMS perm og kjemikaliene registrert i Stoffkartoteket.

<u>Kap 8 Vurdering av operasjonell sikkerhet</u>
Sikrer at etablerte prosedyrer dekker alle identifiserte risikoforhold som må håndteres gjennom operasjonelle barrierer og at operatører og teknisk utførende har tilstrekkelig kompetanse.

8.1 Prosedyre Hazop
Prosedyre-HAZOP gjennomføres som en systematisk gjennomgang av den aktuelle prosedyren ved hjelp av fastlagt HAZOP-metodikk og definerte ledeord. Prosedyren brytes ned i enkeltstående arbeidsoperasjoner (noder) og analyseres ved hjelp av ledeordene for å avdekke mulige avvik, uklarheter eller kilder til mangelfull gjennomføring og feil.

8.2 Drifts og nødstopp prosedyrer
Utarbeides for alle forsøksoppsetninger.
Driftsprosedyren skal stegvis beskrive gjennomføringen av et forsøk, inndelt i oppstart, under drift og avslutning. Prosedyren skal beskrive forutsetninger og tilstand for start, driftsparametere med hvor store avvik som tillates før forsøket avbrytes og hvilken tilstand riggen skal forlates.
Nødstopp-prosedyre beskriver hvordan en nødstopp skal skje, (utført av uinnvidde),
hva som skjer, (strøm/gass tilførsel) og
hvilke hendelser som skal aktivere nødstopp, (brannalarm, lekkasje).

Kap 9 Risikomatrise

9 Tallfesting av restrisiko, Risikomatrisen

For å synliggjøre samlet risiko, jevnfør skjema for risikovurdering, plottes hver enkelt aktivitets verdi for sannsynlighet og konsekvens inn i risikomatrisen. Bruk aktivitetens IDnr.
Eksempel: Hvis aktivitet med IDnr. 1 har fått en risikoverdi D3 (sannsynlighet 3 x konsekvens D) settes aktivitetens IDnr i risikomatrisens felt for 3D. Slik settes alle aktivitetenes risikoverdier (IDnr) inn i risikomatrisen.

I risikomatrisen er ulike grader av risiko merket med rød, gul eller grønn. Når en aktivitets risiko havner på rød (= uakseptabel risiko), skal risikoreduserende tiltak gjennomføres. Ny vurdering gjennomføres etter at tiltak er iverksatt for å se om risikoverdien er kommet ned på akseptabelt nivå.

KONSEKVENS	Svært alvorlig	E1	E2	E3	E4	E5
	Alvorlig	D1	D2	D3	D4	D5
	Moderat	C1	C2	C3	C4	C5
	Liten	B1	B2	B3	B4	B5
	Svært liten	A1	A2	A3	A4	A5
		Svært liten	Liten	Middels	Stor	Svært Stor
		SANSYNLIGHET				

Prinsipp over akseptkriterium. Forklaring av fargene som er brukt i risikomatrisen.

Farge		Beskrivelse
Rød		Uakseptabel risiko. Tiltak skal gjennomføres for å redusere risikoen.
Gul		Vurderingsområde. Tiltak skal vurderes.
Grønn		Akseptabel risiko. Tiltak kan vurderes ut fra andre hensyn.